A framework for 210Pb model selection and its application to 37 cores from Eastern Canada to identify the dynamics and drivers of lake sedimentation rates

Alexandre Baud[1], Candice Aulard[2], Hamid Ghanbari[3], Maxime Fradette[4], Dermot Antoniades[3], Paul Del Giorgio[2], Yannick Huot[3], Pierre Francus[5], John Smol[6], and Irene Gregory-Eaves[1]

[1]Biology Department, McGill University
[2]Département des sciences biologiques, Université du Québec à Montréal
[3]Département de géographie, Université Laval
[4]Département de géomatique appliquée, Université de Sherbrooke
[5]Centre Eau Terre Environnement, Institut National de la Recherche Scientifique (INRS)
[6]Biology Department, Queen's University

November 18, 2022

Abstract

Lake sedimentation rate represents a synthetic metric of ecosystem functioning. Many localized studies have reported a significant association between land use/land cover changes and lake sediment mass accumulation rates, with a few global syntheses echoing these findings at larger scales. In the literature, studies evaluating lead-210 (210Pb) for establishing sediment chronologies will report at least one of three dating models, but the constant rate of supply (C.R.S.) model is the most widely used. However, it is often unclear how or why this model is selected, despite its influence on the interpretation of many subsequent analyses about ecosystem dynamics and functioning. It would thus be advantageous to design an objective and semi-automated way of choosing among dating models. We measured radioisotopic activities in 37 sediment cores across four ecozones of eastern Canada and developed an approach to assess model fit for the three commonly applied dating models. The derived chronologies were then used to evaluate the spatial and temporal variation in sedimentation rates across four ecozones in Canada (covering a surface area of 2.2 x 10^6 km2). We observed a recent increase in lake sedimentation rates across most lakes, as has been observed globally, albeit with significant differences in the magnitude of sedimentation rates across ecozones. Across all lakes, we found that regional human population counts and mean annual air temperatures were significant temporal predictors of variation in mass accumulation rates. Overall, this analytical framework offers an objective approach for assessing fit and selecting among sediment age models, which contributes to a more robust quantification of sedimentation rates. With this first application, we provide a quantitative assessment of how lake sedimentation rates vary across a northern lake-rich region and have responded to environmental change.

A framework for ^{210}Pb model selection and its application to 37 cores from Eastern Canada to identify the dynamics and drivers of lake sedimentation rates

Alexandre Baud[1,2,3], Candice Aulard[3,4], Hamid Ghanbari[3,5], Maxime Fradette[6], Dermot Antoniades[3,5], Paul del Giorgio[3,4], Yannick Huot[3,5], Pierre Francus[2,7], John Smol[8] and Irene Gregory-Eaves[1,3]

[1]Biology Department, McGill University, Montréal, Québec, H3A 1B1, Canada

[2]Centre Eau Terre Environnement, Institut National de la Recherche Scientifique (INRS), Québec City, Québec, G1K 9A9, Canada

[3]Group for Interuniversity Research in Limnology and Aquatic Environments (GRIL);

[4]Département des sciences biologiques, Université du Québec à Montréal, Montréal, Québec, H2X 3X8, Canada

[5]Département de géographie, Université Laval, Québec City, Québec G1V 0A6, Canada

[6]Département de géomatique appliquée, Université de Sherbrooke, Sherbrooke, Québec, J1K 2R1

[7]GEOTOP, Geochemistry and Geodynamics Research Centre, Université du Québec à Montréal, Montréal, Québec H3C 3P8, Canada

[8]Biology Department, Queen's University, Kingston, Ontario, K7L 3N6, Canada

Corresponding author:

Alexandre Baud,

Biology Department, McGill University,

Montréal, Québec, H3A 1B1, Canada

Telephone: +1 (514) 398 4119

Email: alexandre.baud@mail.mcgill.ca

Abstract

Lake sedimentation rate represents a synthetic metric of ecosystem functioning. Many localized studies have reported a significant association between land use/land cover changes and lake sediment mass accumulation rates, with a few global syntheses echoing these findings at larger scales. In the literature, studies evaluating lead-210 (^{210}Pb) for establishing sediment chronologies will report at least one of three dating models, but the constant rate of supply (C.R.S.) model is the most widely used. However, it is often unclear how or why this model is selected, despite its influence on the interpretation of many subsequent analyses about ecosystem dynamics and functioning. It would thus be advantageous to design an objective and semi-automated way of choosing among dating models. We measured radioisotopic activities in 37 sediment cores across four ecozones of eastern Canada and developed an approach to assess model fit for the three commonly applied dating models. The derived chronologies were then used to evaluate the spatial and temporal variation in sedimentation rates across four ecozones in Canada (covering a surface area of 2.2×10^6 km^2). We observed a recent increase in lake sedimentation rates across most lakes, as has been observed globally, albeit with significant differences in the magnitude of sedimentation rates across ecozones. Across all lakes, we found that regional human population counts and mean annual air temperatures were significant temporal predictors of variation in mass accumulation rates. Overall, this analytical framework offers an objective approach for assessing fit and selecting among sediment age models, which contributes to a more robust quantification of sedimentation rates. With this first application, we provide a quantitative assessment of how lake sedimentation rates vary across a northern lake-rich region and have responded to environmental change.

Keywords: Radiochronology, ^{210}Pb, Dating Models, C.R.S., C.I.C., C.F.C.S., Paleolimnology, Sedimentation Rates, Land-use

Introduction

Lakes are critical ecosystems, acting as hotspots of biogeochemical cycling and biodiversity (Schallenberg et al., 2013). Using proxies of past conditions preserved in lake sediments, paleolimnologists can reconstruct shifts in lake ecosystem properties and of their surrounding watersheds, on scales spanning decades to millennia (Last et al., 2003; Korosi et al., 2013). While paleolimnology can provide insights and context for local and regional environmental changes over extended timescales, the study of lake sediment cores also provides key insights into ecosystem functioning (Millet et al., 2010; Winegardner et al., 2017). In particular lake sediment mass accumulation rates (MAR) are reflective of both the export of materials from the watershed and of material processing and burial within lakes, and in turn strongly influence the biogeochemical functioning of lakes. Several authors have recently evaluated the temporal change in lake sedimentation regimes and the factors controlling them across large regions. For example, sedimentation rates have increased globally during the mid to late Holocene, coincident with forest clearance and the onset of European-style agriculture (Jenny et al., 2016). Considering a more recent time frame, Baud et al. (2021) found global

sedimentation rates to have increased 3- to 4-fold since ca. 1850 CE, associated with further expansion of agriculture and urbanization.

The development of reliable sediment chronologies is critical to establishing sedimentation rates, which in absence of annual laminae (i.e., varves) are most often derived through the quantification and analysis of naturally occurring radioisotopes, such as radioisotopic lead (^{210}Pb) for recent sediments. ^{210}Pb has a half-life of 22.23 years (DDEP, 2010), and thus is an obvious candidate for the chronological dating of recent sediments. While the account of the lead radioisotopic decay series has been described elsewhere (Goldberg, 1963; Krishnaswami, 1978; Appleby and Oldfield, 1983), it is important to note that radioactive lead is part of the natural decay series of uranium. ^{210}Pb activities in sediment records originate from two components: 1) a supported ^{210}Pb component, derived from the in situ radioactive decay series of uranium-238 (^{238}U) in soils and from the transfer of radon-222 (^{222}Rn) via surface run-off or groundwater contribution; and 2) an unsupported ^{210}Pb fraction, derived from ^{222}Rn that first diffuses from the Earth's surface into the atmosphere and subsequently decays into ^{210}Pb (Ghaleb, 2009) (Figure 1). This unsupported ^{210}Pb component is expected to follow a first order-decay rate while the supported ^{210}Pb component is expected to have a constant, near-zero activity. The supported ^{210}Pb fraction is often measured via gamma spectroscopy by quantifying the activity of short-lived daughter products of radium-226 (^{226}Ra) such as lead-214 (^{214}Pb) or bismuth-214 (^{214}Bi) (Martz et al., 1991). With gamma spectroscopy, additional radioisotopes independent of the ^{210}Pb decay series are routinely measured, providing validation for ^{210}Pb dating methods. These radioisotopes include cesium-137 (^{137}Cs) and americium-214 (^{241}Am), both of which are associated with radioactive fallout. Cesium-137 is expected to begin rising in the sedimentary record around 1950, when the first nuclear weapons tests were initiated, and reach peak activities ca. 1963 CE (Pennington et al., 1976), the year of maximum atmospheric nuclear testing (Wright et al., 1999). Likewise, ^{241}Am has been reported to reach maximum abundance around 1963 (Appleby et al., 1991). The meltdown of the Chernobyl reactors (1986 CE) created a second peak in ^{137}Cs, mainly over northern Europe.

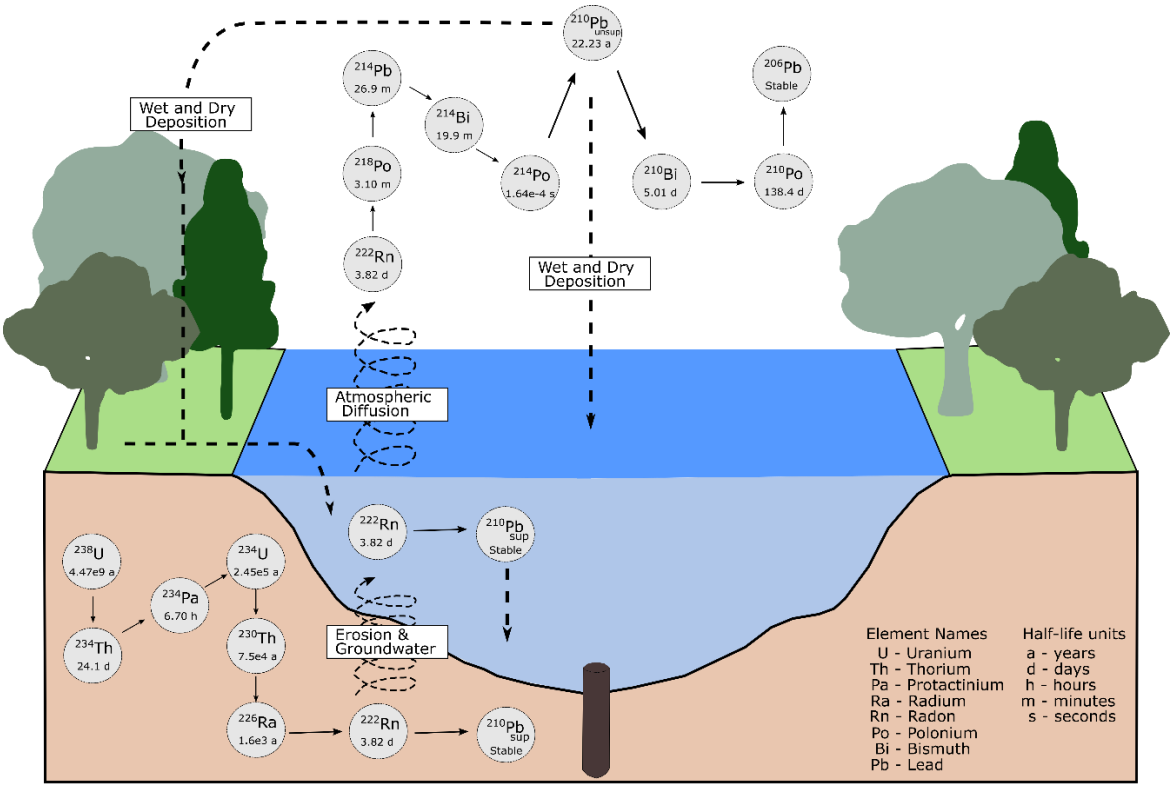

Figure 1. The ^{238}U (uranium) decay series accounting for the deposition of supported ^{210}Pb and unsupported ^{210}Pb into lake sediments via wet and dry deposition on the landscape. Solid lines represent the radionuclide transitions while curved dashed lines account for the transfer of ^{222}Rn from the lithosphere into lakes via erosion and from lakes into the atmosphere via diffusion.

Stemming from the behavior of the measured ^{210}Pb activity in sediment cores, different dating models have emerged, each with different assumptions and applications. There are three main models: the Constant Flux Constant Sedimentation model (C.F.C.S.); the Constant Initial Concentration model (C.I.C.); and the Constant Rate of Supply model (C.R.S.). All three models have a central assumption of an unmixed temporal structure of the sediment core where the ^{210}Pb incorporated within it follows its natural accumulated order and is not affected by any subsequent redistribution processes. However, the three models differ in the fraction of ^{210}Pb investigated and its expected decay function, thereby yielding divergent age models (Table 1). The choice of model therefore has implications for the estimates of the age of individual sediment layers, but perhaps more importantly, may greatly influence not only the sediment mass accumulation rates that are derived from these modeled ages, but also any assessment of potential changes in these accumulation rates that may have occurred over past decades, the latter being a fundamental and yet unresolved issue in contemporary limnology.

When confronted with the outputs from the three dating models for any one sediment core, selecting the model that best reflects the core chronology is not a straightforward procedure. An in-depth evaluation of the sediment properties and possible changes in the sediment stratigraphy, the lake and its watershed and airshed as well as a clear account of historical events (human settlement, known flood

events) are often necessary to gain full confidence in the derived chronology. This knowledge, which is also clearly useful for more than just developing a chronology, can be difficult to obtain, especially when considering large numbers of lakes or sites in remote regions. When dealing with model selection, previous regional coring efforts have used independent markers to validate the derived ^{210}Pb-based chronology, including other radioisotopes (e.g., ^{137}Cs and ^{241}Am), modern contaminants, forest fires or pollen markers indicative of recent settlement activities (e.g., the *Ambrosia* rise in eastern North America) (Blais et al., 1995; Smol, 2008).

Most commonly, only peak activities of ^{137}Cs and (more rarely) ^{241}Am are considered when evaluating ^{210}Pb-based chronologies. Given that gamma spectroscopy measures these radioisotopes at the same time as ^{210}Pb activities, many investigators have easy access to these data. Most studies publishing ^{210}Pb profiles measured from gamma spectroscopy will report the use of ^{137}Cs (Turner and Delorme, 1996). However, several papers have emerged over the past few decades highlighting the potential for post-depositional mobility of ^{137}Cs (Davis et al., 1984; Klaminder et al., 2012). Unfortunately, other independent measures can require extensive laboratory processing, or are simply not possible due to shortages of sediment material.

Based on several large, regional paleolimnological studies, a few key observations regarding sediment dating have emerged. For example, in a study of ~30 North American lakes, Binford et al. (1993) compared chronologies derived from the C.I.C. and C.R.S. models with multiple independent markers (^{137}Cs, fly ash, and the *Ambrosia* rise were analyzed in cores from Florida, New-England Adirondack Mountains and Minnesota). While the authors reported having considered both dating models, they later state that they relied exclusively on C.R.S.-derived ages. This choice was mainly motivated by the fact that previous studies had reported variable sedimentation rates and dilution of the ^{210}Pb in surficial sediment by higher sediment accumulation rates (Binford and Brenner 1986). In another study of 22 lake sediment cores from the Canadian Prairies, Turner and Delorme (1996) also considered multiple dating models and generally observed a good agreement (in over 50% of the cores) between the dates derived from C.I.C and C.R.S. models. Having validated their chronologies using ragweed (*Ambrosia*) pollen, the authors also noted that, in some instances, the close agreement in core chronologies between models only held true for the upper most (recent) section of the sediment cores, beyond which the C.R.S. model started to assign much older dates as a function of small increases in core depth. This account of age over-estimation of the C.R.S. model in deeper sediments was also noted in more recent work (Bruel and Sabatier, 2020). It is thus recommended to be careful or to avoid extrapolating C.R.S. age models beyond the point where the ^{210}Pb inventory has reached background activity. As reported from a global synthesis of published sediment chronologies from the *Journal of Paleolimnology*, the C.R.S. model was the most popular dating model, being reported in over 75% of the studies establishing recent sediment radiochronology (Baud et al., 2021).

In this study, we have explicitly applied and compared the three dating models to radioisotopic sediment profiles for 37 lakes spanning four ecozones of eastern Canada to develop a robust and consistent framework for the selection of lake sediment age models. We then applied the resulting framework to estimate mass sedimentation rates for these lakes, to assess both cross lake patterns in sedimentation and potential temporal shifts in these rates. Given the substantial differences in land use, vegetation and climate across these ecozones, we expected both differences in mean mass sedimentation rates as well as variation in recent sediment mass accumulation rates among ecozones. Furthermore, given that human population and land use have emerged as significant predictors of

sedimentation rates in a global database (Baud et al., 2021), we tested the hypothesis that catchment-scale human population would be a significant predictor of sedimentation rates across time and among lakes in our four Canadian ecozones.

Methodology and Methods

Core collection and shipment

A total of 37 sediment cores was collected from lakes across four ecozones of Eastern Canada as part of the NSERC LakePulse network. Virtually all lakes greater than 0.1km^2 and within 1km of a road were considered for selection by the modified stratified design whereby an equal number of lakes would be sampled across different ecozones (CCEA Canada Ecozones V5b, 2014) as well as lake area and human impact classes (Huot et al., 2019). Ecozones are defined as regional delineations of shared geological, climatic and ecological characteristics (Ecological Stratification Working Group, 1996). Logistical considerations meant that full cores were collected once a week, on the day before sample shipment, and thus slightly altered the original stratified design. Sediment cores were retrieved using the NLA Gravity corer (built by Aquatic Research Instruments) from the deepest point of the lake detected, or from the deepest point of one of the lake's sedimentary basins. On the same day as core collection, sodium polyacrylate was slowly added to a small volume of overlying water within the core tube to stabilize the water-sediment interface for shipping (Tomkins et al., 2008). The addition was done in increments (e.g., adding and waiting for stabilization) to limit porewater absorption. Once the sodium polyacrylate had formed a gel, the sediment cores were stored in a cooler at 4°C until shipping (usually within 24 hrs). Additional cores were also collected on the same day and extruded in the field for surface and pre-industrial sediment layers (Top-Bottom), and ^{210}Pb activities from these secondary cores were compared to the full cores. Full sediment cores were shipped on freezer packs to Laval University. Shortly after arrival, these sediment cores were split longitudinally for core scanning. One of the sediment core halves was kept as an archive while the other, "working half" was subsequently subsampled at 1 cm intervals and placed in Whirl-pak sampling bags that were kept frozen until freeze drying.

Gamma Spectroscopy

For each of the 37 full sediment cores, ~15 discrete sediment intervals along the depth of each core were prepared for gamma spectroscopy and analyzed at the Paleoecological Environmental Assessment and Research Laboratory (PEARL) at Queen's University, Canada. Briefly, sediment intervals were freeze-dried, placed into gamma tubes to a height of about 2.5 cm and sealed using 2-ton epoxy over a silicone septum and left to reach equilibrium for three weeks. An Ortec® high purity Germanium gamma spectrometer (Oak Ridge, TN, USA) was then used to measure the gamma activity of the radioisotopes ^{210}Pb, ^{214}Pb, ^{214}Bi and ^{137}Cs. The chronologies for these cores were derived from the measured radioisotopic activity using ScienTissiME 2.1.4 software (Apr 2017) for the three dating models described above.

Overview of the Three Dating Models (C.F.C.S., C.I.C., C.R.S.)

The *simplest* model of the three is the C.F.C.S. model. It assumes a constant sedimentation rate throughout the entire sediment sequence, such that the activity of unsupported ^{210}Pb is expected to decay as a function of the cumulative dry mass of sediment in a core (Crozaz et al., 1964; Koide et al., 1972). Dates for sediment intervals are derived graphically from the slope of the log-transformed unsupported ^{210}Pb against cumulative dry mass (Sanchez-Cabeza and Ruiz-Fernandez, 2009). This dating model is described as the most appropriate for lakes where erosive processes in the catchment have been steady and in-lake productivity has been constant (Appleby and Oldfield, 1983), as exemplified by many remote and large Alaskan lakes (Rogers et al., 2013).

The C.I.C. model assumes a 1st order decay of the unsupported ^{210}Pb activity. However, the C.I.C. model relies on the assumption that there will be a constant activity of unsupported ^{210}Pb in each sediment layer as it is formed. This model allows for variation in sedimentation rates but assumes that increases in the flux of sedimentary particles from the water column will proportionally increase the ^{210}Pb deposited to the sediment floor, thus yielding constant initial unsupported ^{210}Pb activities irrespective of any variations in sediment accumulation rate (Appleby and Oldfield, 1983).

Finally, the C.R.S. model also assumes a 1st order decay rate but is based on the decay of the total cumulative unsupported ^{210}Pb activity, also known as the total ^{210}Pb inventory (A_0). A_0 is the cumulative, density-corrected unsupported ^{210}Pb measured across sediment intervals (Sanchez-Cabeza and Ruiz-Fernandez, 2009). In this model, the underlying hypothesis is that there is a constant fallout of ^{210}Pb from the atmosphere, yielding a constant rate of supply of unsupported ^{210}Pb to the sediment surface (Appleby and Oldfield, 1983). However, across different layers, the unsupported ^{210}Pb of the initial activity (at time zero) will be inversely proportional to the mass accumulation rate, such that increases in sediment erosion or autochthonous production could result in a dilution of unsupported ^{210}Pb.

Table 1. Summary of dating models highlighting the key assumption and equations across each of the three main dating models. See symbols and abbreviation table.

Model	Assumption	Equations
Constant Flux Constant Sedimentation model (C.F.C.S.)	• Assumes a constant sedimentation rate along the entire core • Activity of unsupported ^{210}Pb is expected to decay as a function of the cumulative dry mass of the sediment in the core	Log-C_{t_x} = Log-C_0 $e^{-\lambda \frac{m}{MAR}}$ $MAR_{CFCS} = \frac{-\lambda}{b}$
Constant Initial Concentration model (C.I.C.)	• Assumes a constant activity of unsupported ^{210}Pb in each sediment layer as it is formed • Increases in the flux of sedimentary particles from the water column will proportionally increase amounts of unsupported ^{210}Pb deposited to the sediment floor	$C_{t_x} = C_0 e^{-\lambda t_x}$ $MAR_{CIC} = \frac{m_j - m_i}{\Delta t}$
Constant Rate of Supply model (C.R.S.)	• Assumes a constant fallout of ^{210}Pb from the atmosphere, yielding a constant rate of supply of unsupported ^{210}Pb to the sediment surface • Unsupported ^{210}Pb of the initial activity (at time zero) will be inversely proportional to the mass accumulation rate, such that increases in burial driven by sediment erosion or autochthonous production results in dilution of unsupported ^{210}Pb	$A_{t_x} = A_0 e^{-\lambda t_x}$ $MAR_{CRS} = \lambda \times \frac{A_{t_x}}{C_{t_x}}$

Symbols used in tables: $\boldsymbol{\lambda}$, ^{210}Pb disintegration constant (λ = 0.03114 year^{-1}); $\boldsymbol{m}$, Cumulative dry mass of sediment (g); $\boldsymbol{MAR}$, Sediment mass accumulation rate (g cm^{-2} year^{-1}); $\mathbf{b}$, Slope of log-transformed C_{t_x} with cumulated dry mass ($\frac{1}{g\ cm^{-2}}$); $\boldsymbol{C_{t_x}}$, Unsupported ^{210}Pb activity at time t_x (Bq kg^{-1}); $\boldsymbol{t_x}$, Time x (year); $\boldsymbol{\Delta t}$, Elapsed time between the deposition of two intervals (Δt=t_i-t_j , years); $\boldsymbol{A_{t_x}}$, ^{210}Pb$_{unsupp.}$ accumulated below interval corresponding to time t_x (Bq m^{-2});

Dating Model Selection

To evaluate the performance of the different dating models generated by the ScienTissiME software (http://www.scientissime.net/), we plotted for each lake the pattern of the unsupported ^{210}Pb (^{210}Pb$_{Unsupp.}$) content measured throughout the cores as a function of the expected decaying trends across each model as detailed in Appleby and Oldfield (1983).

For the C.F.C.S. model, the log-transformed unsupported ^{210}Pb$_{Unsupp.}$ was plotted against the cumulative dry mass of sediment. As described in Appleby et al. (1983), for the C.F.C.S. model to be considered valid, log-^{210}Pb$_{Unsupp.}$ must follow a linear relationship with cumulative dry mass.

$$\text{Log-}C_{t_x} = \text{Log-}C_0\, e^{-\lambda \frac{m}{MAR}} \quad \text{(Equation 1)}$$

Where $log\text{-}C_{t_x}$ is the log-transformed activity of $^{210}Pb_{Unsupp.}$ (Bq kg^{-1}), $log\text{-}C_0$ the initial log-transformed activity of $^{210}Pb_{Unsupp.}$, λ the ^{210}Pb disintegration constant (λ = 0.03114 year^{-1}); m the cumulative dry mass of the sediment core (g) and MAR the sediment mass accumulation rate (g cm^{-2} year^{-1}).

To evaluate performance of the C.I.C. model, we modeled the expected decay of the measured $^{210}Pb_{Unsupp.}$ activity as a function of cumulative dry mass. To allow for the 1st order reaction to reach "background" activity (= where the unsupported ^{210}Pb level reaches the supported ^{210}Pb activity; ~1900 CE) at the observed cumulative dry mass, we incorporated the measured cumulative dry mass where background is reached (m_{bdg}) as the denominator of the decaying-section of the equation (= exponent denominator) and replaced $\lambda * t_x$ by the ratio of age-background (t_{bgd} = 1900 CE) and ^{210}Pb half-life ($t_{1/2}$=22.23 years).

$$C_{t_x} = C_0 e^{-\lambda t_x} = C_0 e^{-\frac{\frac{t_{bgd}}{t_{1/2}}}{m_{bgd}} \cdot g\ cm^{-2}\ yr^{-1}} \quad \text{(Equation 2)}$$

The expected decay rate associated with validation of the C.R.S. models followed a similar methodology as for the C.I.C. expected decay profile, but further considered the 1st-order decay rate of the ^{210}Pb inventory, which evaluates the density-corrected cumulative content of $^{210}Pb_{Unsupp.}$: A_0 (Bq m^{-2}). Similar to what has been previously described, the ^{210}Pb inventory was modeled to decay as a function of cumulative dry mass where ^{210}Pb inventory reaches background supported ^{210}Pb.

$$A_{t_x} = A_0 e^{-\lambda t_x} = A_0 e^{-\frac{\frac{t_{bgd}}{t_{\frac{1}{2}}}}{m_{bgd}} \cdot g\ cm^{-2}\ yr^{-1}} \quad \text{(Equation 3)}$$

To compare models and select the most robust among them, we evaluated the fit (R^2) between observed ^{210}Pb content and predicted ^{210}Pb quantities derived from the expected decaying trends. To remove the scale impact in relation to the different ^{210}Pb quantities evaluated (log-$^{210}Pb_{Unsupp.}$ for C.F.C.S., $^{210}Pb_{Unsupp.}$ for C.I.C. and ^{210}Pb Inventory for C.R.S.), we Z-transformed the observed and the predicted ^{210}Pb quantities and calculated the resulting *Z-scaled* Root Mean Squared Error (Z-RMSE). The model returning the greatest R^2 and the lowest Z-RMSE values was then selected. A summary of the steps taken towards model selection is available in the supplementary materials (Fig S1). Chronologies from selected dating models yielding non-increasing age-depth relationships were rejected, and instead were selected chronologies from the dating model returning the second highest R^2 and second lowest Z-scaled RMSE. Lake sediment cores displaying both a uniform $^{210}Pb_{Total}$ distribution along core depth and the lack of a distinct ^{137}Cs peak should also qualify for rejection because of concerns over potential

mixing and/ or re-distribution of $^{210}Pb_{Total}$, thereby violating dating model assumptions. In general, a thorough investigation of the resulting mass accumulation rates should be performed, leading to the potential rejection of the chronology when anomalous MAR estimates have been identified.

General errors and chronological uncertainty

Analytical errors linked with gamma detection of the naturally occurring radioisotopes were reported following the equation provided in Sanchez-Cabeza and Ruiz-Fernandez (2012). This error was propagated to the calculation of age estimates using empirical equations as it is generated in ScienTissiME 2.1.4. Another error in establishing core chronologies using ^{210}Pb is if the uppermost unconsolidated section is not retrieved by the coring device (Crusius and Anderson, 1991) or was potentially influenced by the sodium polyacrylate addition. To evaluate these processes, we compared ^{210}Pb unsupported activities from the first subsampled interval of our full sediment cores (0-1 cm) to the *Top* (0-1 cm) sample collected from the additional sediment cores (Top-Bottom) retrieved the same day and extruded in the field. This comparison yielded a robust correlation coefficient (R^2 = 0.64) indicative that the ^{210}Pb activities in the top intervals of the full sediment cores were similar between cores. Due to the large-scale nature of the sampling protocol the full sediment cores were sub-sectioned horizontally every cm in the lab. This coarse subsampling led to a reduction in the number of intervals available for dating model selection in regions of low sedimentation rates, likely reducing the robustness in model selection. For each derived chronology, age estimates were compared to the natural ^{137}Cs maximum abundance found within each sediment core, but with full knowledge that the ^{137}Cs peak may be mobile within the sediment column (see Metadata). To compensate for the coarse subsampling resolution when investigating naturally occurring ^{137}Cs maximum in sediment stratigraphies, we used a spline interpolation to model the raw abundance of ^{137}Cs across sediment intervals. A graphical representation of each radioisotope profile was made against the expected decay profile across each model, and the fit between expected ^{210}Pb, generated from empirical equations, and observed ^{210}Pb activity measured across intervals was compared by linear regression (Figure 2).

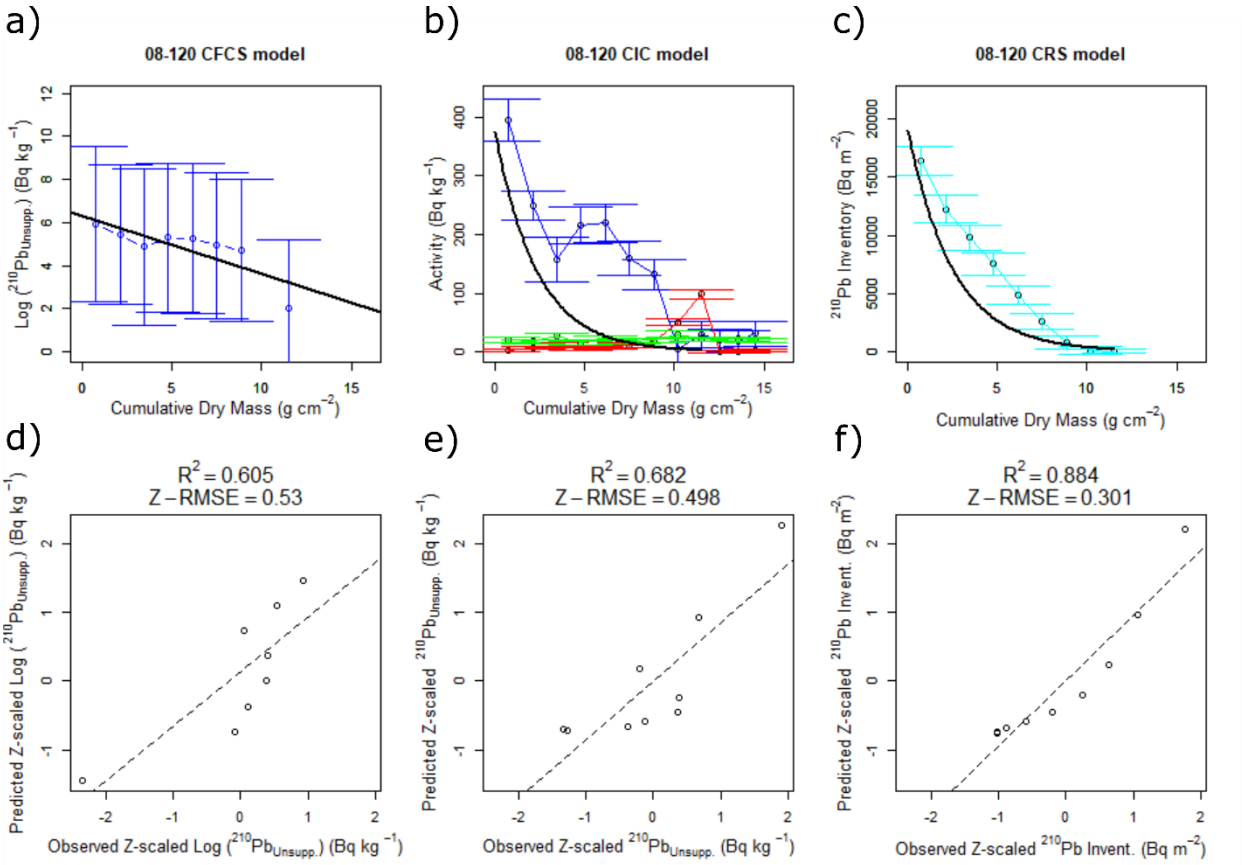

Figure 2. Multi-panel plot summarizing the empirical ^{210}Pb dating model fitting (detailed in Appleby and Oldfield (1983), and evaluation using linear regression for lake 08-120 (Lac des Chicots – Ste Therese, QC). a) Log-transformed $^{210}Pb_{Unsupp}$, with error bars in blue as a function of cumulative dry mass. The black line represents the best linear model fit. b) Graphical representation of the measured ^{210}Pb (Bq kg^{-1}) in blue with corresponding errors as a function of cumulative dry mass. The red line is the ^{137}Cs activities (Bq kg^{-1}) and the ^{214}Bi activities are in green. The black line is the expected decay curve for $^{210}Pb_{Unsupp.}$ c) Graphical representation of the observed ^{210}Pb inventory and corresponding errors in cyan, as a function of cumulative dry mass. The black line is the expected decay curve for ^{210}Pb inventory. d) Linear regression evaluating the fit of the predicted log Z-transformed $^{210}Pb_{Unsupp.}$ activities (Bq kg^{-1}) against observed log Z-transformed $^{210}Pb_{Unsupp}$. e) Linear regression evaluating the fit of the predicted Z-transformed $^{210}Pb_{Unsupp.}$ activities (Bq kg^{-1}) against observed Z-transformed $^{210}Pb_{Unsupp}$. f) Linear regression evaluating the fit of the predicted Z-transformed ^{210}Pb inventory (Bq m^{-2}) against the observed Z-transformed ^{210}Pb inventory. The R^2 of the relationship and the RMSE of the Z-transformed observed and predicted ^{210}Pb quantities for each of the three models appears on top of each graph from d – f.

Sediment Mass Accumulation Rate Calculation

Lake sediment mass accumulation rates were calculated following model-specific equations.

For the C.F.C.S. model, sediment Mass Accumulation Rate (MAR_{CFCS}, g cm^{-2} year^{-1}) was calculated based on the slope of the natural log unsupported ^{210}Pb (Log-C_{tx}) regression as a function of cumulative dry

mass. Following the parametric equation "y = a + bx", *a* equals log-transformed C_0 and *b* ($\frac{1}{g\ cm^{-2}}$) is the slope of the log-transformed Cx relationship with cumulative dry mass. MAR can be derived using the following:

$$MAR_{CFCS} = \frac{-\lambda}{b} \quad \text{(Equation 4)}$$

For the C.I.C. model, sediment mass accumulation rate (MAR_{CIC}, g cm^{-2} year) was calculated from the mass difference between two intervals i and j (m_i and m_j) and the associated elapsed time between the deposition of these two layers ($\Delta t = t_i - t_j$, years)

$$MAR_{CIC} = \frac{m_j - m_i}{\Delta t} \quad \text{(Equation 5)}$$

For the C.R.S. model, sediment mass accumulation rate (MAR_{CRS}, *kg* m^2 *year*$^{-1}$) was calculated for each interval based on the proportion of unsupported ^{210}Pb (C_{t_x}, Bq kg^{-1}) to cumulative ^{210}Pb inventory from the bottom of the core to interval corresponding to time t_x (Bq m^{-2}).

$$MAR_{CRS} = \lambda \times \frac{A_{t_x}}{C_{t_x}} \quad \text{(Equation 6)}$$

MAR_{CRS} is obtained by means of a ratio, and low C_i values can be measured when approaching background supported ^{210}Pb activity; as a result, artificially elevated values in MAR_{CRS} can be detected. For this reason, we removed one estimate of MAR_{CRS} associated with lake 08-179 where the specific MAR_{CRS} was 87 times greater than the rest of MAR_{CRS} for this lake.

Census Population Reconstruction

We delineated the hydrologically conditioned watersheds of the lakes using a 20 m flow direction raster layer acquired from the 0.75 arc second Canadian Digital Elevation Model dataset (Government of Canada, 2015). The delineation uses the union of all sub-drainage basins that reach each point along a lakeshore based on the National Hydro Network lakes polygon data (Government of Canada, 2017). We then acquired Census Subdistrict (CSD) boundary files from 1911 CE to 2016 CE (accessible from: http://geo.scholarsportal.info/) along with the relevant microstatistics table files that feature the total population within each CSD (accessible from: http://odesi2.scholarsportal.info/webview/). In an effort to normalize the geographical data and to overcome issues of the Modifiable Areal Unit Problem (MAUP) (Openshaw, 1983), we used the WordPop UN dataset to redistribute CSD population counts across each CSD. To reduce the error associated with new urban development arising during the 20th century, digitized historical topographic maps were used when available. These historical maps were acquired from national and university libraries (Scholar Geoportal for Ontario, BaNQ for Quebec and from an online repository from the University of Ottawa). These maps were produced from 1909 to 1989 CE at a resolution of 1:63,360 or 1:50,000. These maps were georeferenced using the WGS84 coordinates present on the map. Each "house" on the maps was accounted for by a point feature. We

then compared our redistributed population against the georeferenced point feature layer to ensure our population estimates were adequate.

Temporal Temperature and Precipitation reconstruction

Historical (1841 CE – 2017 CE) monthly records of air temperature and precipitation were obtained from Environment and Climate Change Canada using the rclimateca package (Dunnington, 2018). Only stations with at least a complete year of monthly data were selected to create mean annual temperature and total annual precipitation estimates for each station. Rather than assigning air temperature and precipitation estimates based on the nearest station (which can be hundreds of km away), estimates from stations within 75 km of the study site were spatially interpolated, forming rings of raster values (estimated temperature and precipitation) around the input station. This step ensured that the estimated temperatures for any site were reflective of station input data.

Lake Morphometric and Watershed Land Use, Bedrock Geology and Soil Composition

Basic lake morphometric information was recorded across all lakes featured in this study. Lake maximum depth (m) was estimated as the maximum depth measured by the field teams during sampling with aid of bathymetric maps when available. Lake surface area (km^2) was obtained via Canvec/HydroLakes and altitude (m a.s.l.) calculated from The Canadian Digital Elevation Model (CDEM).

Since the methodology developed for the LakePulse pan-Canadian sampling of lakes involved the classification of lakes according to the relative proportion of natural to more intensive land uses (e.g. Agriculture, Urban, Mines; see Huot et al. (2019) for details) in their watersheds, we explored the influence of each of these land-use types on the variation observed in lake sediment mass accumulation rates. A table summarizing data sources included in Huot et al. (2019) is available in the supplementary materials of this study (Table S1). We simplified the original land use definitions found in *Annual Space-Based Crop Inventory for Canada* (2016) and in *Land Use* (2010) into seven categories (NoData, Water, Natural Landscape, Forestry, Urban, Agriculture, Pasture and Mines). A table summarizing the original class definition and the simplified categories is also available in the electronic supplementary materials (Table S2).

To investigate the role of watershed soil and geological composition on the variation observed in mass accumulation rates, we acquired bedrock geology from the Geological Survey of Canada (1996) and computed the intersection between the watershed polygons and the bedrock geology polygons. With one of the lakes' watersheds spanning outside of Canada into the USA, "NoData" has been assigned for this portion of the watershed. Soil properties maps generated by the International Soil Reference and Information Centre (ISRIC) were retrieved from *soilgrids.org.* From the available soil horizon depths, we selected the 0-5m depth layer and computed for each watershed the mean abundance of all soil property values.

Statistical analyses

All statistical modelling was performed using R (R Core Team, 2013) and all occurrences of log-transformed variables refer to the common (i.e., base 10) logarithms. Specific packages used include *davies.test::segmented* for the analysis of breakpoints in the regression parameter in the linear predictor (Muggeo, 2003). General additive mixed effects models (GAMMs) were fitted using the r package *mgcv* (Wood, 2012). A random factor was assigned to lake identity (LakeID) to structure errors in the model's residuals. In GAMMs, the estimated degree of freedom (e.d.f.) summarizes the degree of non-linearity of the modelled trends, with values of 1 being linear and with any value above 1 reflecting a departure from linearity. To establish the potential significant differences in lake sediment mass accumulation across different timesteps instructed from Davies' test, we first assessed the normality in the paired MAR differences (pre and post breakpoint) for each of the four ecozones using a Shapiro-Wilk test. Since all ecozone specific Shapiro-Wilk tests returned p-values greater than $p = 0.05$, the paired MAR differences were considered to be normally distributed and the significant difference in means was evaluated using a paired t-test. To establish a predictive model of recent mean lake mass accumulation rates, we selected and averaged MAR estimates ranging from 2000 to 2017 (the latter indicative of the year when the cores were retrieved). Using a post-2000 period was mainly motivated by the limited availability of environmental datasets that are necessary to explore the drivers of recent lake MARs. Lake specific recent mean MARs were then used in a multiple linear regression model. For this predictive model, the explanatory variables that were considered included climatic variables (mean annual air temperature (MAT, °C) and total annual precipitation (mm)), watershed land-use variables (fraction of agriculture in the catchment (%), population count (individuals), soil and bedrock geology fractions (%)), watershed size (km^2), and lake morphological variables (lake depth (m), lake surface area (km^2)).

Results

Assessing the Performance of Dating Models

Across the 37 sediment cores considered, the C.R.S. model returned higher R^2 values for 30 lakes when assessing the fit between observed and predicted values of unsupported ^{210}Pb. The C.I.C. model typically had the lowest fit, while the C.F.C.S. equation performed well in only a handful of lakes (Table 2). Considering each of the four ecozones separately, the C.R.S. model always returned the highest R^2 for lakes in the Mixedwood Plains region. In contrast, the C.F.C.S. model was selected as having the best fit in several Boreal Shield sites, although the C.R.S. was still deemed appropriate for most lakes in this ecozone. Lakes set in the two Atlantic ecozones (Atlantic Highlands and Atlantic Maritime) also predominantly followed the C.R.S. exponential decay of ^{210}Pb inventory quantities (Table 2). While the C.R.S. model generally produced a higher R^2 than the other models, for some lakes the C.F.C.S. model and the C.R.S. model generated similar R^2 values (Table 3, Figure S2). Lakes with higher proportions of urban land cover in their watersheds tended to display a greater R^2 difference between C.F.C.S. and C.R.S. models. While the agriculture fraction within watersheds was also tested, it was not a significant predictor of this difference. There was no clear spatial distribution signal in the selected chronological model (Figure 3).

Table 2. Distribution of the selected dating model percentage across the four Eastern Canadian ecozones. Lakes sample size across ecozone is indicated between parentheses.

Ecozone	C.F.C.S.	C.I.C.	C.R.S.
Atlantic Highlands (11)	9%	9%*	82%
Atlantic Maritime (7)	14%	0%	86%
Boreal Shield (10)	30%	0%	70%
Mixedwood Plains (8)	0%	0%	100%

*Despite the C.I.C. model being selected for one of the lakes (17-067) in the Atlantic Highlands, dates for this core could not be derived using the C.I.C. equation as it generated non-decreasing age with depth (see metadata). For core 17-067, we thus generated dates using the C.R.S. model which returned similar R^2 to that of the C.I.C. model (see Figure S2).

Table 3. Summary of the linear model R^2 for the three dating models tested (n=111). The *Estimate* parameter accounts for the mean R^2 value obtained across all 37 lakes.

Dating Model	Mean R^2	Standard Error of R^2	p-value
C.F.C.S.	0.788	0.035	< 0.001
C.I.C.	0.667	0.039	0.002
C.R.S.	0.944	0.039	< 0.001

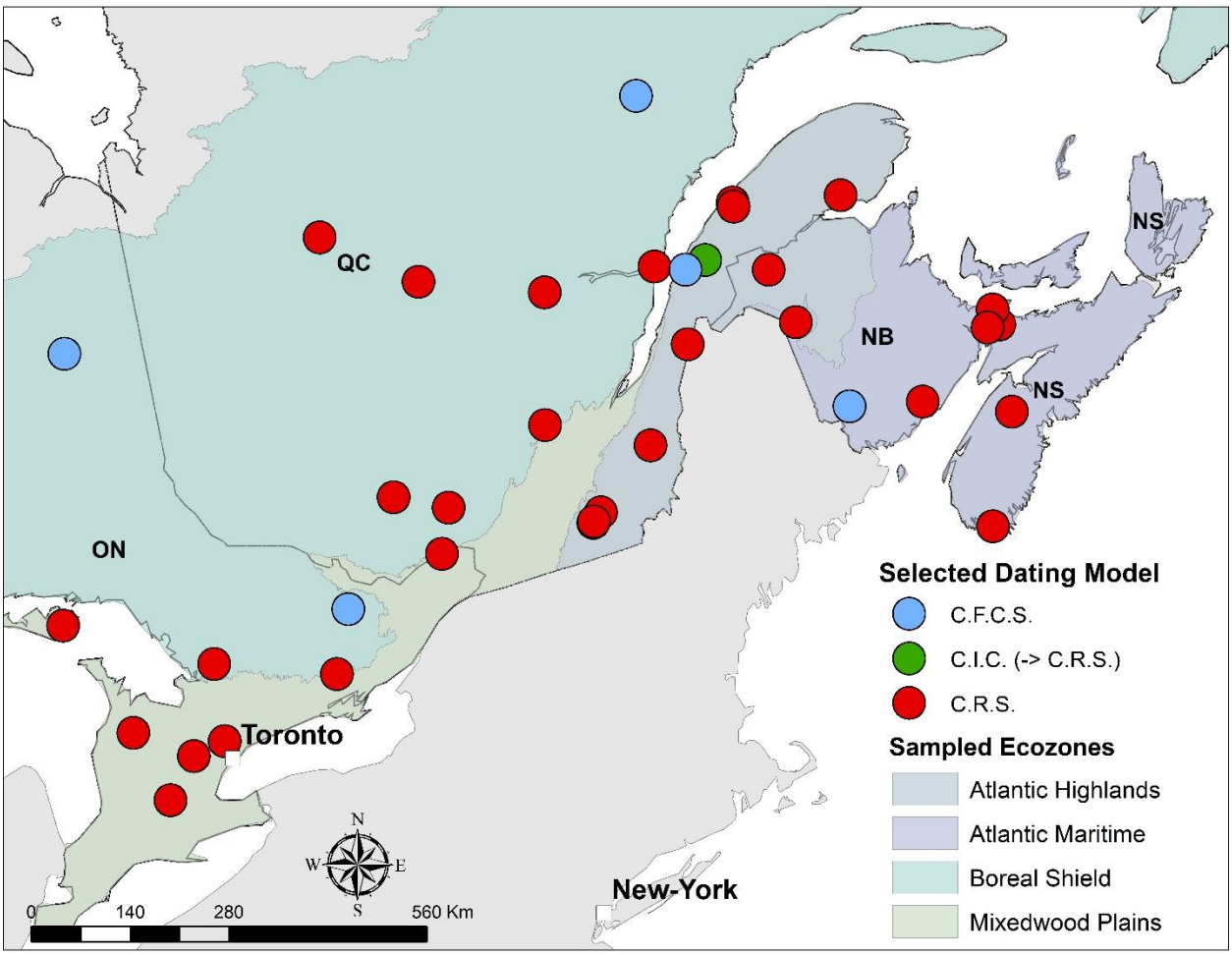

Figure 3. Map showing the distribution of the selected dating models across the four sampled Eastern Canadian ecozones.

Temporal variation in sediment mass accumulation rates

Using the selected dating model identified for each ecozone, we considered region-specific change in lake MARs. While pre-industrial (pre-1900) lake sediment MARs exhibited similar values across all four ecozones, with estimates ranging from 6.3×10^{-3} to 1.5×10^{-2} g cm^{-2} year^{-1}, there was a marked difference across ecozones, with lakes in the Mixedwood Plains (M.P.) accumulating a greater amount of sediment than lakes in the other 3 ecozones (Figure 4a). One lake set in the Boreal Shield (B.S.) had highly elevated MAR estimates compared to other lakes in this ecozone. This site is located in the floodplain of Lac St-Jean (QC), and the ^{210}Pb profile suggested numerous rapid-deposit events (see Metadata). Given that this lake (Lac à la Croix, 06-103) was not representative of its region's sedimentation rate patterns, it was removed from the dataset for any further analysis. Region-specific

modelled trends provided evidence of non-linear variation in MARs across three of the four ecozones evaluated, with GAM-estimated degree of freedom (e.d.f.) values ranging from 1.12 - 1.49 (Figure 4b). The Atlantic Maritime (A.M.) and Atlantic Highlands (A.H.) as well as the Mixedwood Plains displayed nearly constant rates of sedimentation prior to the 1940s. Between 1947 and 1956, rates of sedimentation accelerated across these three ecozones (supported by the Davies test results, Figure 4b). In the case of the Boreal Shield, the GAM did not detect any support for nonlinear temporal variation of MAR.

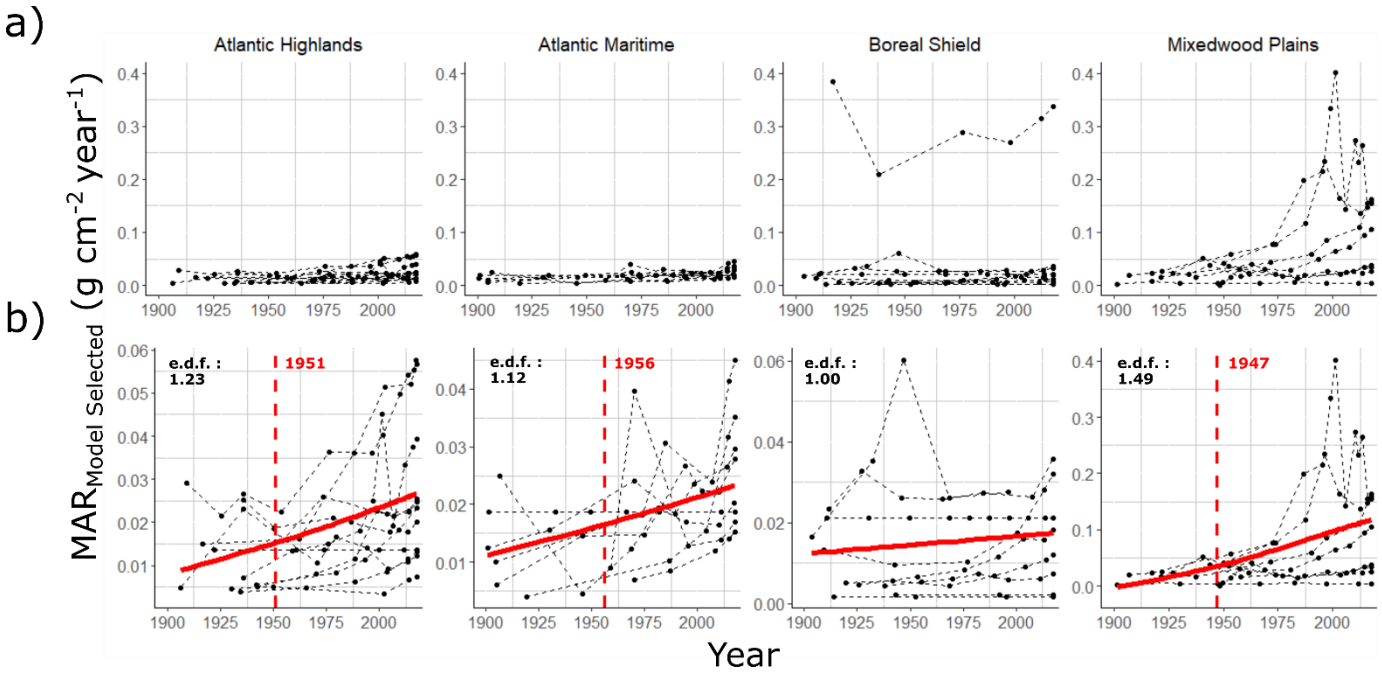

Figure 4. Temporal variation in sediment dry weight mass accumulation rate across the four ecozones of Eastern Canada as determined from dating model selection. a) The upper panels display the raw measured sedimentation rates across the 37 lakes. b) The lower panels show the general additive model (GAMM) trends of ecozone-specific MAR temporal variation. The estimated degrees of freedom (e.d.f.) associated with the GAMM is also reported, as is the estimated onset of the MAR acceleration across each ecozone based on a breakpoint analysis. Note: One lake (06-103) for the Boreal Shield was identified as having anomalously high MAR and was also found to be a site in a floodplain, and was thus removed from GAMM analyses.

Considering the continuous temporal variation observed for MAR and the marked acceleration in lake MAR as evidenced from the Davies test (Figure 4a and b), we considered a former timestep defined as *pre-1955 CE*, which includes MAR estimates prior to the acceleration recorded across Eastern Canada. A second timestep – post-2000 CE, reflective of the last ~20 years of MAR – was also considered as it is the focus of a subsequent analysis in this study where we evaluate the predictors of recent lake MARs. As described previously, using a post-2000 timestep was partly motivated by the limited

availability of environmental datasets which are necessary to explore the drivers of recent lake MARs. Shapiro-Wilks tests of normality demonstrated the normal distribution of the paired MAR differences in all four ecozones. Paired t-tests for each of the four ecozones evidenced significant differences in lake sediment mass accumulation rates (Figure 5). For both the Atlantic Highlands and Maritimes regions, mean MAR between time steps doubled: A.H. $t(10) = -3.17$, $p = 1.0 \times 10^{-3}$; A.M. $t(5) = -3.30$, $p = 2.1 \times 10^{-2}$. For the Mixedwood Plains, mean MAR quadrupled: $t(7) = -2.42$, $p = 4.6 \times 10^{-2}$. In contrast, the change in mean MAR across the two time periods in the Boreal Shield was more modest, but paired t-tests still detected a significant difference in lake MARs across the two timesteps considered (B.S. $t(8) = -2.72$, $p = 2.6 \times 10^{-2}$).

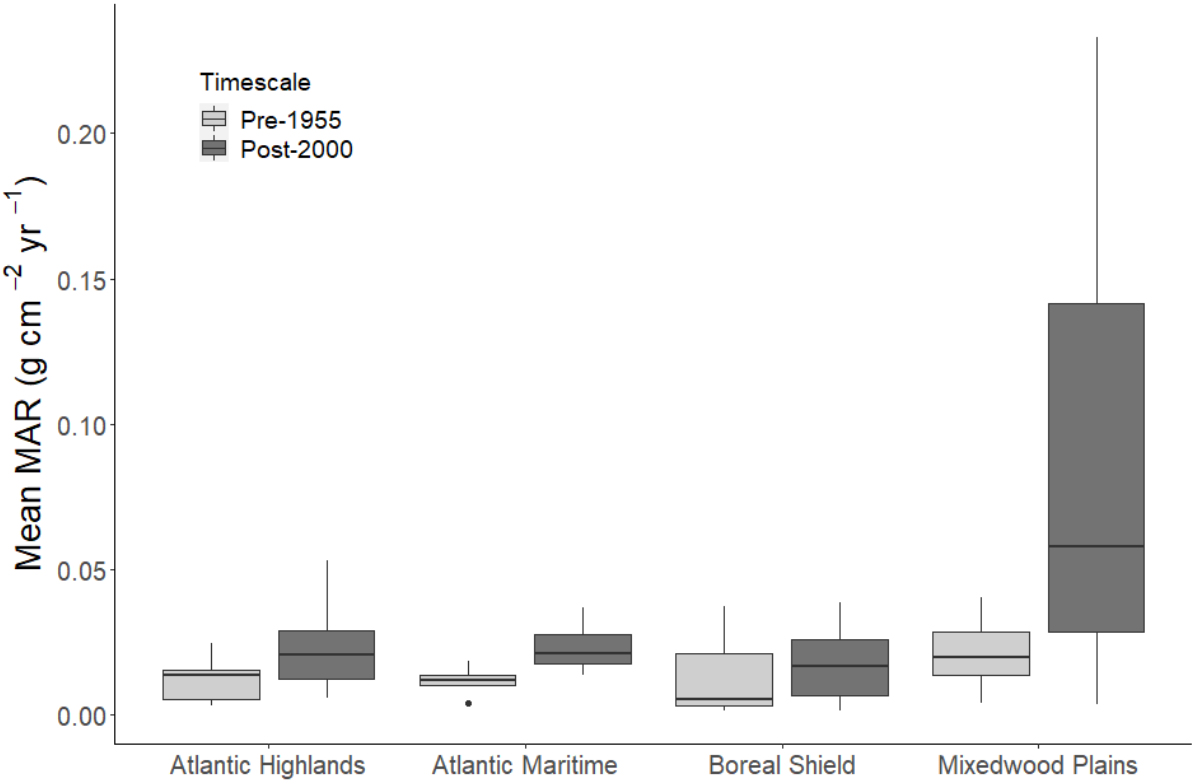

Figure 5. Mean Mass Accumulation Rate (MAR: g cm^{-2} $year^{-1}$) across the four sampled Eastern Canadian ecozones for two timesteps: "Pre-1955" ($n_{MARPre\text{-}1955}$ = 34), "and "Post-2000" ($n_{MARPost\text{-}2000}$ = 36). While pre-1955 includes MAR estimates prior to the acceleration recorded across Eastern Canada, we also considered a post-2000 timestep, reflective of the recent MAR estimates. This timestep was considered as it is the focus of a predictive model assessing the drivers of recent lake MARs. Using this former timestep was also motivated by the limited availability of contemporary environmental datasets which are necessary to explore the drivers of recent lake MARs.

Temporal drivers responsible for increased lake sediment mass accumulation rates

We applied a linear mixed effects model, correlating our estimates of mass accumulation rates year by year with population counts (number of individuals; measured approximately every 5 years), climate estimates (Mean Annual air Temperature (MAT, ºC) and total annual precipitation (mm)) linearly approximated to the same year as the MAR estimate, to evaluate the temporal drivers of variation and the spatial component of the dataset as accounted for by using lakeID as a random effect. We found that mass accumulation rates (log-transformed) were positively related to log(x+1) transformed population count in the watershed (Slope = 0.177 (± 0.046), D.F. = 146, p-value = < 0.001). MAT (ºC) was also found to be positively related to log-transformed lake MAR, but its contribution to the model was smaller than that of population count (Slope = 0.0912 (± 0.046), D.F. = 146, p-value = 0.0515). Overall, our regression model, which considered ~120 years of sedimentation rates for 37 sediment cores, was capable of accounting for 22% of the variation in its fixed effects. We also tested mean total annual precipitation (derived from Environment and Climate Change Canada monitoring stations) as a predictor for temporal variation in MAR, but it was not a significant parameter in the linear mixed effects model. However, LakeID as a random factor explained a large proportion (49%) of the residual variation (Table 4).

Table 4. Summary of the linear mixed effects model assessing the temporal variation in log-transformed Mass Accumulation Rate (MAR) across the 37 cores. t-value refers to the t statistics. LLR refers to the log-likelihood ratio.

Effect	Estimate (Std. Error)	Degree of Freedom	t-value	LLR	p-value
(Marginal R^2 = 0.222,	**Conditional R^2 = 0.696)**				
Intercept	-5.29 (0.30)	146	-17.52		
Log-(Population+1) (numbers of individuals)	0.177 (0.046)	146	3.84	17.17	0.0002
MAT (ºC)	0.0912 (0.046)	146	1.96	3. 85	0.0515
Random effects (Proportion of variance explained by LakeID = 0.710)					
LakeID	0.714 (0.51)			116.12	< .001
Residual	0.571 (0.32)				

Predictive model for recent lake sediment average mass accumulation rates

Through multiple linear regression, we investigated the cross-lake variation in modern mean MAR post-2000 CE (all MAR estimates from a single lake averaged between 2000 – 2017 and expressed $MAR_{2000\text{-}Present}$, g cm^{-2} $year^{-1}$) to identify significant predictors of this variation. Anthropogenic indicators, specifically the fraction of agriculture expressed in percent (p-value = 2.5×10^{-4}) and log-transformed human population count (number of individuals) (p-value = 1.1×10^{-4}) in lakes' watersheds averaged between 2000 and 2016 explained the greatest amount of variation in recent lake sediment mass accumulation rates. Another variable that accounted for a significant portion of the variation was mean total annual precipitation (over the post-2000 CE period; p-value = 2.4×10^{-4}). Altogether these variables accounted for 57% of the variation observed in average recent lake sediment mass accumulation rates (post-2000 CE) (Figure 6). Additional variables, such as the proportion of sand in the lake watershed and log-transformed lake maximum depth, were also found to be weakly significant (p-value < 0.1) but were omitted from the regression equation to prevent over-fitting of the model. The final model is expressed as:

$$\text{Log}(\text{Mean MAR}_{2000\text{-Present}})\ (\text{g cm}^{-2}\ \text{year}^{-1}) = -8.86 + 4.3 \times \text{Mean Agriculture}_{2000\text{-Present}}\ (\%) + 0.22 \times \text{Log}(\text{Population Count}_{2000\text{-Present}} + 1)\ (\text{individuals}) + 0.0036 \times \text{Mean Precipitation}_{2000\text{-Present}}\ (\text{mm})$$

(Equation 6)

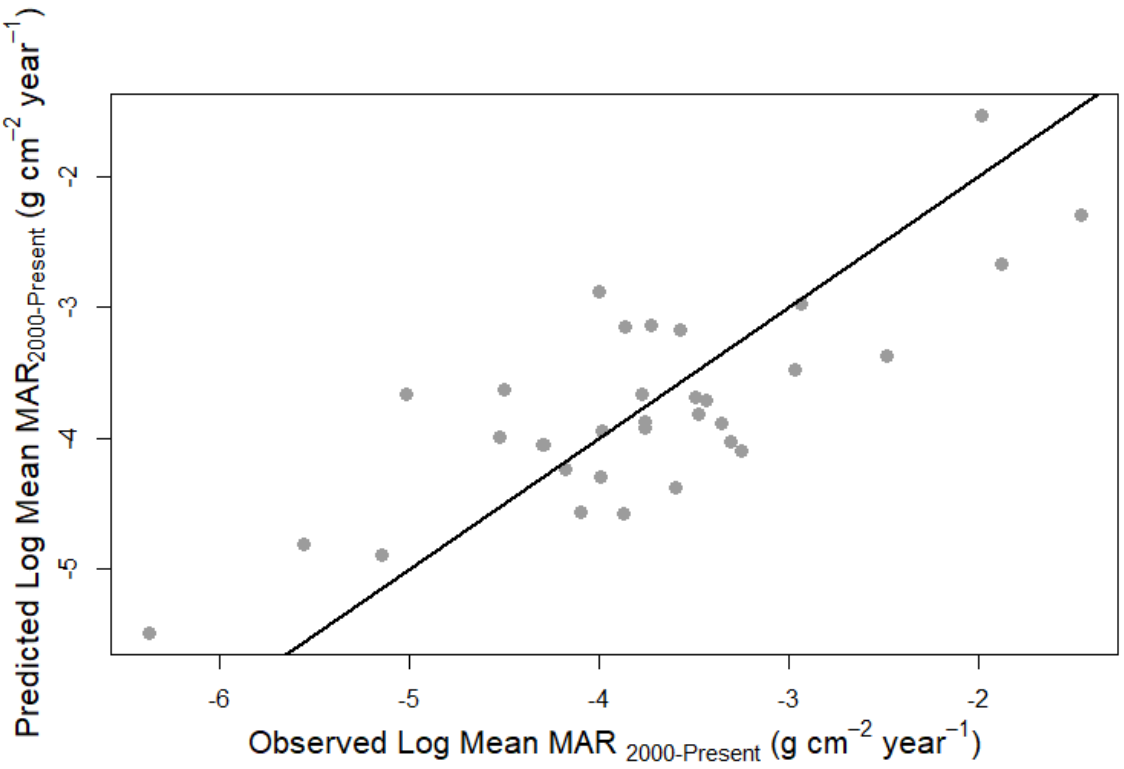

Figure 6. Observed versus predicted log-transformed Mean Mass Accumulation Rate (post-2000 CE, from equation 6).

Discussion

Developing a robust chronology and calculating mass sediment accumulation data are critical steps in most paleolimnological and biogeochemical lake studies. The new insights gained from our inter-regional study of lake core dating and sedimentation rates are methodological and data-driven. On the methodological front, we present a robust empirical framework for evaluating the three most commonly used chronological dating models. Applying this new framework whereby we fit model-specific empirical equations and compared the outcomes statistically to 37 sediment core records from across 4 ecozones, we clearly showed substantial spatio-temporal variation, for which we identified significant predictors.

Earlier work had shown that the C.R.S. model dating results are those most frequently reported in the literature, but it is not always clear why this approach was adopted. The difficulty of dating model selection becomes even greater when the number of sediment cores to be dated increases, or with growing spatial coverage. However, this challenge can now be met with the approach we have described for assessing how closely the measured isotopic activities are in accordance with the specific assumptions of the chronological model. This standardized method of evaluating different chronologies will further facilitate identification of the most reliable chronological dating model where model assumptions are respected. Interestingly, Barsanti et al. (2020) recently conducted an interlaboratory calibration exercise with 14 different laboratories worldwide to evaluate a single lake sediment isotopic profile and no consensus was reached with regard to dating model selection: seven laboratories selected the C.R.S. model, five adopted the C.F.C.S. model, another one chose the C.I.C model, and finally the last group selected a modified version of the C.F.C.S. model. Clearly, there is a need to standardize approaches to model selection.

From a mathematical perspective, there is a greater probability of obtaining a better R^2 value when considering the C.R.S. or the C.F.C.S. model assumption over the C.I.C. model. Specifically, the C.F.C.S. model is based on analyses of log-transformed ^{210}Pb activity, which reduces to some extent the stochastic nature of radioisotopic measurements in sediment and thus one can expect a stronger fit relative to C.I.C. model results. For the C.R.S. model, the analyses are based on the cumulative ^{210}Pb inventories and it is thus less sensitive to inter-sample variation that could be apparent with C.I.C. models. Independent of the dating model, the establishment of a robust chronology also depends on the number of sediment intervals with measurable $^{210}Pb_{unsupp.}$ exceeding equilibrium with $^{210}Pb_{supp.}$. For this reason, it is recommended to adjust sediment core subsampling according to empirical regional sedimentation rates.

The selection of chronological dating models across the 37 sediment cores using our framework was in line with findings from the literature, where the C.R.S. model was selected the most frequently (Dillon et al., 1986; Appleby, 2002). Our observation that the C.R.S. model was the most appropriate for 100% of lakes studied from the Mixedwood Plains suggests that changes in sedimentation rate are common in this region, which is a plausible hypothesis as this ecozone is the most densely populated region of Canada. In the Atlantic Highlands and Atlantic Maritimes, a majority of cores (> 80%) displayed ^{210}Pb

activities best modeled following the C.R.S. model assumptions *and* showed increased sedimentation rates. Increased sedimentation rates were not unexpected, either, given the long history of settlement in the area. By contrast, 30% of the cores from the Boreal Shield had ^{210}Pb activities that matched most strongly with the C.F.C.S. model's assumption (i.e., a consistent a log-linear decay of ^{210}Pb activities with cumulative dry mass). The C.F.C.S. model was designed for lakes where erosive processes in the catchment are steady and in-lake productivity is constant (Appleby and Oldfield, 1983), which aligns with the more pristine and remote lakes settings of many lake-watershed ecosystems in the Boreal Shield. It is also interesting that while only one of the 37 sediment cores followed the C.I.C. model's assumptions, dates generated by this model could not be applied due to non-decreasing age with depth. While Appleby and Oldfield (1992) described an example where the chronological C.R.S. model was invalidated due to discontinuity within the sediment stratigraphy, the lake in our study for which C.I.C. was selected was not one exhibiting the most drastic stratigraphic changes. We thus recommend a careful contextualization of stratigraphical facies with radioisotope profiles (^{210}Pb, ^{137}Cs and ^{241}Am).

One of the challenges with developing an empirical means to estimate chronologies from ^{210}Pb is the establishment of the expected ^{210}Pb decay trend. We must assume the age associated with the sediment cumulative dry mass where unsupported ^{210}Pb activity has reached supported ^{210}Pb activity (= t_{bgd}) (see Equations 2- 3). Depending on lake location, one can often detect 4-5 half-lives before reaching the supported ^{210}Pb activity. However, at high latitudes, where the flux of atmospheric ^{210}Pb can be lower (Baskaran and Naidu, 1995; Tomkins et al. 2009) or at locations where elevated autochthonous production leads to the dilution of unsupported ^{210}Pb in the sediment (Binford and Brenner, 1986; Arias-Ortiz et al., 2018), the number of half-lives detected can decrease on the order of 1-3 half-lives. In our study, the estimated age of background was selected to be 110 years, which corresponds to 5 half-lives. Results of the sensitivity analysis (Fig S3) demonstrated that the model selection we present in this manuscript was consistent across the range of naturally expected values for t_{bgd} (80 – 130 years) and did not elicit any analytical artifacts as can be seen outside of this range.

While we have highlighted the models with the best fit, it should be noted that in many cases the R^2 values were very close across dating models for the same core (Fig S2). In such cases there was an important overlap between dating models, at least for the uppermost section of the cores (see Metadata) prior to C.R.S. model yielding older age estimates for bottom samples. While this phenomenon has been described elsewhere (Turner al., 1995; Bruel and Sabatier, 2020), our results further reinforce the need to cautiously consider these older dates and evaluate different dating models. With only a few lakes not returning C.R.S. as the best dating model, we did not observe striking regional differences when using MAR estimates derived solely from the C.R.S. models (Figure S4).

Mass accumulation rates across ecozones generally matched previous estimates from the literature and varied substantially across lakes within regions and also across ecozones. Set in similar geological environments rich in granite and gneiss, with cool and moist climates, the Atlantic Highlands and Atlantic Maritimes had similar MAR estimates. Greater proportions of sand in these lakes' watersheds were found to negatively influence MAR, and the contemporary anthropogenic development experienced predominantly in the coastal lowland areas of these regions could be at play. The lakes from the Boreal Shield are in a different geological and hydrological region defined by a strong continental climate and Precambrian granitic bedrock and, surprisingly, were not characterized by lower mean mass accumulation rates. Lakes from the Boreal Shield also experienced less development of anthropogenic land use within their watersheds (Huot et al., 2019). In contrast, lakes from the

Mixedwood Plains which are associated with a warmer climate and lie in watersheds with fertile soils, along with more extensive anthropogenic development, accumulated a significantly greater mass of sediment than the three other ecozones. When breaking down the temporal variation into two timeframes (pre-1955 and post-2000 CE), it is apparent that all 37 lakes accumulated comparable amounts of sediment prior to the 20th century. With all four ecozones having similar baseline mass accumulation rates, ranging from ~ 6.3×10^{-3} to 1.5×10^{-2} g cm^{-2} year^{-1}, it is lakes from the Mixedwood Plains that have recorded the largest increases in sediment MAR.

From the ecozone-specific General Additive Models, we can conclude that MAR estimates in the Boreal Shield exhibited a linear temporal increase while the other 3 ecozones displayed non-linear temporal variation in MARs with GAM e.d.f. values ranging from 1.12 to 1.49. Another commonality found across these three ecozones was the timing of the MAR acceleration onset. Lakes in the Mixedwood Plains and Atlantic Highlands ecozones were first to experience MAR acceleration with estimated onset occurring around 1947 and 1949, respectively. Lakes in the Atlantic Highlands closely followed with a recorded MAR onset around 1958. These reported onset MAR values are similar to those identified from global lake sediment assessments. For example, in Baud et al. (2021), an onset of global MAR acceleration was identified around 1941 and was explained by widespread increases in anthropogenic landscape transformations and application of fertilizer. Echoing these findings, our results from the linear mixed effects model detected significant associations between sediment MAR and anthropogenic land-use variables, where percent agriculture and population count in lake watersheds were found to be significant predictors. While climate accounted for some variation in sediment mass accumulation rates when evaluating recent average MAR, it did not account for a significant part of the variation when assessing the temporal variation in MAR. The lack of historical climate data that are distributed in sufficiently close proximity to our sites in Eastern Canada may be part of the problem. Indeed, only a few stations in the Boreal Shield region were available, limiting the scope of the analysis. When considering additional variables, such as the geological characteristics of the watershed or lake morphometric variables (lake area, lake maximum depth), the fraction of sand present in the lake watershed and log-transformed lake maximum depth were only marginally significant (p-value < 0.1).

Conclusion

We generated a framework to examine ^{210}Pb activities to enable dating model selection following a repeatable and quantifiable approach. Using this approach, the C.R.S. dating model was selected as the most robust model for a majority of sites. We identified heterogeneity across ecozones of eastern Canada in terms of the amount of sediment that lakes accumulate. Mixedwood Plains lakes accumulated on average 4 times more sediment than any of the three other ecozones. While all four ecozones of Eastern Canada have recorded temporal increases in lake sediment MAR since 1880 CE, it is the Mixedwood Plains ecozone that recorded the greatest increase with over a 4-fold increase from baseline rates. We conclude that the likely influence of population size in the watershed and increasing temperatures were significant predictors for this MAR temporal variation. We also found that current mean lake sediment MAR can be predicted using anthropogenic land-use variables (population count and percent agriculture) along with precipitation within the watershed. Bridging the analytical model selection and the derived implication for lake sedimentation provides a comprehensive approach for

dealing with sedimentation rate variations, which in turn is critical for the establishment of mass-balance models evaluating sediment constituents such as carbon and heavy metals.

Acknowledgements

This work has been supported by a FRQNT Fellowship and an Excellence award from the Department of Biology at McGill University awarded to AB. In addition, we acknowledge funding from an FRQNT Team grant awarded to IGE, DA, PdG and PF, the NSERC LakePulse network as well as CRC grants awarded to IGE, DA and PF. We'd also like to thank Yohanna Klanten and Julie Nadeau for subsampling the 2017 LakePulse cores, Michelle Gros for processing the core samples and Chris Grooms for running the gamma spectroscopy.

Author Contributions

AB & IGE designed the study. IGE, PF, DA, PdG, JS & YH are responsible for funding acquisition. AB responsible for methodological development. AB, MF & CA were involved in data collection. AB, CA & HG participated in data investigation. All participating authors were also involved in reviewing and editing of the manuscript.

References

Appleby, P. G. and Oldfield, F. (1978). The calculation of lead-210 dates assuming a constant rate of supply of unsupported 210Pb to the sediment. *Catena*, 5(1), 1-8.

Appleby, P. (2002). Chronostratigraphic techniques in recent sediments. In: Last, W. and Smol, J.P. Editors. Tracking environmental change using lake sediments: Vol 1. Basin analysis, coring, and chronological techniques. (pp. 171-203) *Springer*.

Appleby, P. and Oldfield, F. (1983). The assessment of ^{210}Pb data from sites with varying sediment accumulation rates. *Hydrobiologia*, 103(1), 29-35.

Appleby, P., Richardson, N. and Nolan, P. (1991). ^{241}Am dating of lake sediments. *Hydrobiologia*, 214(1), 35-42.

Arias-Ortiz, A., Masqué, P., Garcia-Orellana, J., Serrano, O., Mazarrasa, I., Marbà, N., Lovelock, C.E., Lavery, P.S. and Duarte, C.M., (2018). Reviews and syntheses: ^{210}Pb-derived sediment and carbon accumulation rates in vegetated coastal ecosystems–setting the record straight. *Biogeosciences*, 15(22), 6791-6818.

Barsanti, M., Garcia-Tenorio, R., Schirone, A., Rozmaric, M., Ruiz-Fernández, A.C., Sanchez-Cabeza, J.A., Delbono, I., Conte, F., Godoy, J.D.O., Heijnis, H. and Eriksson, M., (2020). Challenges and limitations of the ^{210}Pb sediment dating method: Results from an IAEA modelling interlaboratory comparison exercise. *Quaternary Geochronology*, 59, 101093.

Baskaran, M. and Naidu, A. (1995). ^{210}Pb-derived chronology and the fluxes of ^{210}Pb and ^{137}Cs isotopes into continental shelf sediments, east Chukchi Sea, Alaskan Arctic. *Geochimica Et Cosmochimica Acta*, 59(21), 4435-4448.

Baud A., Jenny J.P., Francus P. and Gregory-Eaves I. (2021) Global spatio-temporal analyses identify an acceleration of lake sedimentation rates associated with modern land-use change. Journal of Paleolimnology.

Binford, M. W. and Brenner, M. (1986). Dilution of ^{210}Pb by organic sedimentation in lakes of different trophic states, and application to studies of sediment-water interactions. *Limnology and Oceanography*, 31(3), 584-595.

Binford, M. W., Kahl, J. S. and Norton, S. A. (1993). Interpretation of ^{210}Pb profiles and verification of the CRS dating model in PIRLA project lake sediment cores. *Journal of Paleolimnology*, 9(3), 275-296.

Blais, J. M., Kalff, J., Cornett, R. J. and Evans, R. D. (1995). Evaluation of ^{210}Pb dating in lake sediments using stable Pb, ambrosia pollen, and ^{137}Cs. *Journal of Paleolimnology*, 13(2), 169-178.

Bruel, R. and Sabatier, P. (2020). Serac: A package for ShortlivEd RAdionuclide chronology of recent sediment cores. *Journal of Environmental Radioactivity*, 225, 106449.

Canadian Council on Ecological Areas (2014) Canada Ecozones. Version 5b [shapefile].

Center for Agroclimate, Geomatics and Earth Observation, Science and Technology Branch, Agriculture and Agri-Food Canada. Annual space-based crop inventory for Canada, Albers conic equal area, 30m [GeoTIFF].

Center for Mapping and Earth Observation, Natural Resources Canada. (2017). CanVec manmade features, NAD83 CSRS, 50k [shapefile].

Center for Mapping and Earth Observation, Natural Resources Canada. CanVec resource management features, NAD83 CSRS, 50k [shapefile].

Crozaz, G., Picciotto, E. and De Breuck, W. (1964). Antarctic snow chronology with Pb^{210}. Journal of *Geophysical Research*, 69(12), 2597-2604.

Crusius, J. and Anderson, R. F. (1991). Core compression and surficial sediment loss of lake sediments of high porosity caused by gravity coring. *Limnology and Oceanography*, 36(5), 1021-1030.

Davis, R. B., Hess, C. T., Norton, S. A., Hanson, D. W., Hoagland, K. D. and Anderson, D. S. (1984). ^{137}Cs and ^{210}Pb dating of sediments from soft-water lakes in New England (USA) and Scandinavia, a failure of ^{137}Cs dating. *Chemical Geology*, 44(1-3), 151-185.

DDEP – DATA DECAY EVALUATION PROJECT. LNELNHB/ CEA. (August 2010). Table de radionucléides 210Pb. Retrieved from http://www.nucleide.org/DDEP_WG/DDEPdata.htm

Dillon, P., Scholer, P. and Evans, H. (1986). ^{210}Pb fluxes in acidified lakes. Sediments and water interactions (pp. 491-499) *Springer*.

Ecological Stratification Working Group (Canada), Center for Land, Biological Resources Research (Canada), & Canada. State of the Environment Directorate. (1996). A national ecological framework for Canada. Centre for Land and Biological Resources Research; Hull, Quebec: State of the Environment Directorate.

Ghaleb, B. (2009). Overview of the methods for the measurement and interpretation of short-lived radioisotopes and their limits. Paper presented at the IOP Conference Series: *Earth and Environmental Science*, 5(1) 012007.

Goldberg, E. (1963). Geochronology with ^{210}Pb radioactive dating. *International Atomic Energy Agency*, Vienna, 121, 130.

Jenny, J.P., Normandeau, A., Francus, P., Taranu, Z.E., Gregory-Eaves, I., Lapointe, F., Jautzy, J., Ojala, A.E., Dorioz, J.M., Schimmelmann, A. and Zolitschka, B. (2016). Urban point sources of nutrients were the leading cause for the historical spread of hypoxia across European lakes. *Proceedings of the National Academy of Sciences of the United States of America*, 113(45), 12655-12660. doi:10.1073/pnas.1605480113 [doi]

Klaminder, J., Appleby, P., Crook, P. and Renberg, I. (2012). Post-deposition diffusion of ^{137}Cs in lake sediment: Implications for radiocaesium dating. *Sedimentology*, 59(7), 2259-2267.

Koide, M., Soutar, A. and Goldberg, E. D. (1972). Marine geochronology with ^{210}Pb. *Earth and Planetary Science Letters*, 14(3), 442-446.

Korosi, J. B., Ginn, B. K., Cumming, B. F. and Smol, J. P. (2013). Establishing past environmental conditions and tracking long-term environmental change in the Canadian maritime provinces using lake sediments. *Environmental Reviews*, 21(1), 15-27.

Krishnaswami, S. and Lal, D. (1978). Radionuclide limnochronology. *Lakes* (pp. 153-177) Springer.

Last, W. M. and Smol, J. P. (2002). Tracking environmental change using lake sediments: Volume 2: Physical and geochemical methods *Springer Science & Business Media*.

Martz, D. E., Langner, G. H., Jr, and Johnson, P. R. (1991). Half-lives of ^{214}Pb and ^{214}Bi. *Health Physics*, 61(4), 511-518. doi:10.1097/00004032-199110000-00006 [doi]

Millet, L., Giguet-Covex, C., Verneaux, V., Druart, J., Adatte, T. and Arnaud, F. (2010). Reconstruction of the recent history of a large deep prealpine lake (lake bourget, france) using subfossil chironomids, diatoms, and organic matter analysis: Towards the definition of a lake-specific reference state. *Journal of Paleolimnology*, 44(4), 963-978.

Muggeo, V. M. R. (2003). Estimating regression models with unknown break-points. *Statistics in Medicine*, 22(19), 3055-3071. doi:10.1002/sim.1545

Openshaw, S. (1983). The modifiable areal unit problem. *Concepts and techniques in modern geography* 38, GeoBooks, Norwich, England.

Pennington, W., Cambray, R., Eakins, J. and Harkness, D. (1976). Radionuclide dating of the recent sediments of Blelham Tarn. *Freshwater Biology*, 6(4), 317-331.

Rogers L.A., Schindler D.E., Lisi P.J., Holtgrieve G.W., Leavitt P.R., Bunting L., Finney B.P., Selbie D.T., Chen G., Gregory-Eaves I., Lisac M.J. and Walsh P.B. (2013) Centennial-scale fluctuations and regional complexity characterize Pacific salmon population dynamics over the past five centuries. *Proceedings of the National Academy of Sciences of the United States of America,* 110: 1750-1755.

Sanchez-Cabeza, J. and Ruiz-Fernández, A. (2012). ^{210}Pb sediment radiochronology: An integrated formulation and classification of dating models. *Geochimica Et Cosmochimica Acta*, 82, 183-200.

Schallenberg, M., de Winton, M. D., Verburg, P., Kelly, D. J., Hamill, K. D. and Hamilton, D. P. (2013). Ecosystem services of lakes. Ecosystem Services in New Zealand: Conditions and Trends. Manaaki Whenua Press, Lincoln, New-Zealand 203-225.

Team, R. C. (2013). R: A language and environment for statistical computing.

Tomkins, J. D., Antoniades, D., Lamoureux, S. F. and Vincent, W. F. (2008). A simple and effective method for preserving the sediment–water interface of sediment cores during transport. *Journal of Paleolimnology*, 40(1), 577-582.

Tomkins, J. D., Lamoureux, S. F., Antoniades, D. and Vincent, W. F. (2009). Sedimentary pellets as an ice-cover proxy in a high arctic ice-covered lake. *Journal of Paleolimnology*, 41(1), 225-242.

Turner, L. and Delorme, L. (1996). Assessment of ^{210}Pb data from Canadian lakes using the CIC and CRS models. *Environmental Geology*, 28(2), 78-87.

Winegardner, A. K., Legendre, P., Beisner, B. E. and Gregory-Eaves, I. (2017). Diatom diversity patterns over the past c. 150 years across the conterminous United States of America: Identifying mechanisms behind beta diversity. *Global Ecology and Biogeography*, 26(11), 1303-1315.

Wood, S. (2012). Mgcv: Mixed GAM computation vehicle with GCV/AIC/REML smoothness estimation.

Wright, S., Howard, B., Strand, P., Nylén, T. and Sickel, M. (1999). Prediction of ^{137}Cs deposition from atmospheric nuclear weapons tests within the Arctic. *Environmental Pollution*, 104(1), 131-143.

Electronic Supplementary Material (ESM)

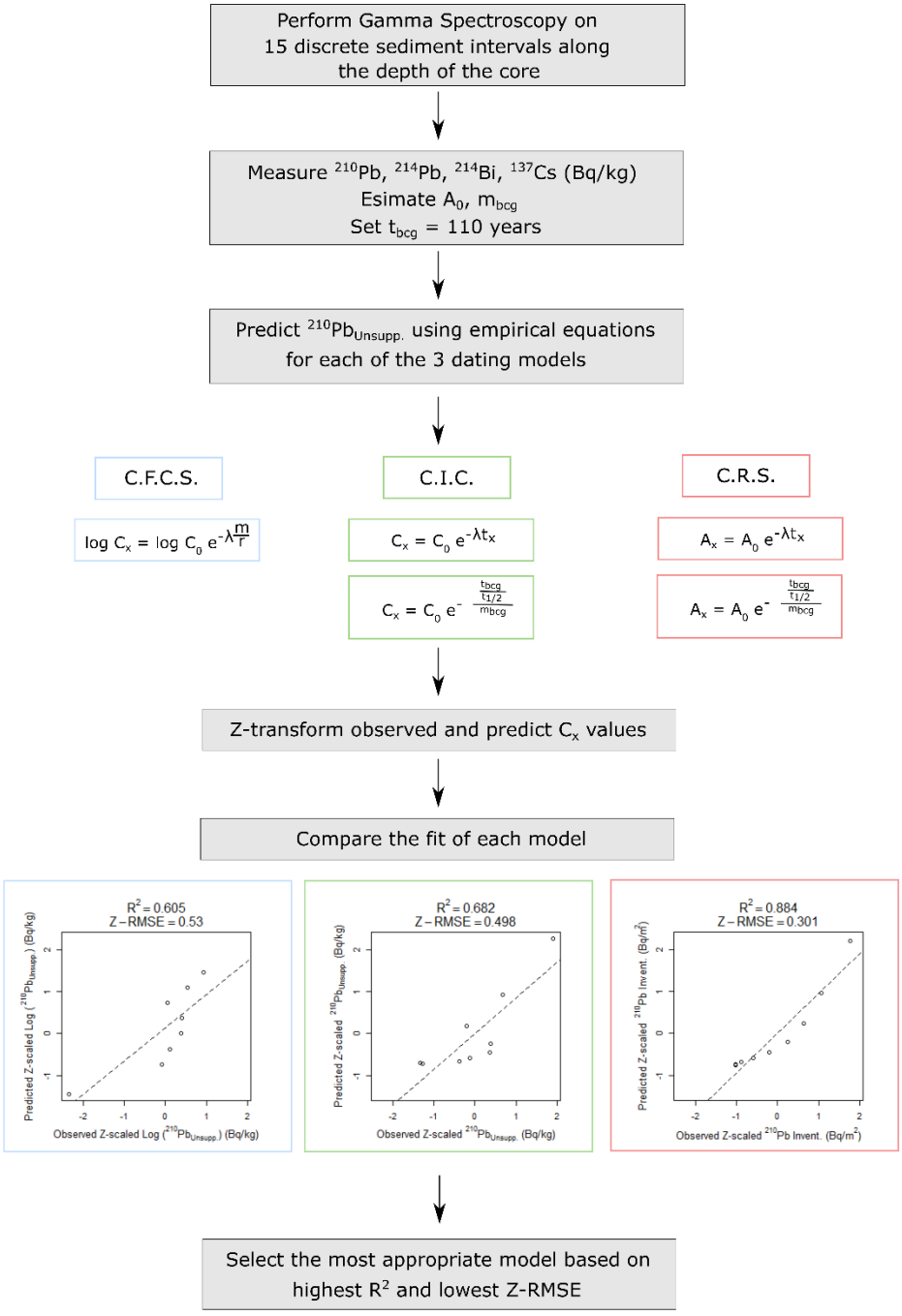

Figure S1. Model selection framework for comparing the ^{210}Pb quantities across 3 dating models using empirical equations from Appleby and Oldfield (1983).

Table S1 Land use, human impact value and data sources. Updated from Huot et al. (2019).

Land Use type	Human impact value	Data source
Urban	1	AAFC Annual Crop inventory 2017; AAFC Land Use 2010; NRCan CanVec Manmade features; USDA NASS Cropland Data Layer 2017; NALCMS Landcover 2010
Mines/Excavation	1	NRCan CanVec Resource Management Features
Agriculture	1	AAFC Annual Crop inventory 2017; AAFC Land Use 2010; USDA NASS Cropland Data Layer 2017; NALCMS Landcover 2010
Pasture	0.5	AAFC Annual Crop inventory 2017; AAFC Land Use 2010; USDA NASS Cropland Data Layer 2017
Recent clearcuts (2012 to 2017)	0.5	Year of gross forest cover loss event (2012 to 2017) from: Hansen et al. 2013; NRCan Natural Burned Area Composite (2010 to 2017)
Natural landscapes	0	NRCan EOSD forest cover map, AAFC Annual Crop inventory 2017; AAFC Land Use 2010; USDA NASS Cropland Data Layer 2017; NALCMS Landcover 2010

Table S2. Class definition and simplified land use categories

Class	Definition	Category simplified
0	No Data	NA
1	Water	Water
10	Exposed Land / Barren / Rock / Snow / Ice	Natural Landscape
20	natural landscape (unclassified)	Natural Landscape
21	Bryoids	Natural Landscape
22	Shrubland	Natural Landscape
23	Herb / Grassland	Natural Landscape
24	Coniferous	Natural Landscape
25	Broadleaf	Natural Landscape
26	Mixedwood	Natural Landscape
27	Forest (undifferentiated)	Natural Landscape
30	Wetland	Natural Landscape
40	Forest Loss (2012-2017)	Forestry
100	Urban / Developed	Urban
101	Sod	Urban
200	Greenhouses	Agriculture
201	Agriculture (undifferentiated)	Agriculture
202	Pasture / Forages	Pasture
203	Too Wet to be Seeded	Agriculture
204	Fallow	Agriculture
205	Cereals	Agriculture
206	Barley	Agriculture
207	Other Grains	Agriculture
208	Millet	Agriculture
209	Oats	Agriculture
210	Rye	Agriculture
211	Spelt	Agriculture
212	Triticale	Agriculture
213	Wheat	Agriculture
214	Switchgrass	Agriculture
215	Sorghum	Agriculture
216	Winter Wheat	Agriculture
217	Spring Wheat	Agriculture
218	Corn	Agriculture
219	Tobacco	Agriculture
220	Ginseng	Agriculture
221	Oilseeds	Agriculture
222	Borage	Agriculture
223	Camelina	Agriculture

224	Canola / Rapeseed	Agriculture
225	Flaxseed	Agriculture
226	Mustard	Agriculture
227	Safflower	Agriculture
228	Sunflower	Agriculture
229	Soybeans	Agriculture
230	Pulses	Agriculture
231	Peas	Agriculture
232	Beans	Agriculture
233	Lentils	Agriculture
234	Vegetables	Agriculture
235	Tomatoes	Agriculture
236	Potatoes	Agriculture
237	Sugarbeets	Agriculture
238	Other Vegetables	Agriculture
239	Fruits	Agriculture
240	Berries	Agriculture
241	Blueberry	Agriculture
242	Cranberry	Agriculture
243	Other Berry	Agriculture
244	Orchards	Agriculture
245	Other Fruits	Agriculture
246	Vineyards	Agriculture
247	Hops	Agriculture
248	Herbs	Agriculture
249	Nursery	Agriculture
250	Buckwheat	Agriculture
251	Canaryseed	Agriculture
252	Hemp	Agriculture
253	Vetch	Agriculture
254	Other Crops	Agriculture
300	mines/excavation	Mines

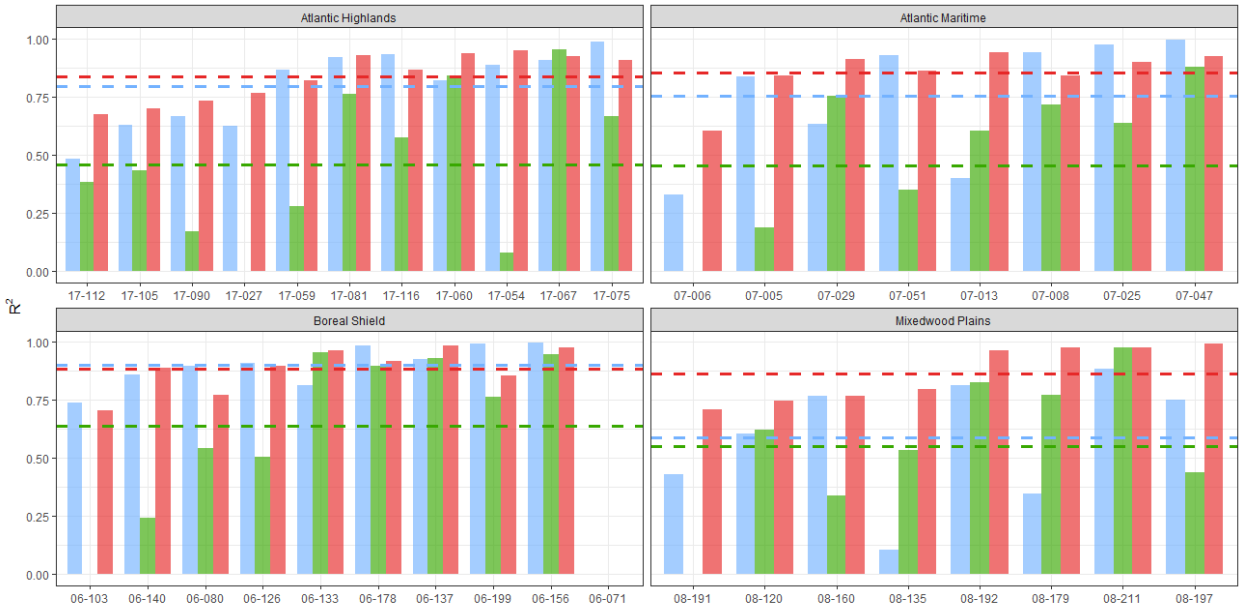

Figure S2. Distribution of predicted and observed R^2 fit across different dating model for all lakes, by ecozone. In blue is the C.F.C.S., green is C.I.C. and red C.R.S. model fit. Lakes are ordered by increasing selected R^2. The colored horizontal dashed lines indicate the mean R^2 for each dating model across each ecozone.

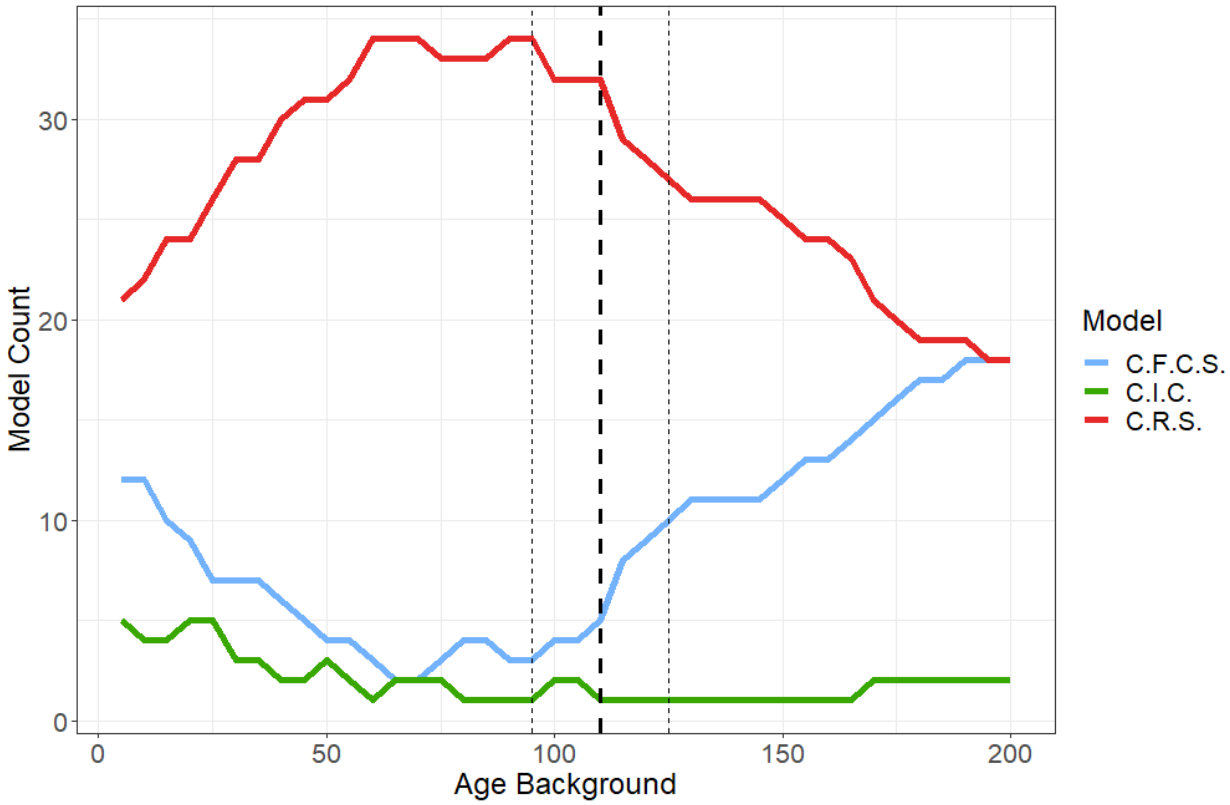

Figure S3. Sensitivity analysis of Age background (= t_{bgd}) parameter used for dating model selection. While t_{bgd}must have environmental significance in accordance with the natural decay of ^{210}Pb (80 – 130 years), represented here by the thin dashed vertical lines, this figure shows the mathematical bias that exists when investigating t_{bgd}outside of this range as well as the model selection stability present within this natural range. The selected t_{bgd} of 110 years is indicated by the thicker dashed line.

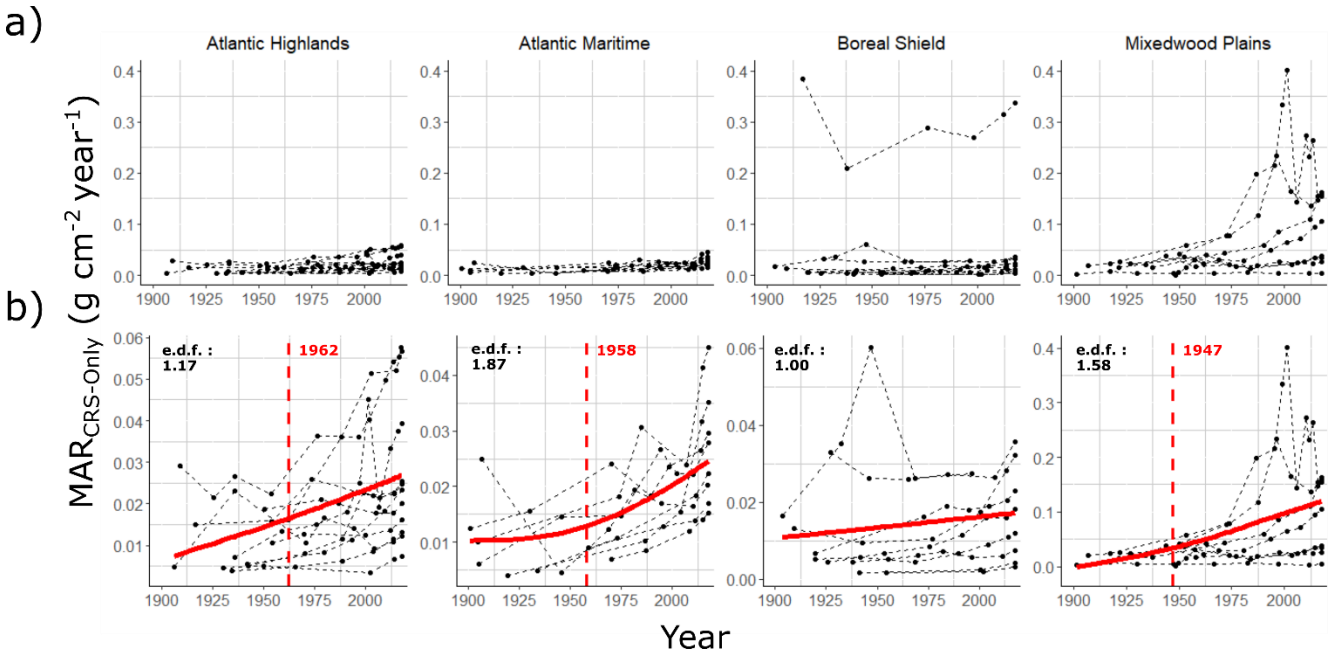

Figure S4. Temporal variation in sediment dry weight mass accumulation rate across the four ecozones of Eastern Canada as determined using only the C.R.S. dating model. The upper panel displays the raw measured sedimentation rates across the 37 lakes. In the lower panel are reported the general additive model (GAM) trends of ecozone specific MAR temporal variation. The estimated degrees of freedom (e.d.f.) associated with the GAM is also reported, as is the estimated onset of the MAR acceleration across each ecozone based on a breakpoint analysis. Lake 06-103 from the Boreal Shield was identified as having anomalously high MAR and was also found to be a site in a floodplain, and thus was removed from our GAM analyses.

Metadata

Activity profiles (Bq kg^{-1}) and high-resolution core photograph scaled to the sediment core depth (cm) for each of the 37 lakes for three radioisotopes; Total ^{210}Pb in blue, ^{137}Cs in red and ^{214}Pb in green. While $^{210}Pb_{Total}$ is expected to follow an exponential decay, ^{137}Cs should indicate, if free of post-depositional movement, the date of 1963 CE and ^{214}Pb accounts for the background, supported quantity of ^{210}Pb present in the sediment.

Age-Depth profiles for three different dating models compared (C.F.C.S. in blue, C.I.C. in green and C.R.S. in red) shown for the 37 sampled lakes. The selected model is indicated in parentheses in the plot title. The location of the measured ^{137}Cs peak concentration in the core is shown in grey, with error bars accounting for its potential location between two sequential dated intervals

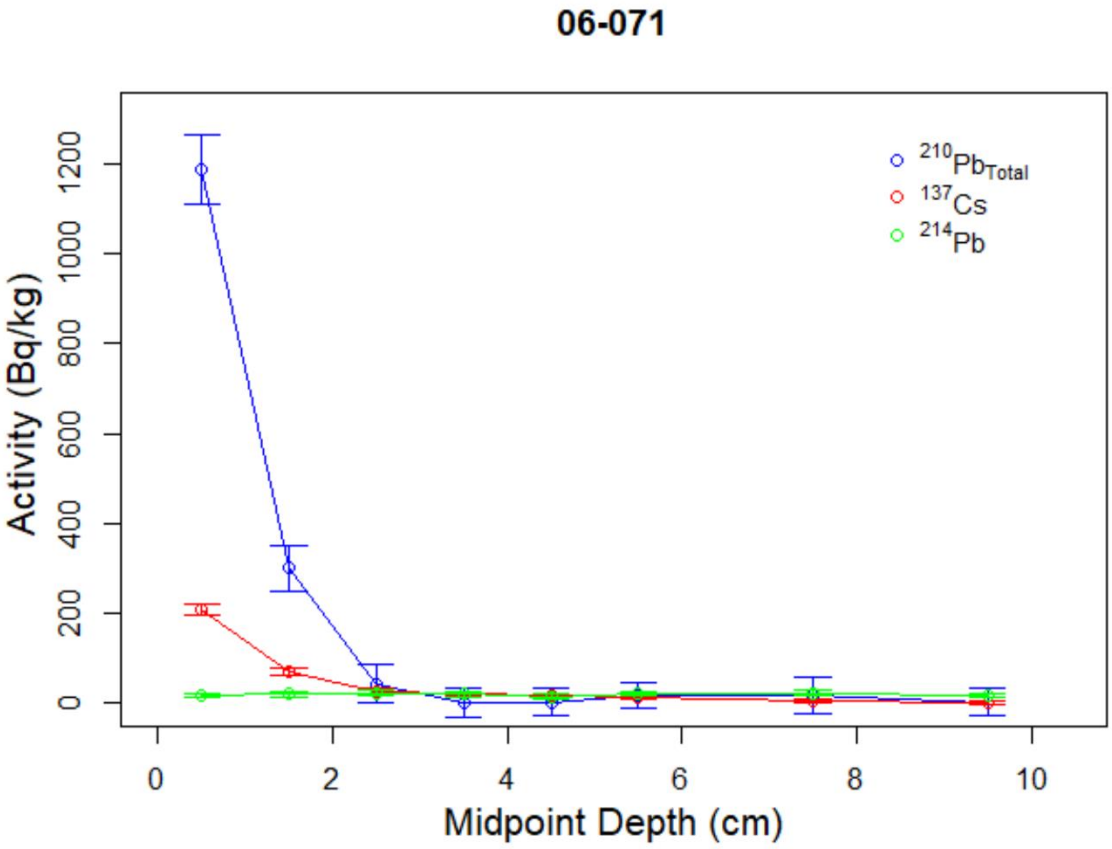
06-071
Activity (Bq/kg)
0
200
400
600
800
1000
1200
0
2
4
6
8
10
Midpoint Depth (cm)
$^{210}Pb_{Total}$
^{137}Cs
^{214}Pb


06-071

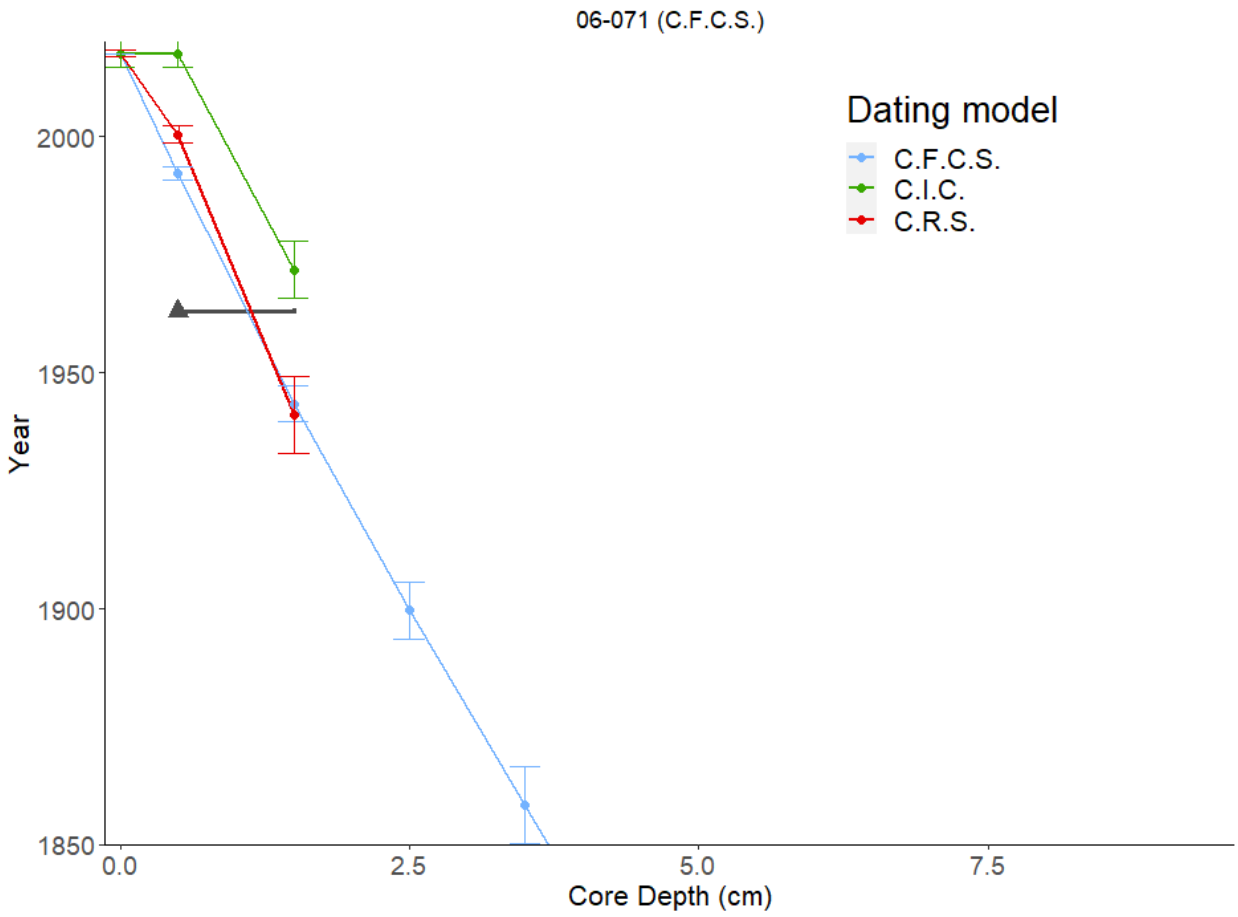
06-071 (C.F.C.S.)
Dating model
C.F.C.S.
C.I.C.
C.R.S.
Year
2000
1950
1900
1850
0.0
2.5
5.0
7.5
Core Depth (cm)

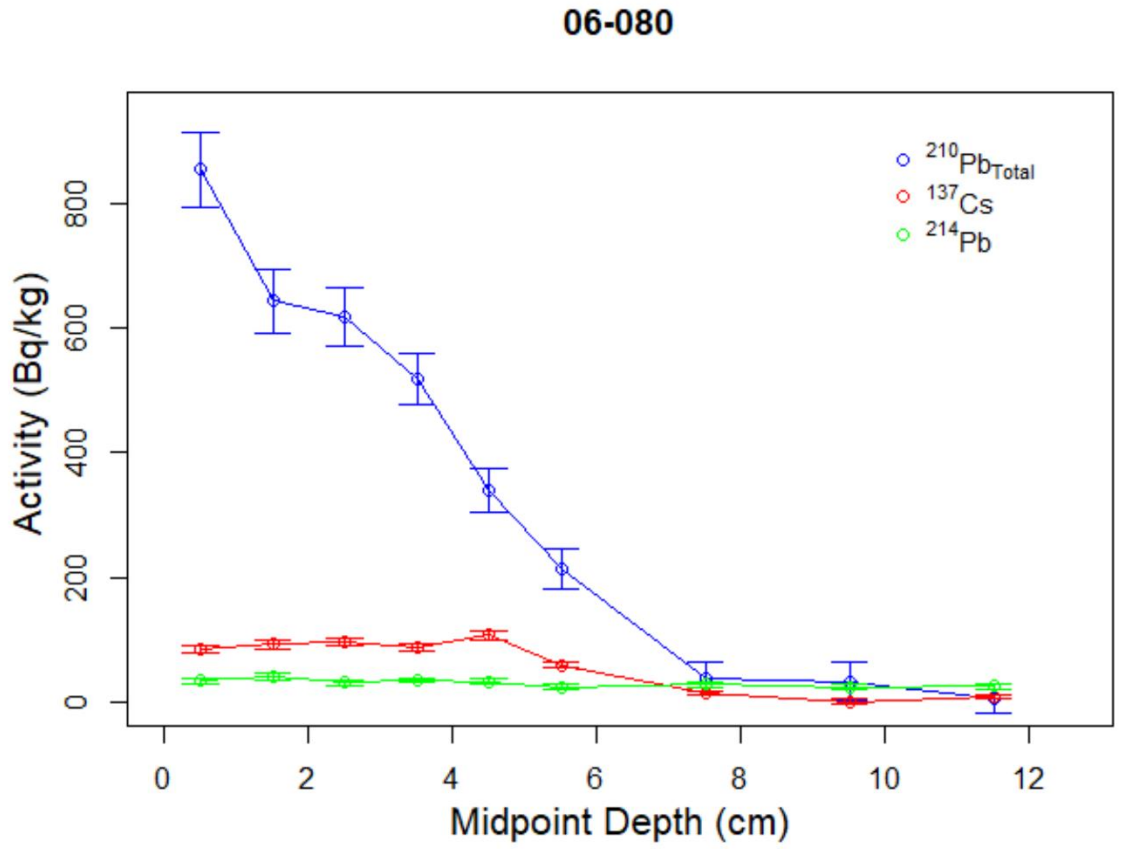
06-080
Activity (Bq/kg)
0
200
400
600
800
0
2
4
6
8
10
12
Midpoint Depth (cm)
$^{210}Pb_{Total}$
^{137}Cs
^{214}Pb


06-071

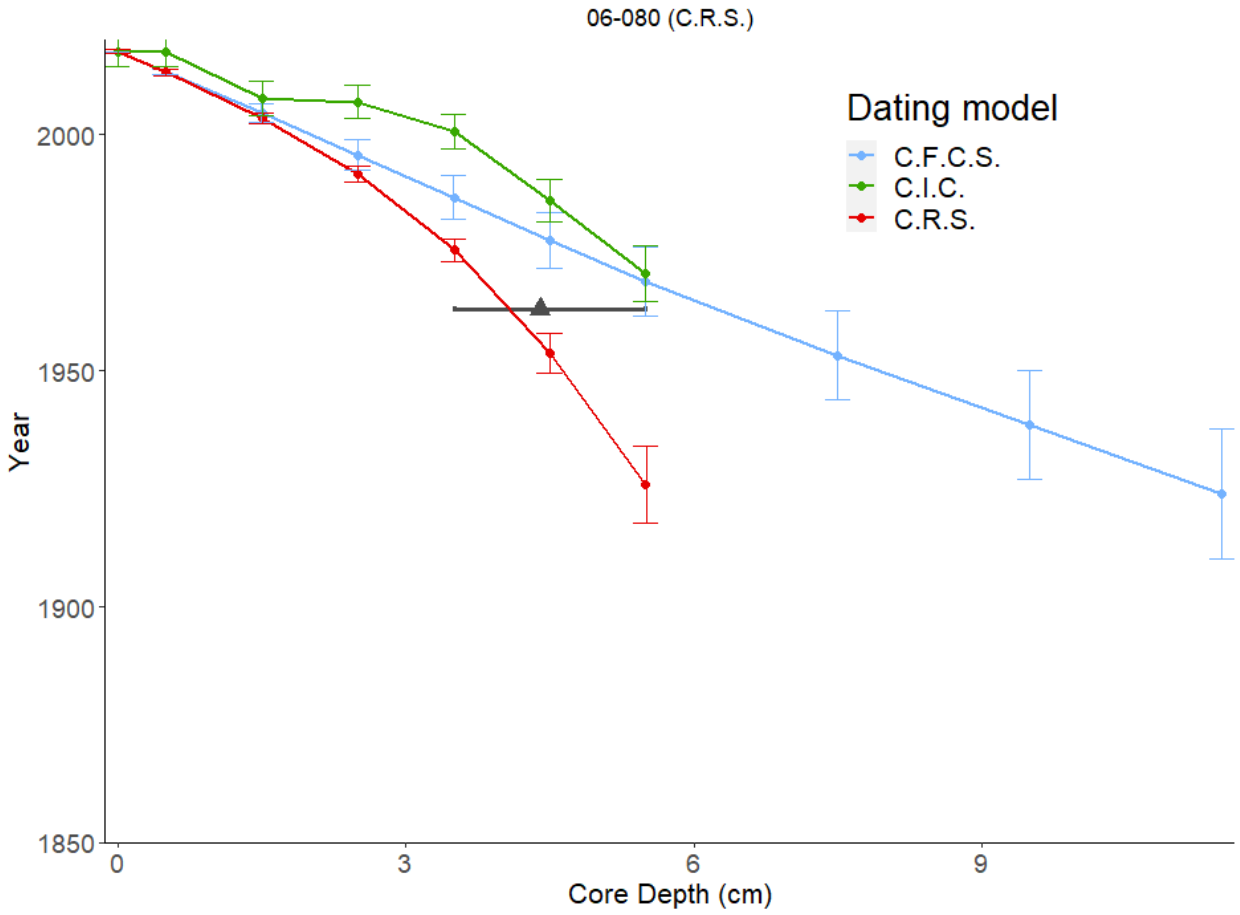
06-080 (C.R.S.)
Dating model
C.F.C.S.
C.I.C.
C.R.S.
Year
2000
1950
1900
1850
0
3
6
9
Core Depth (cm)

15

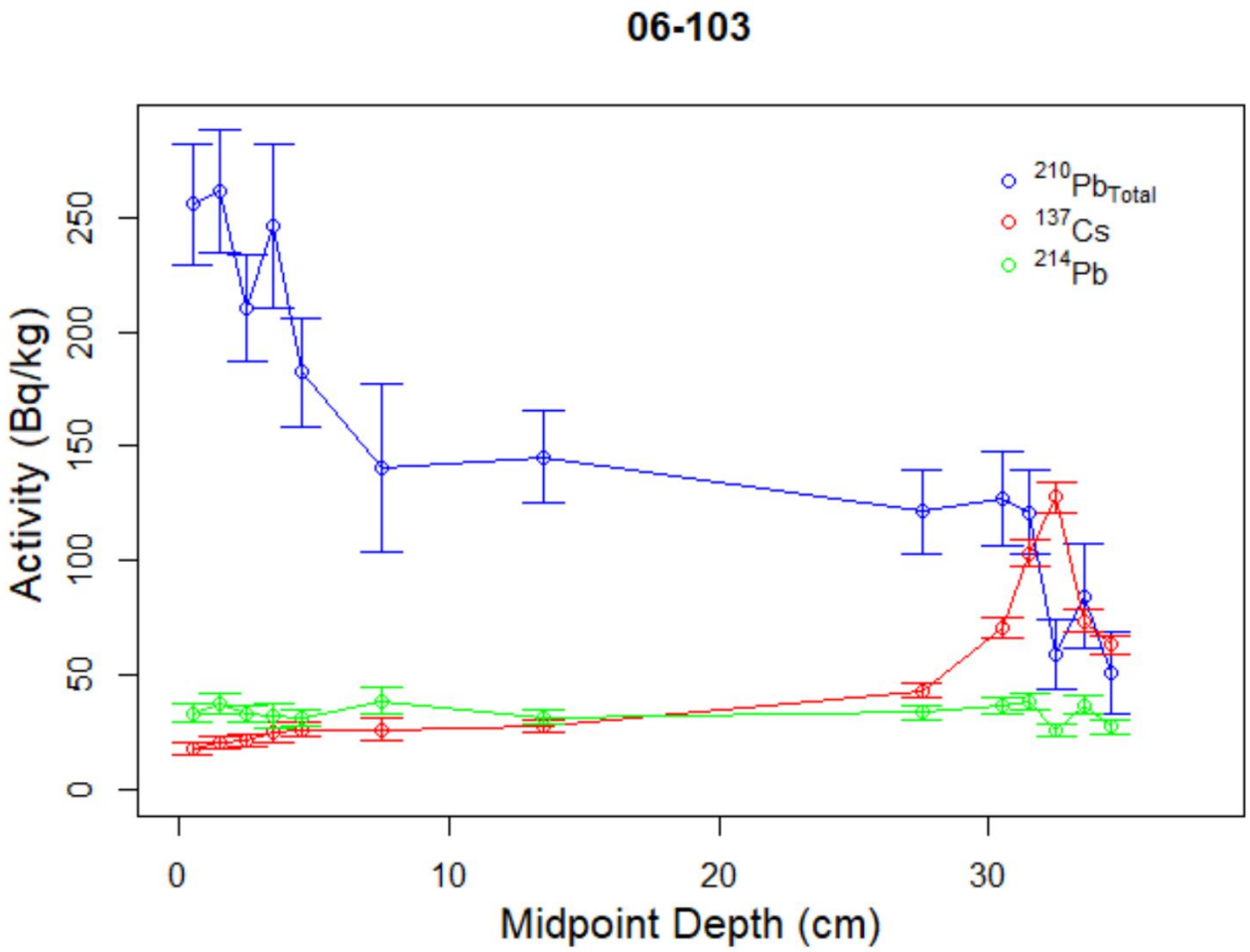
06-103
Activity (Bq/kg)
0
50
100
150
200
250
0
10
20
30
Midpoint Depth (cm)
$^{210}Pb_{Total}$
^{137}Cs
^{214}Pb


06-103

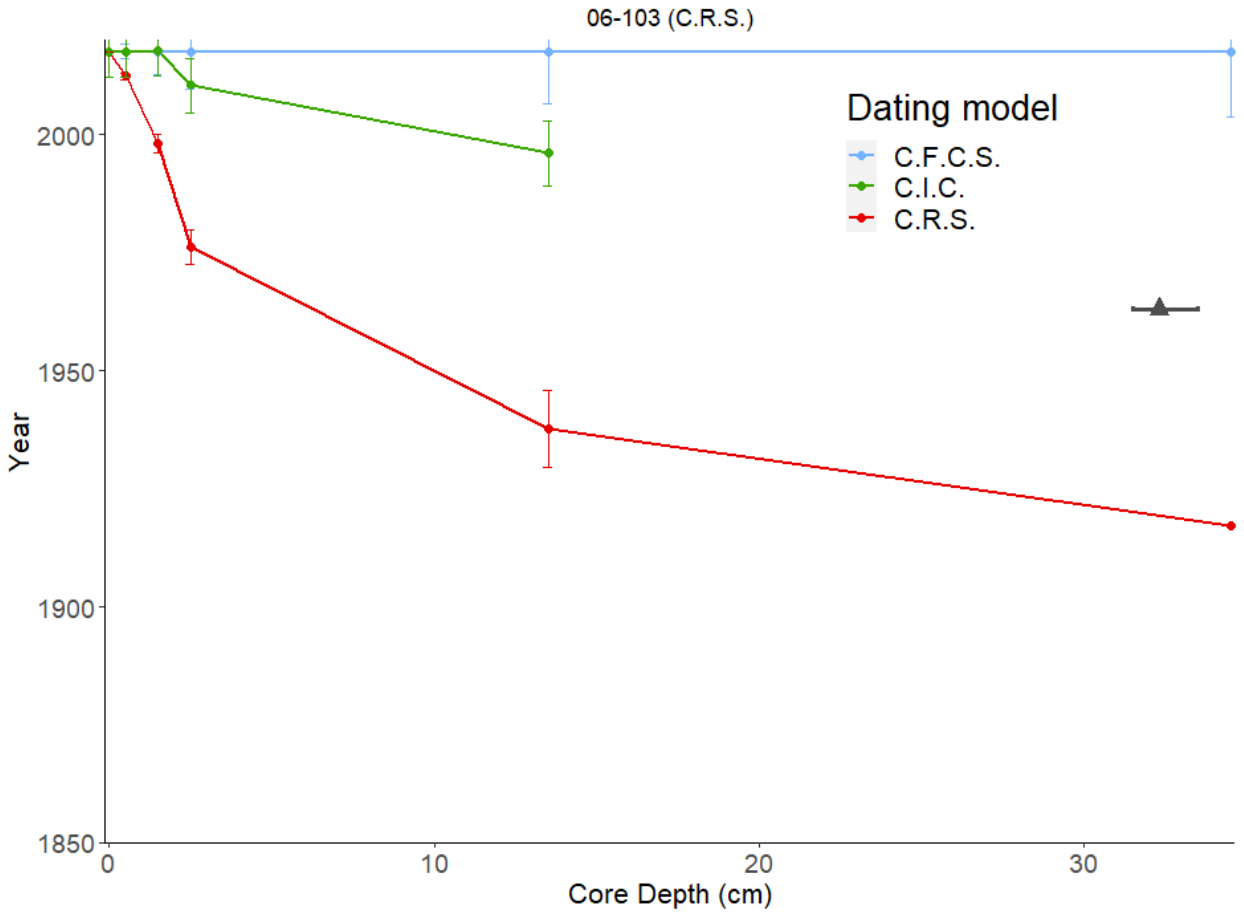
06-103 (C.R.S.)
Dating model
C.F.C.S.
C.I.C.
C.R.S.
Year
2000
1950
1900
1850
0
10
20
30
Core Depth (cm)

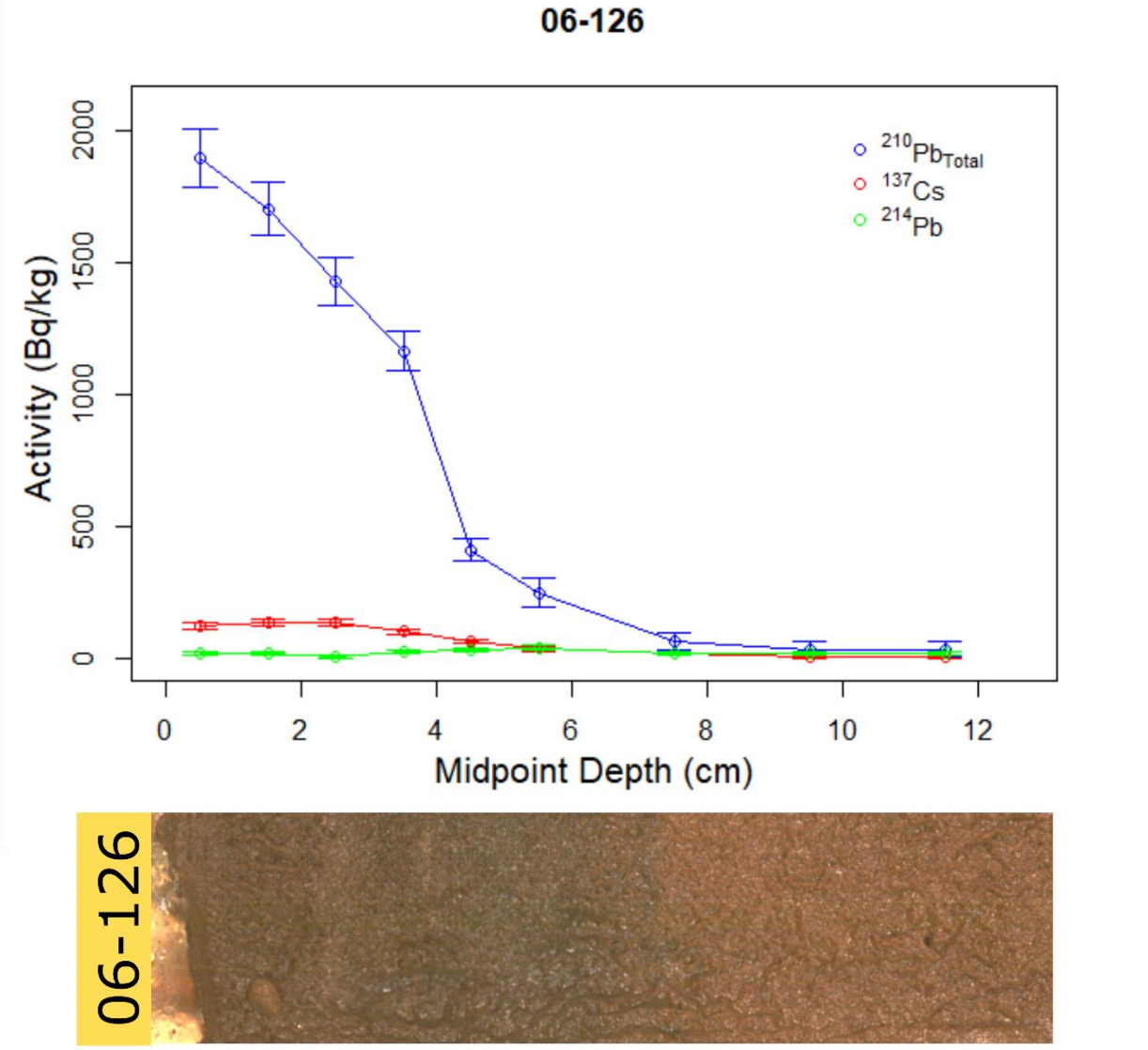
06-126
Activity (Bq/kg)
0
500
1000
1500
2000
0
2
4
6
8
10
12
Midpoint Depth (cm)
$^{210}Pb_{Total}$
^{137}Cs
^{214}Pb
06-126

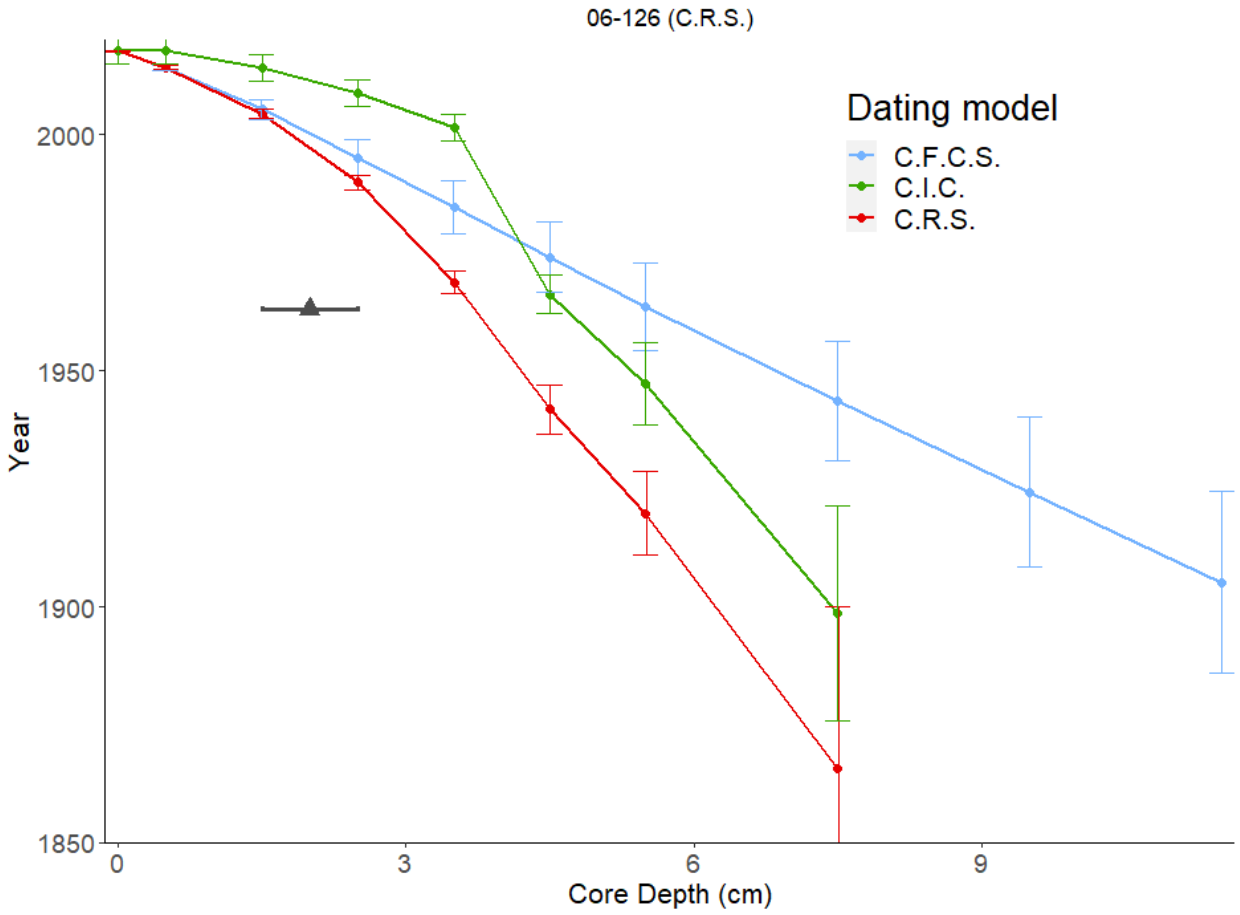
06-126 (C.R.S.)
Dating model
C.F.C.S.
C.I.C.
C.R.S.
Year
2000
1950
1900
1850
0
3
6
9
Core Depth (cm)

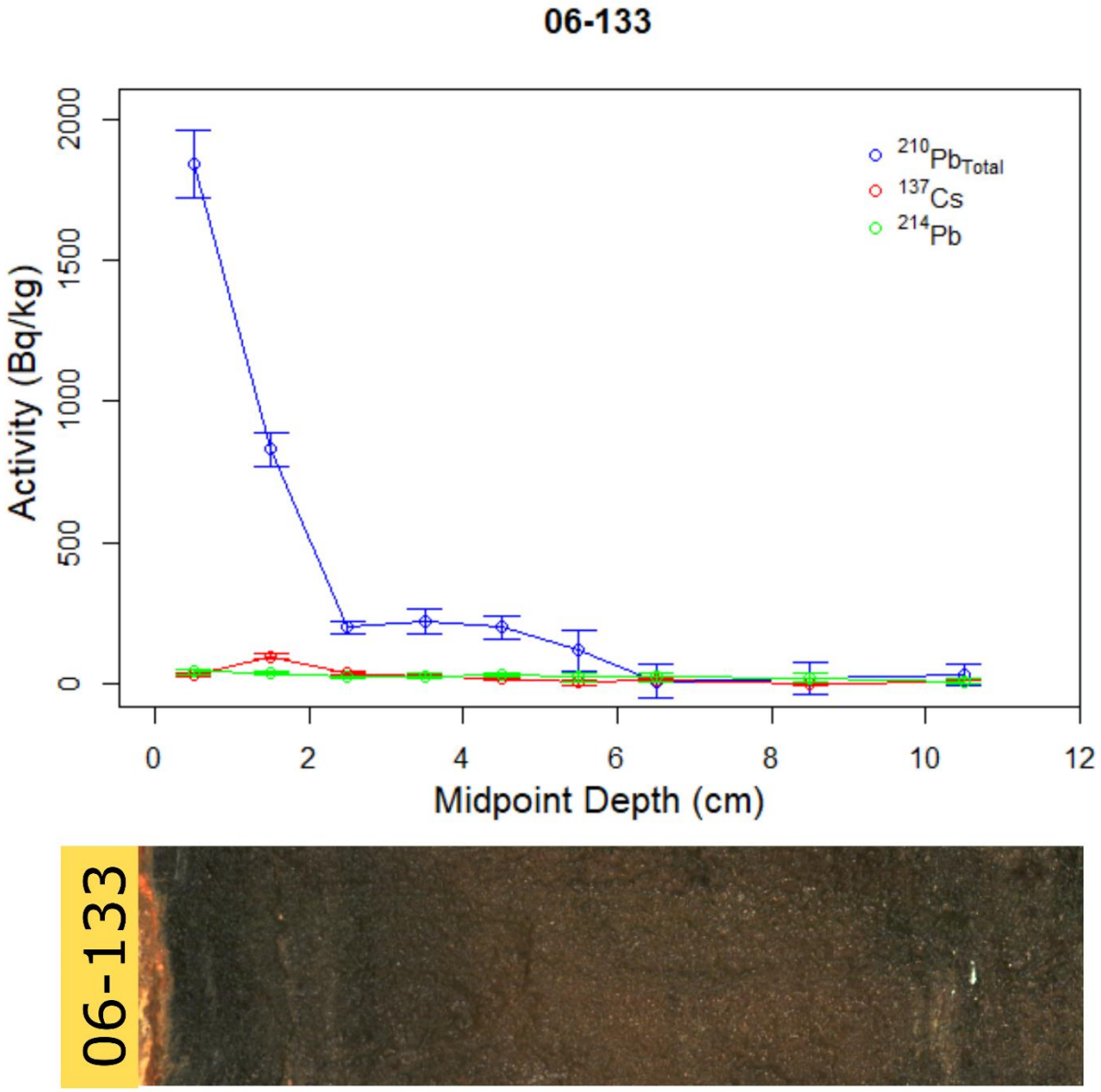
06-133
Activity (Bq/kg)
0
500
1000
1500
2000
0
2
4
6
8
10
12
Midpoint Depth (cm)
$^{210}Pb_{Total}$
^{137}Cs
^{214}Pb

06-133

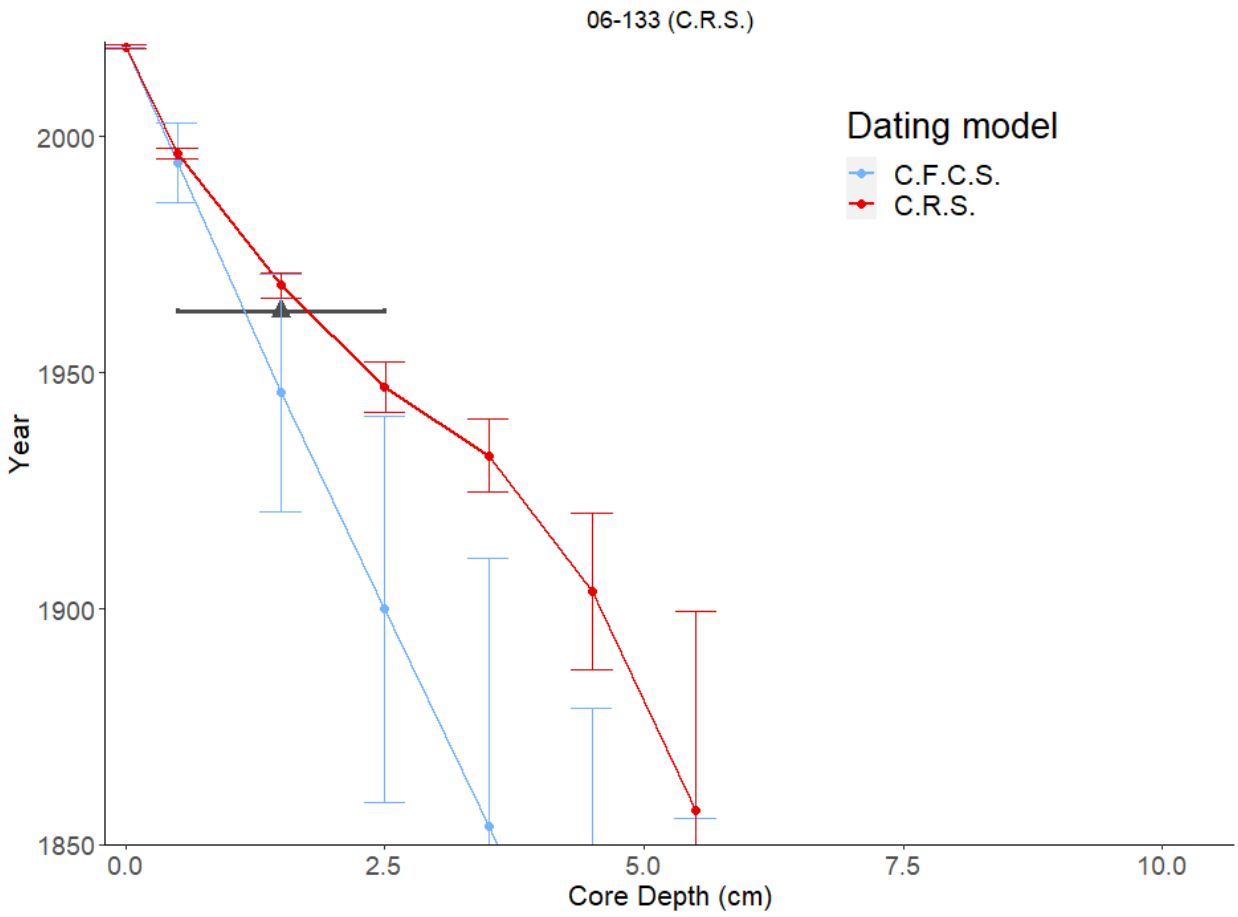
06-133 (C.R.S.)
Dating model
C.F.C.S.
C.R.S.
Year
2000
1950
1900
1850
0.0
2.5
5.0
7.5
10.0
Core Depth (cm)

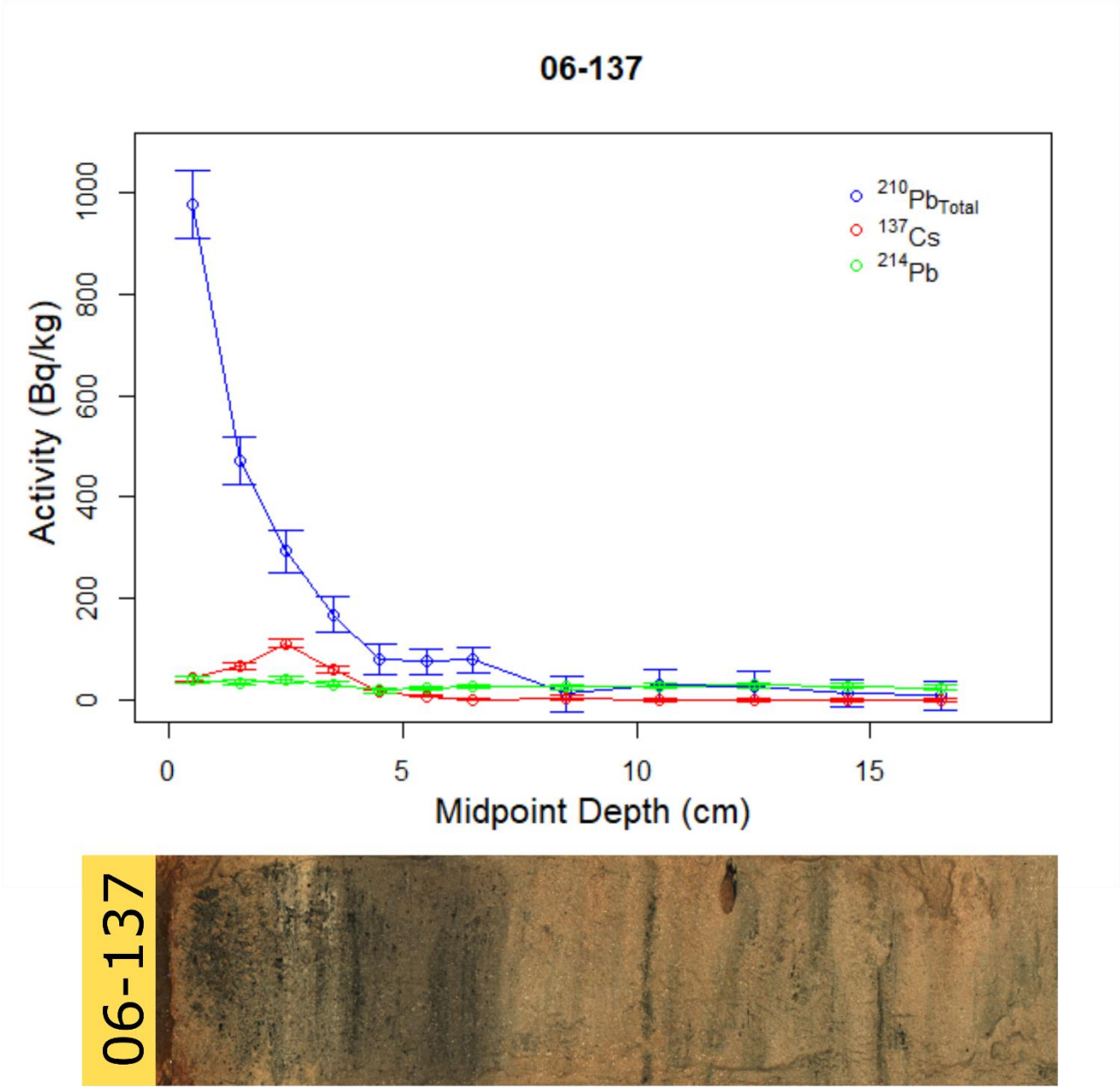
06-137
Activity (Bq/kg)
0
200
400
600
800
1000
0
5
10
15
Midpoint Depth (cm)
$^{210}Pb_{Total}$
^{137}Cs
^{214}Pb
06-137

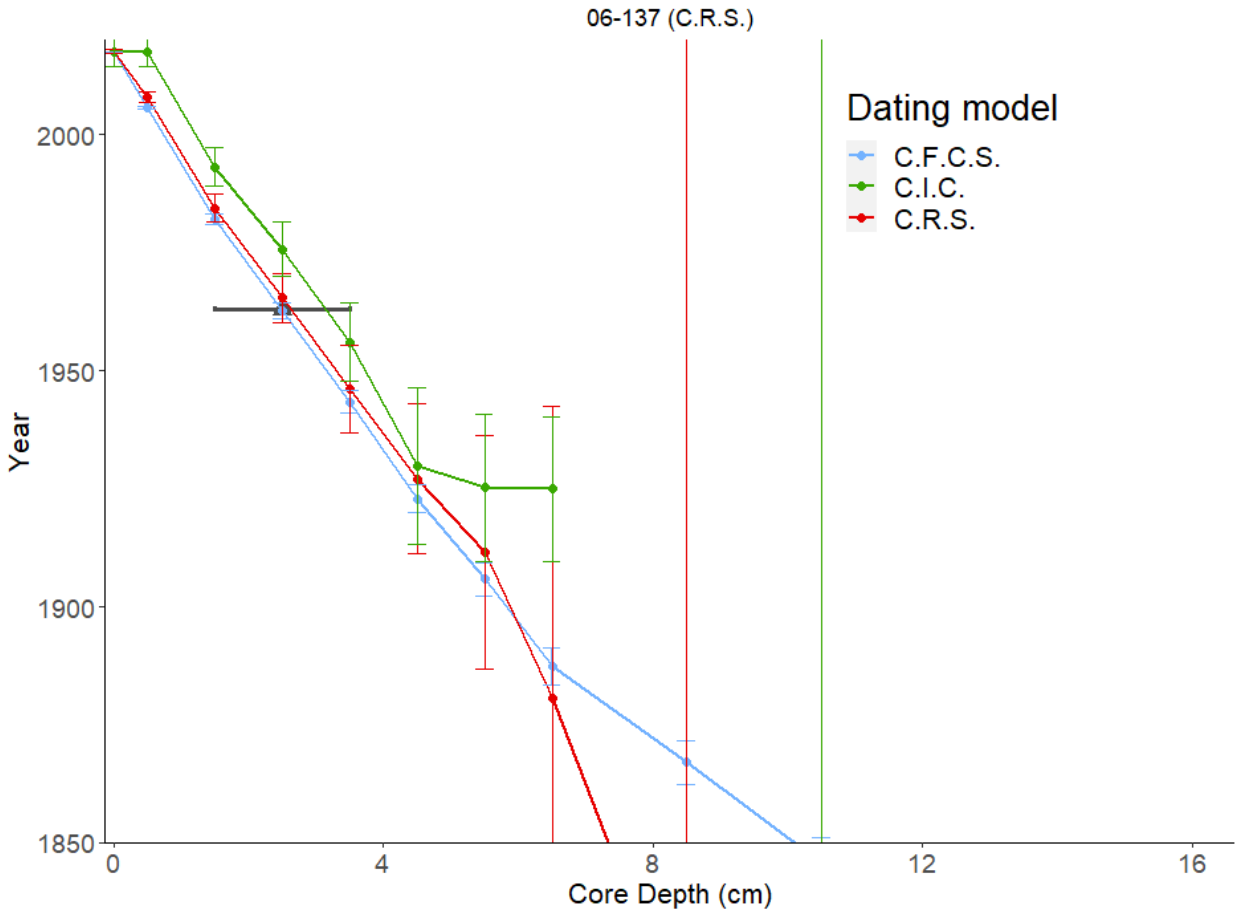
06-137 (C.R.S.)
Dating model
C.F.C.S.
C.I.C.
C.R.S.
Year
2000
1950
1900
1850
0
4
8
12
16
Core Depth (cm)

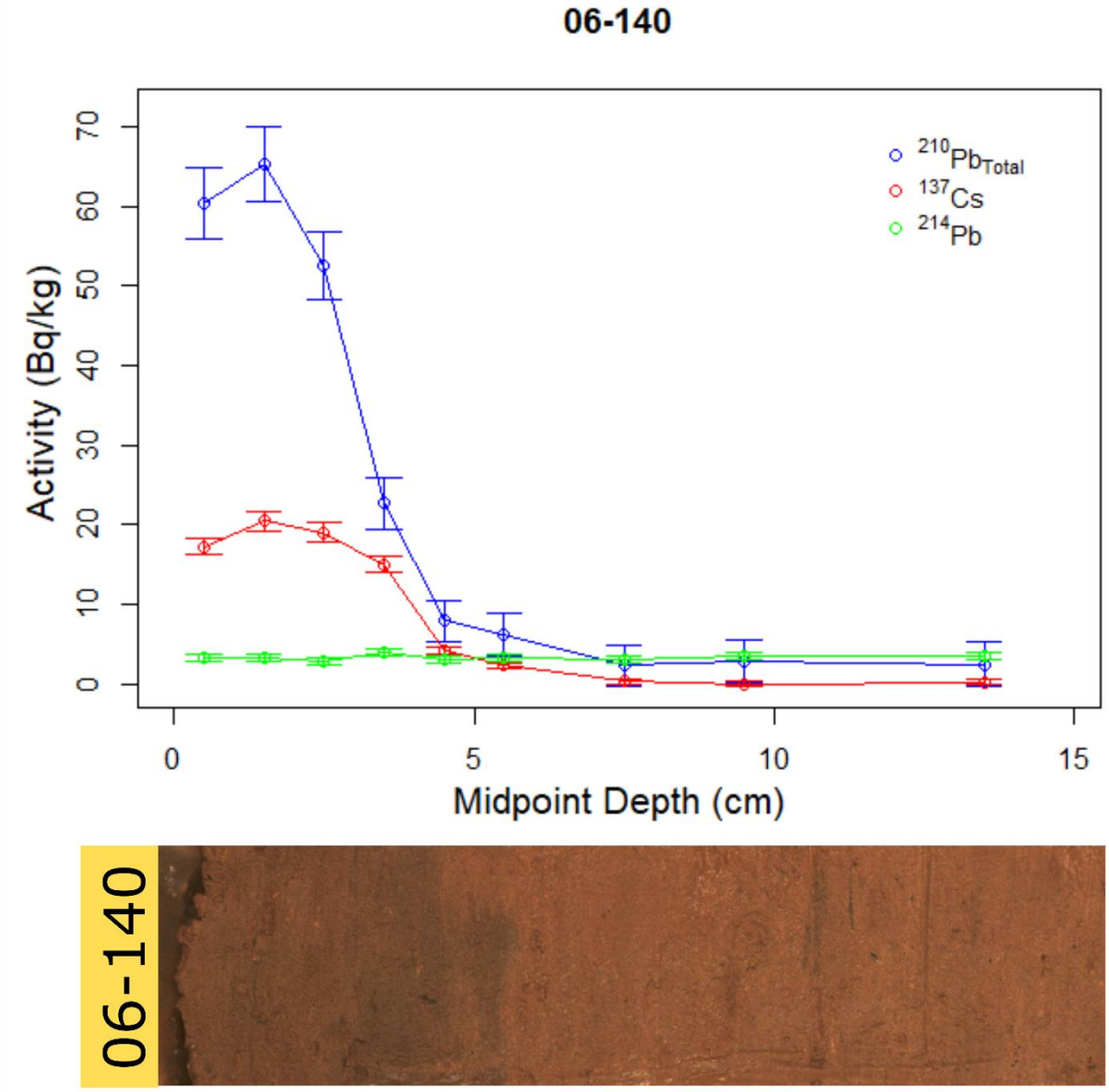
06-140
Activity (Bq/kg)
0
10
20
30
40
50
60
70
0
5
10
15
Midpoint Depth (cm)
$^{210}Pb_{Total}$
^{137}Cs
^{214}Pb
06-140

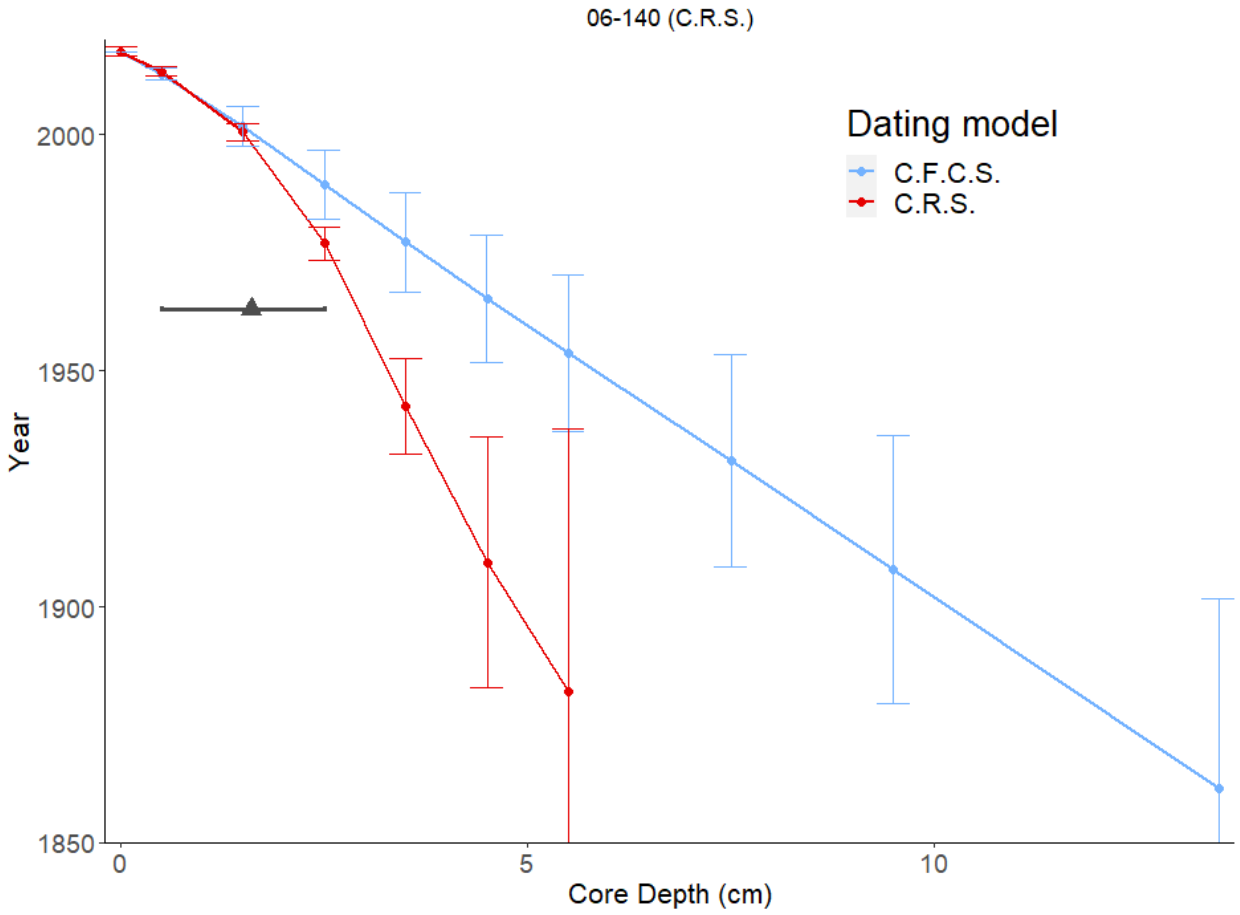
06-140 (C.R.S.)
Dating model
C.F.C.S.
C.R.S.
Year
2000
1950
1900
1850
0
5
10
Core Depth (cm)

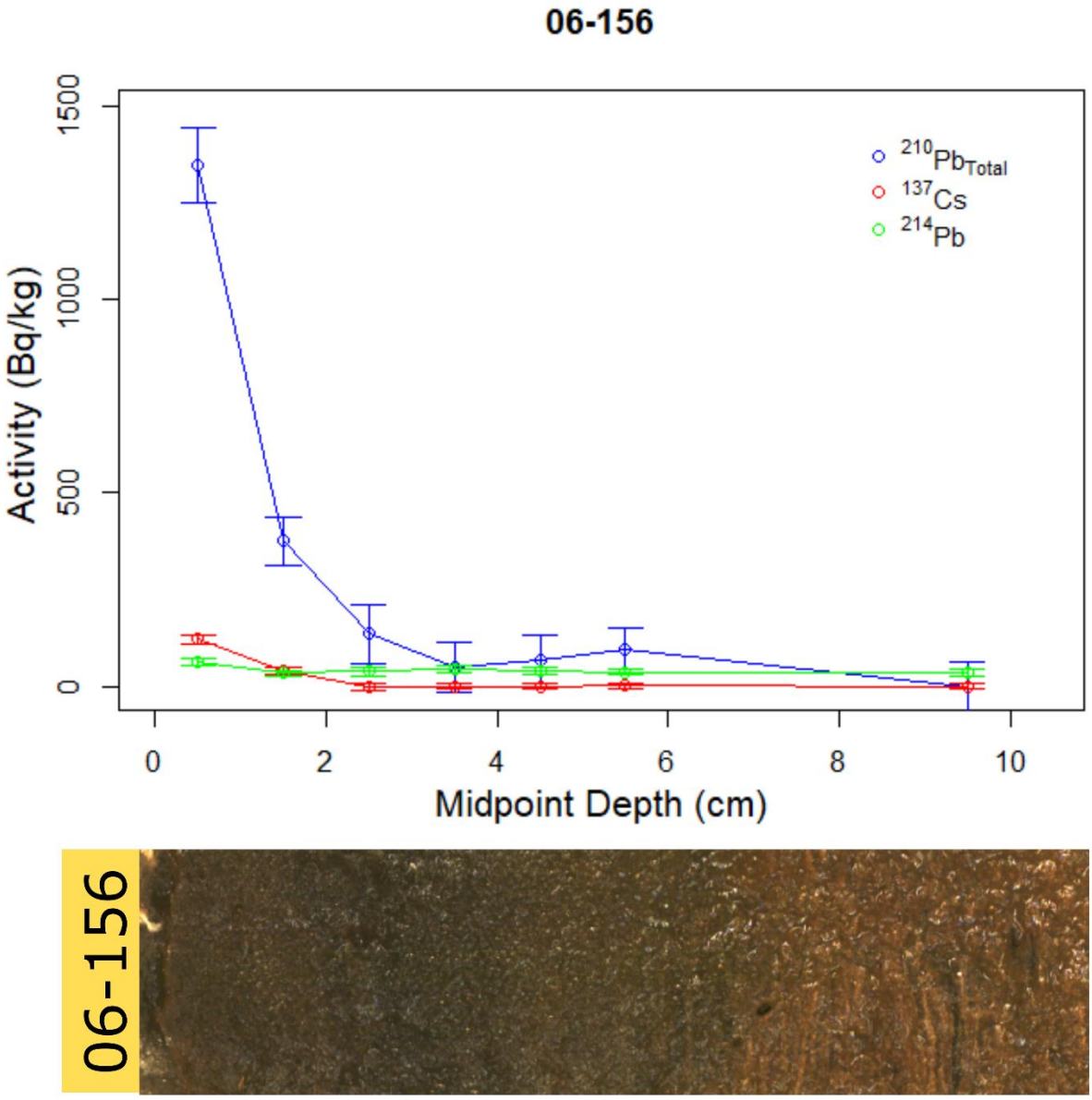
06-156
Activity (Bq/kg)
0
500
1000
1500
0
2
4
6
8
10
Midpoint Depth (cm)
$^{210}Pb_{Total}$
^{137}Cs
^{214}Pb

06-156

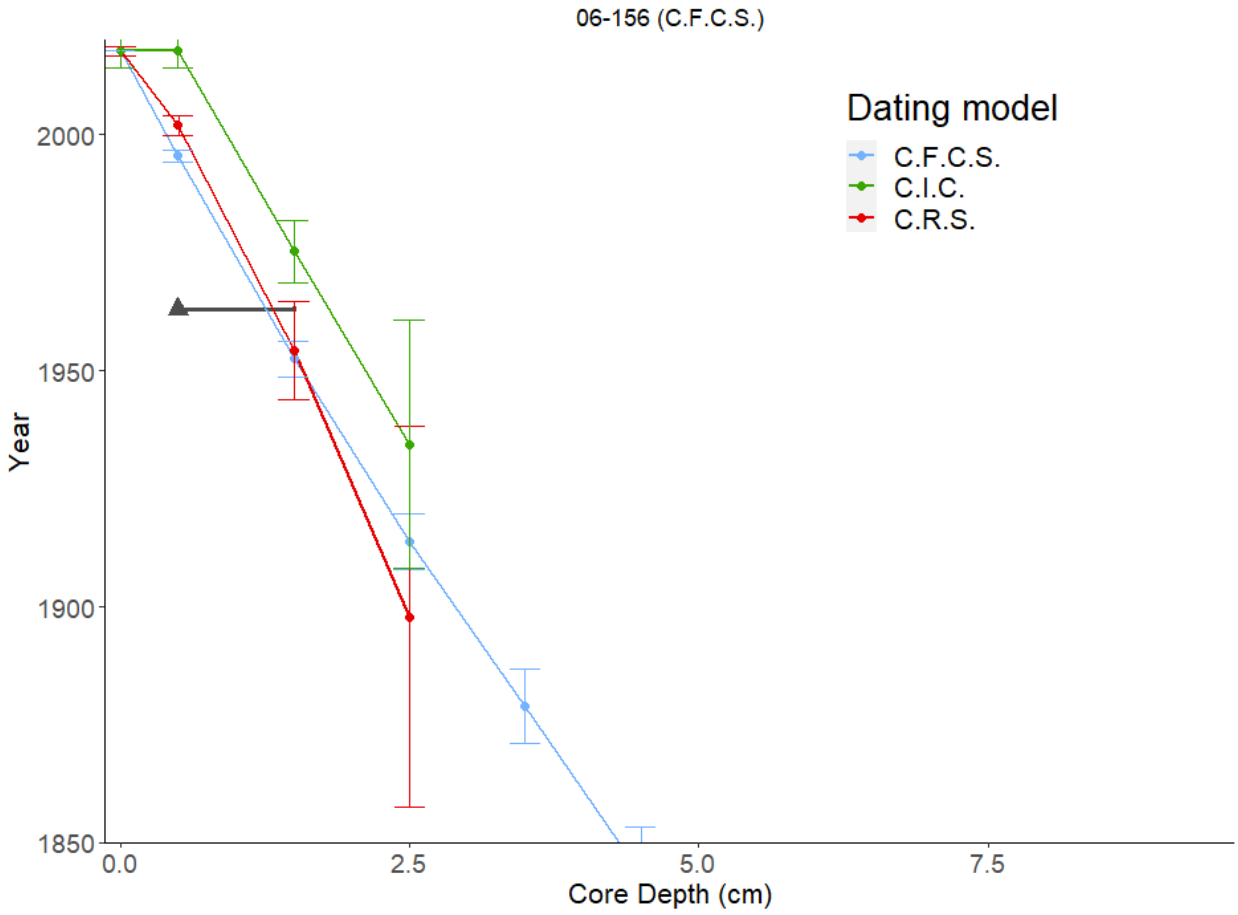
06-156 (C.F.C.S.)
Dating model
C.F.C.S.
C.I.C.
C.R.S.
Year
2000
1950
1900
1850
0.0
2.5
5.0
7.5
Core Depth (cm)

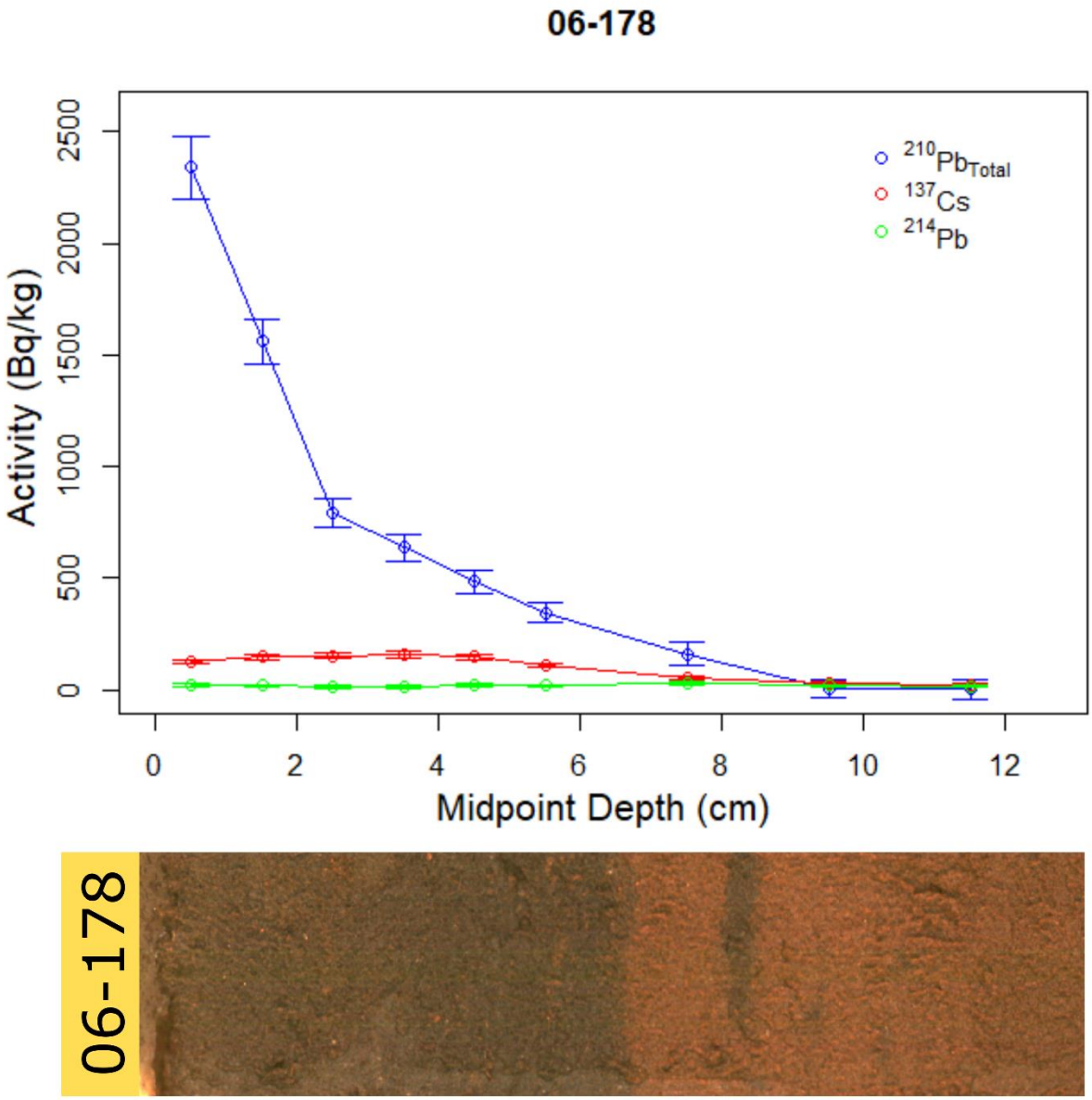
06-178
Activity (Bq/kg)
0
500
1000
1500
2000
2500
0
2
4
6
8
10
12
Midpoint Depth (cm)
$^{210}Pb_{Total}$
^{137}Cs
^{214}Pb
06-178

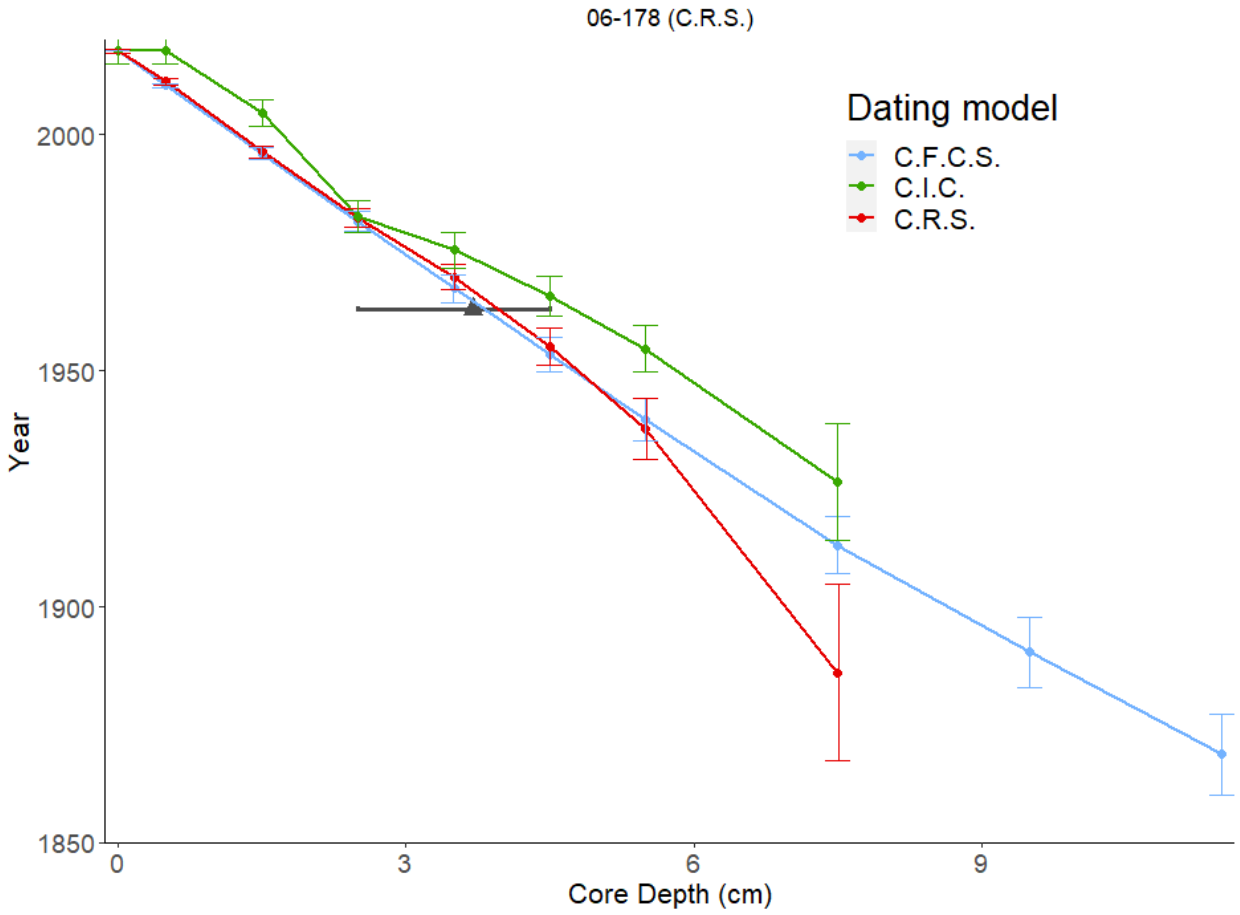
06-178 (C.R.S.)
Dating model
C.F.C.S.
C.I.C.
C.R.S.
Year
2000
1950
1900
1850
0
3
6
9
Core Depth (cm)

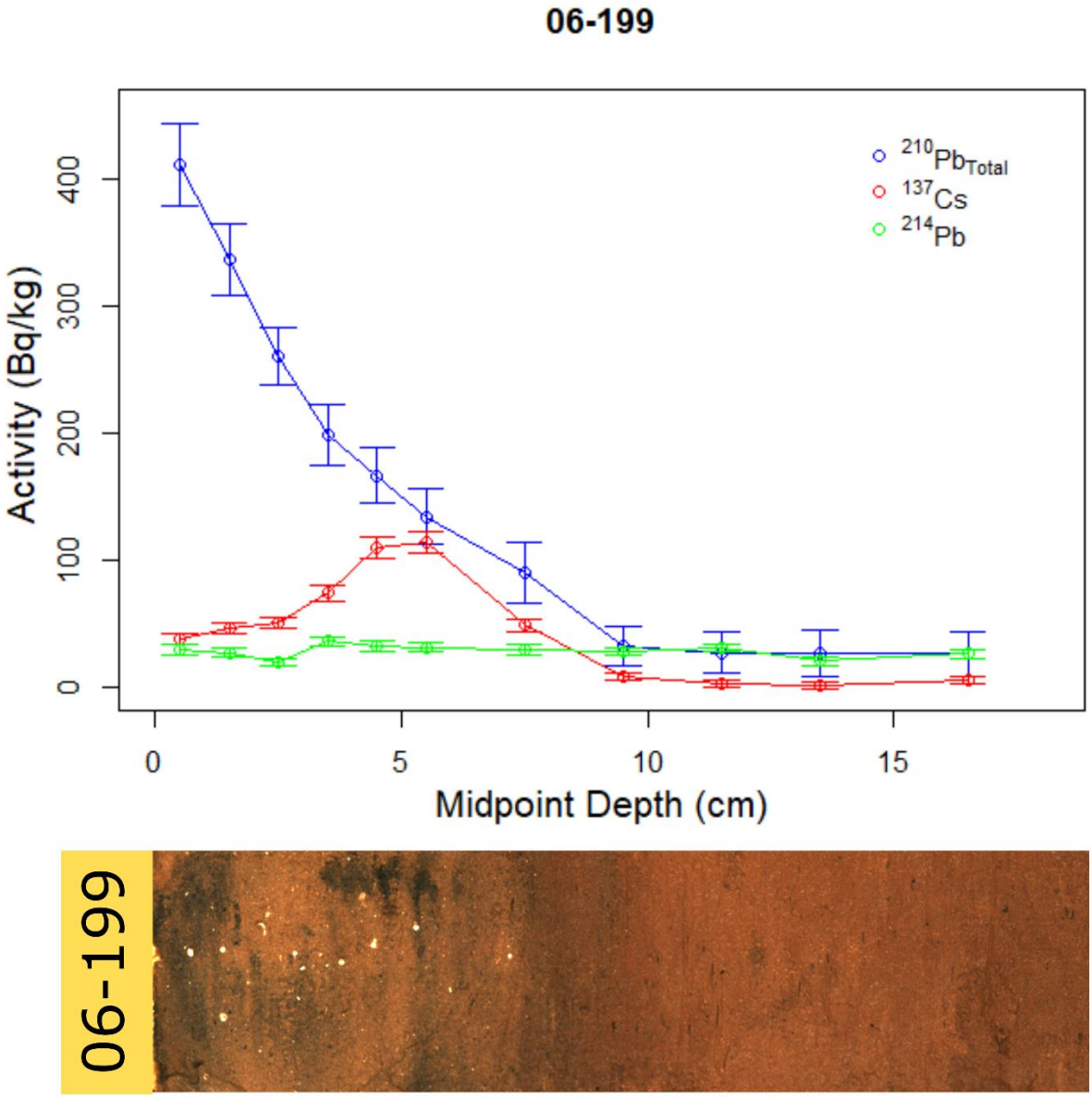
06-199
Activity (Bq/kg)
0
100
200
300
400
0
5
10
15
Midpoint Depth (cm)
$^{210}Pb_{Total}$
^{137}Cs
^{214}Pb

06-199

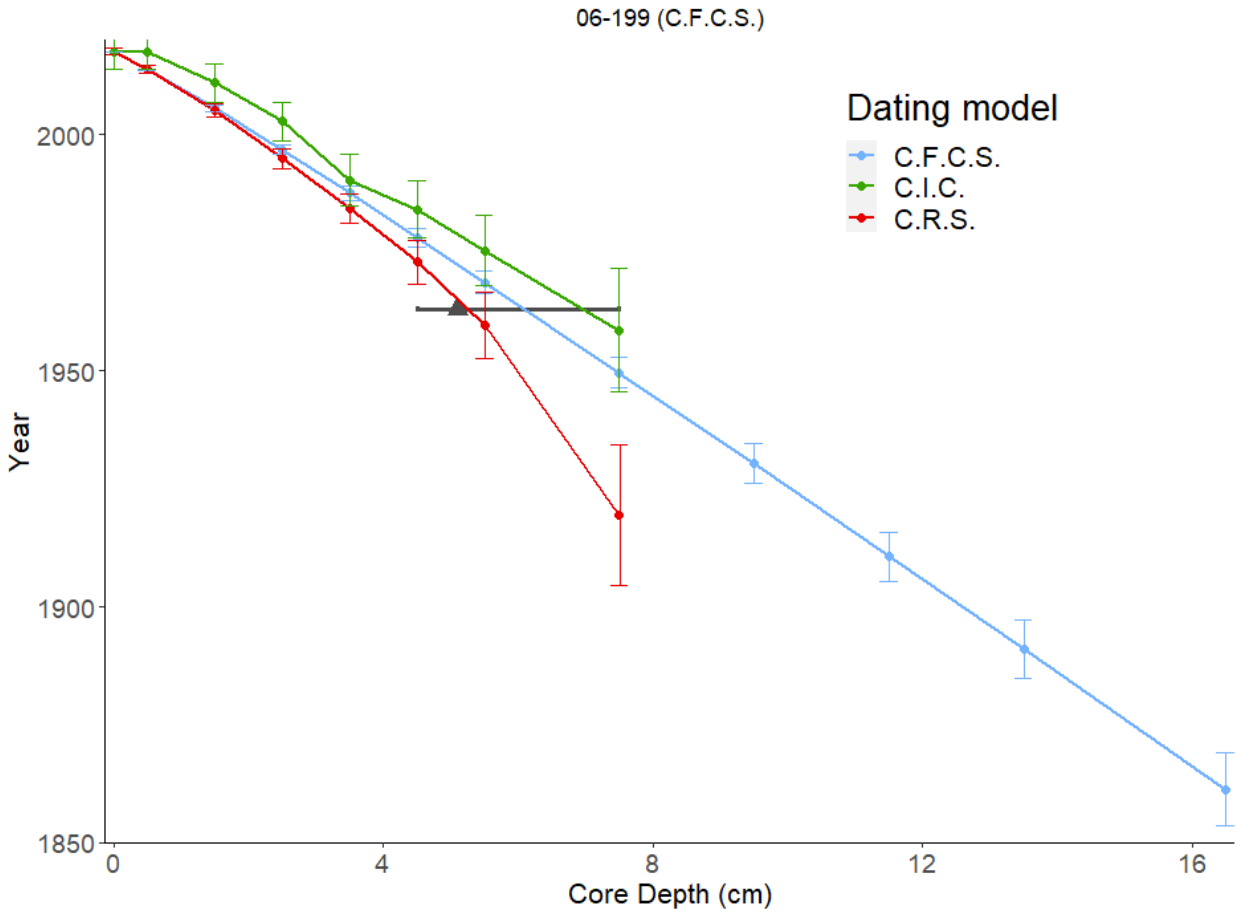
06-199 (C.F.C.S.)
Dating model
C.F.C.S.
C.I.C.
C.R.S.
Year
2000
1950
1900
1850
0
4
8
12
16
Core Depth (cm)

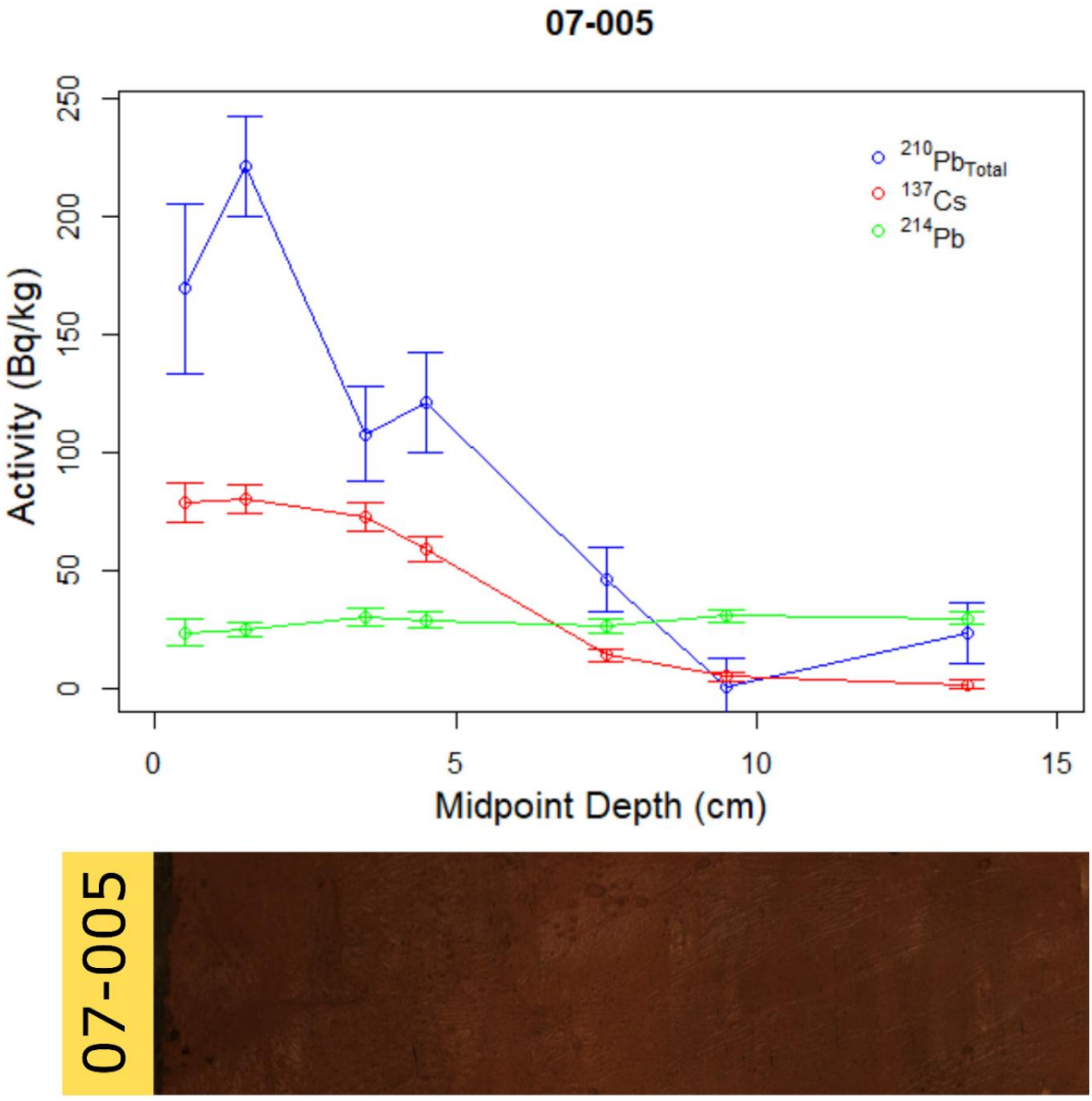
07-005
Activity (Bq/kg)
0
50
100
150
200
250
0
5
10
15
Midpoint Depth (cm)
$^{210}Pb_{Total}$
^{137}Cs
^{214}Pb

07-005

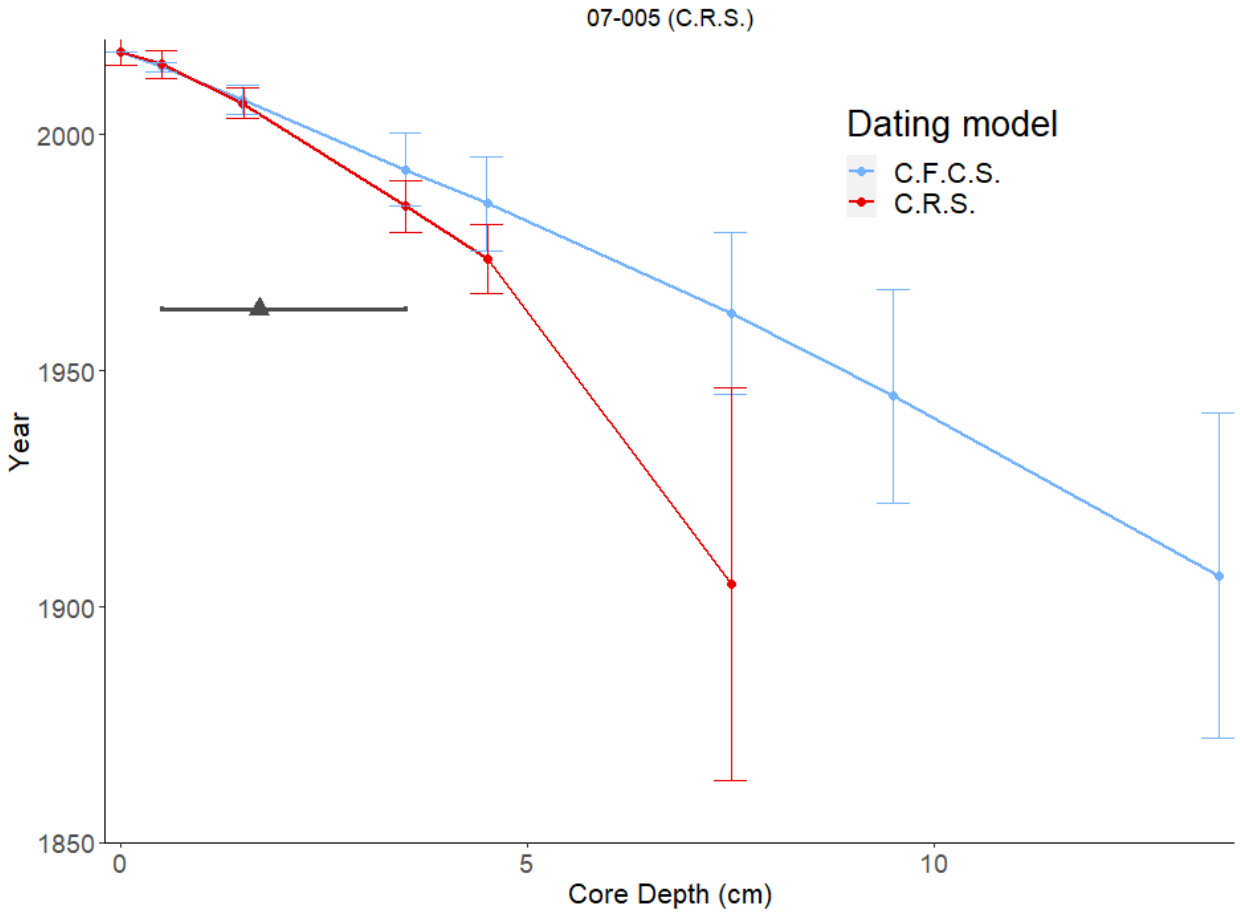
07-005 (C.R.S.)
Dating model
C.F.C.S.
C.R.S.
Year
2000
1950
1900
1850
0
5
10
Core Depth (cm)

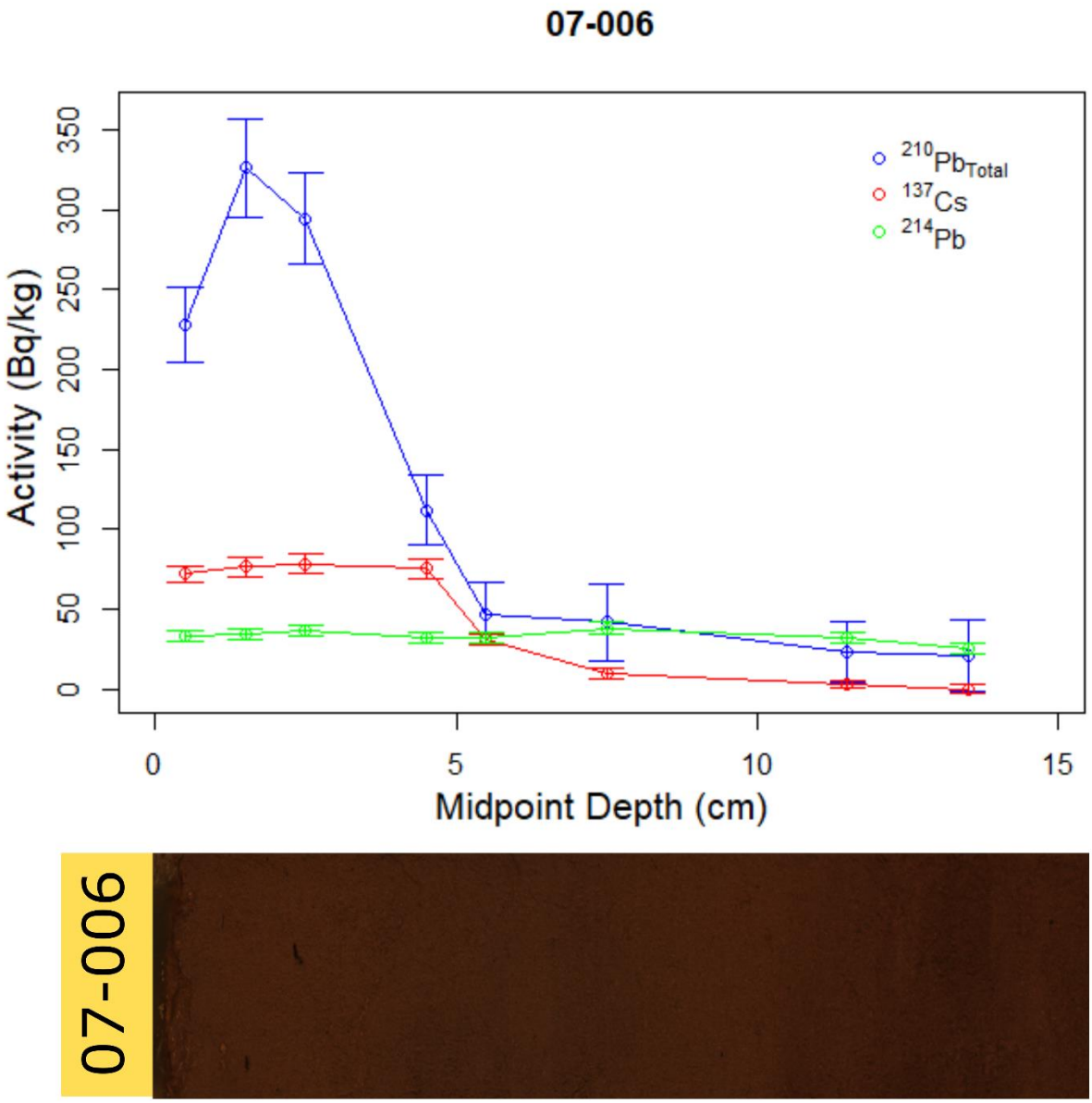
07-006
Activity (Bq/kg)
0
50
100
150
200
250
300
350
0
5
10
15
Midpoint Depth (cm)
$^{210}Pb_{Total}$
^{137}Cs
^{214}Pb

07-006

;;;;

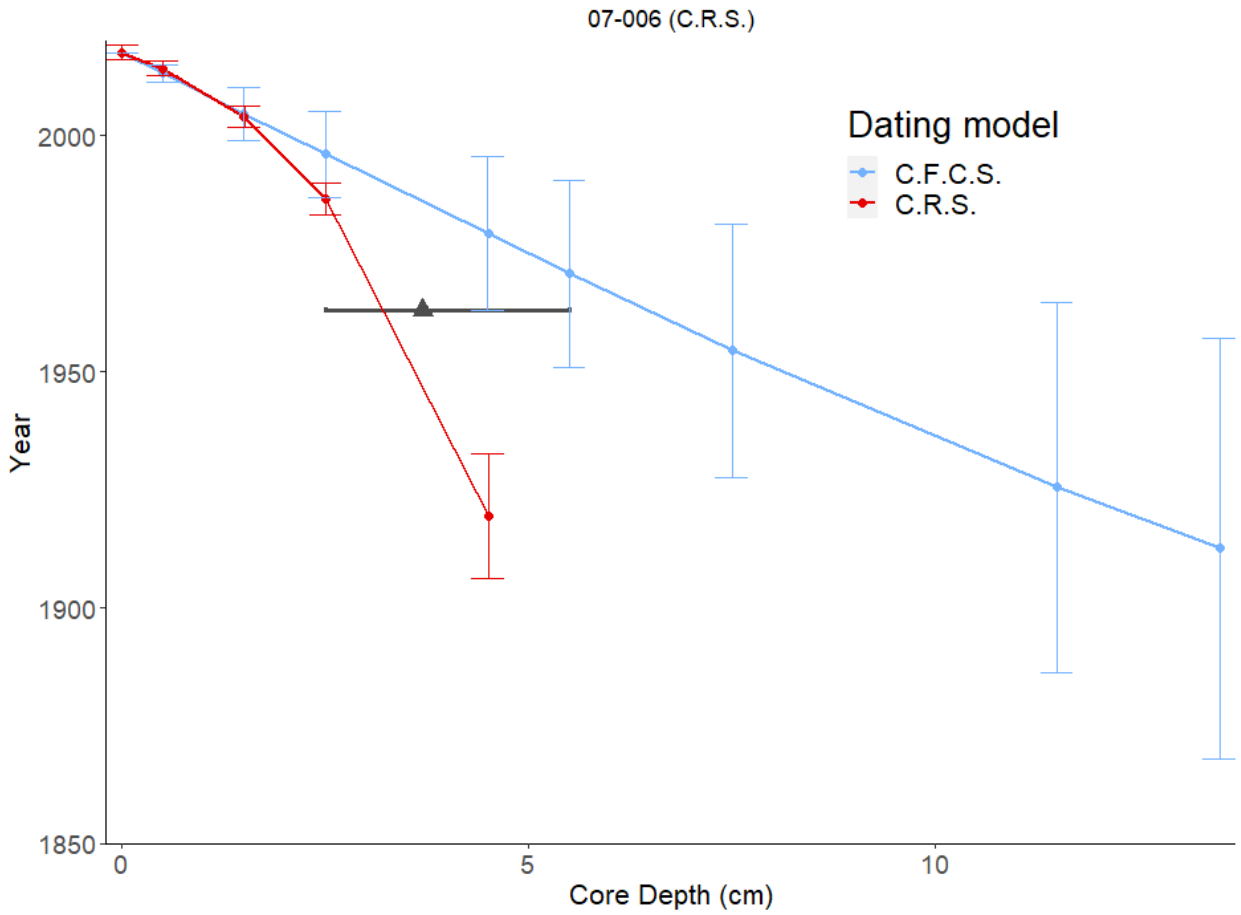
07-006 (C.R.S.)
Dating model
C.F.C.S.
C.R.S.
Year
2000
1950
1900
1850
0
5
10
Core Depth (cm)

;

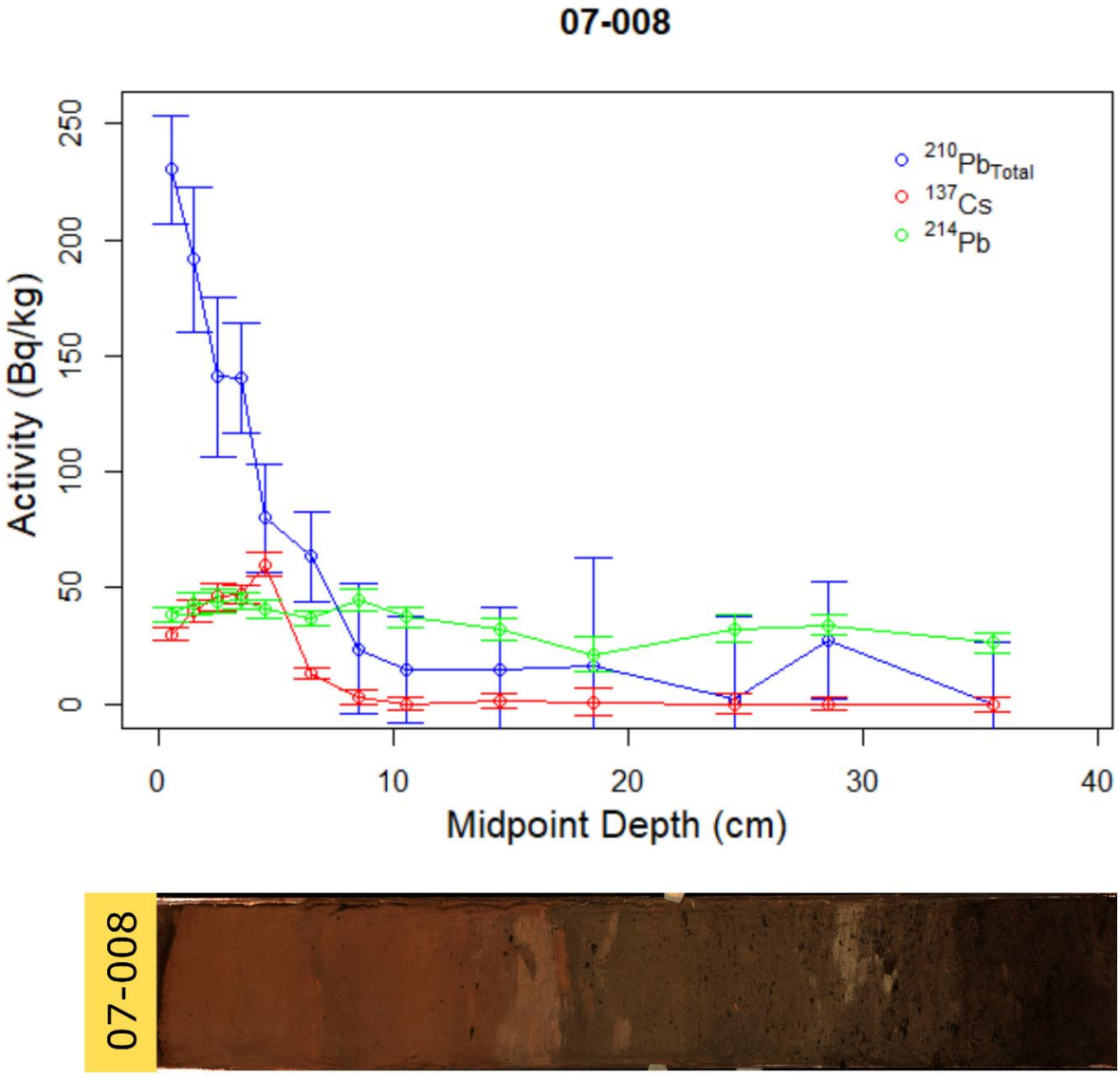
07-008
Activity (Bq/kg)
0
50
100
150
200
250
0
10
20
30
40
Midpoint Depth (cm)
210Pb Total
137Cs
214Pb
07-008

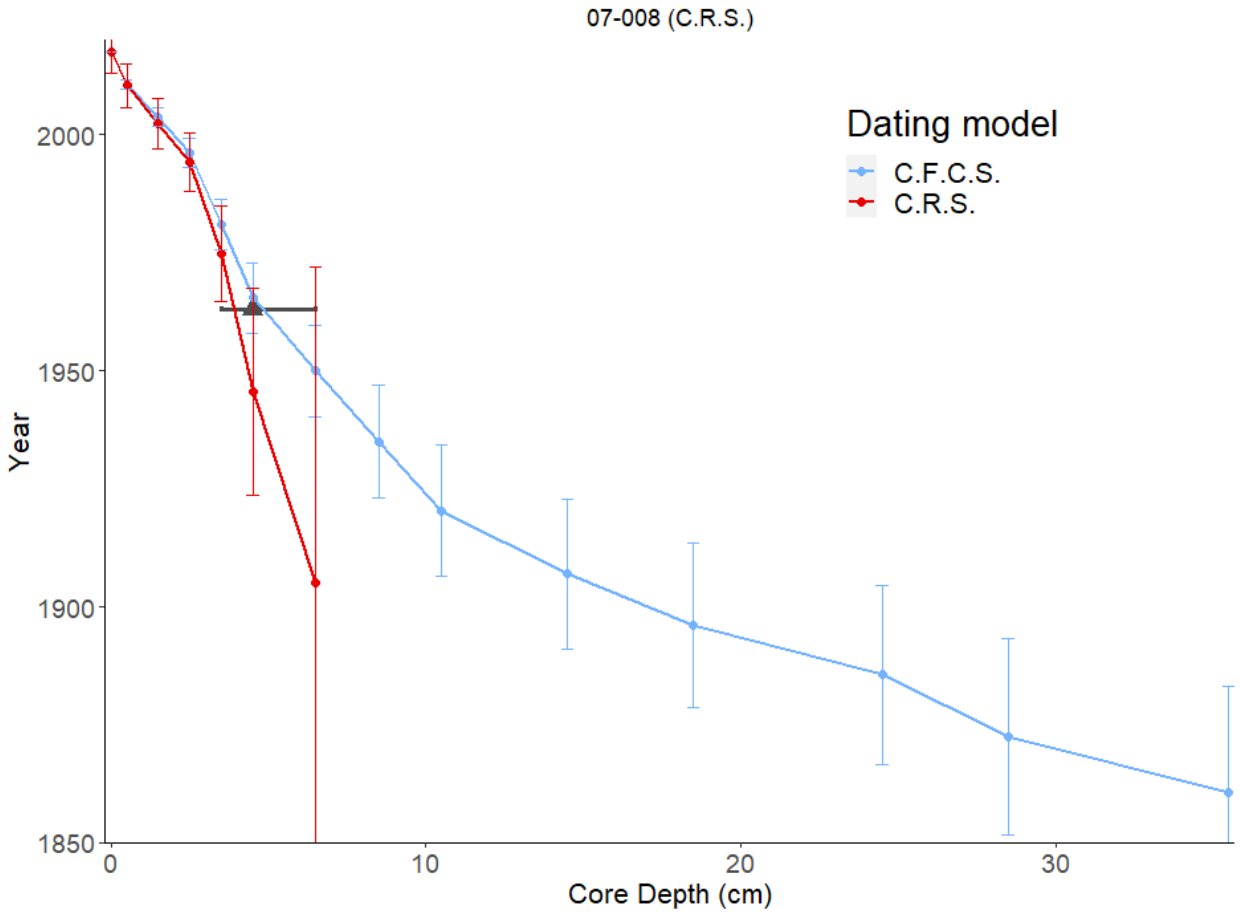
07-008 (C.R.S.)
Dating model
C.F.C.S.
C.R.S.
Year
2000
1950
1900
1850
0
10
20
30
Core Depth (cm)

40

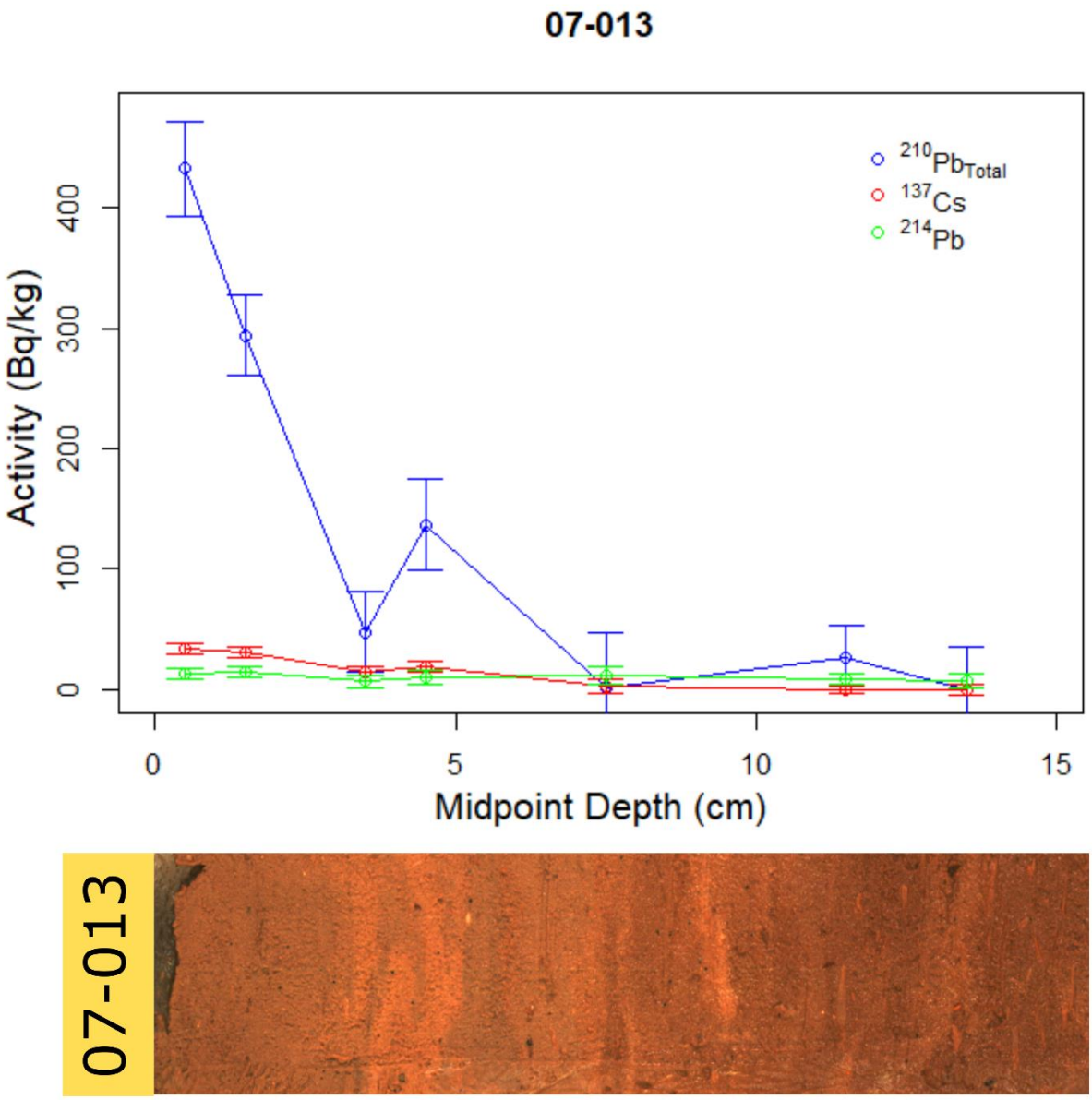
07-013
Activity (Bq/kg)
0
100
200
300
400
0
5
10
15
Midpoint Depth (cm)
$^{210}Pb_{Total}$
^{137}Cs
^{214}Pb

07-013

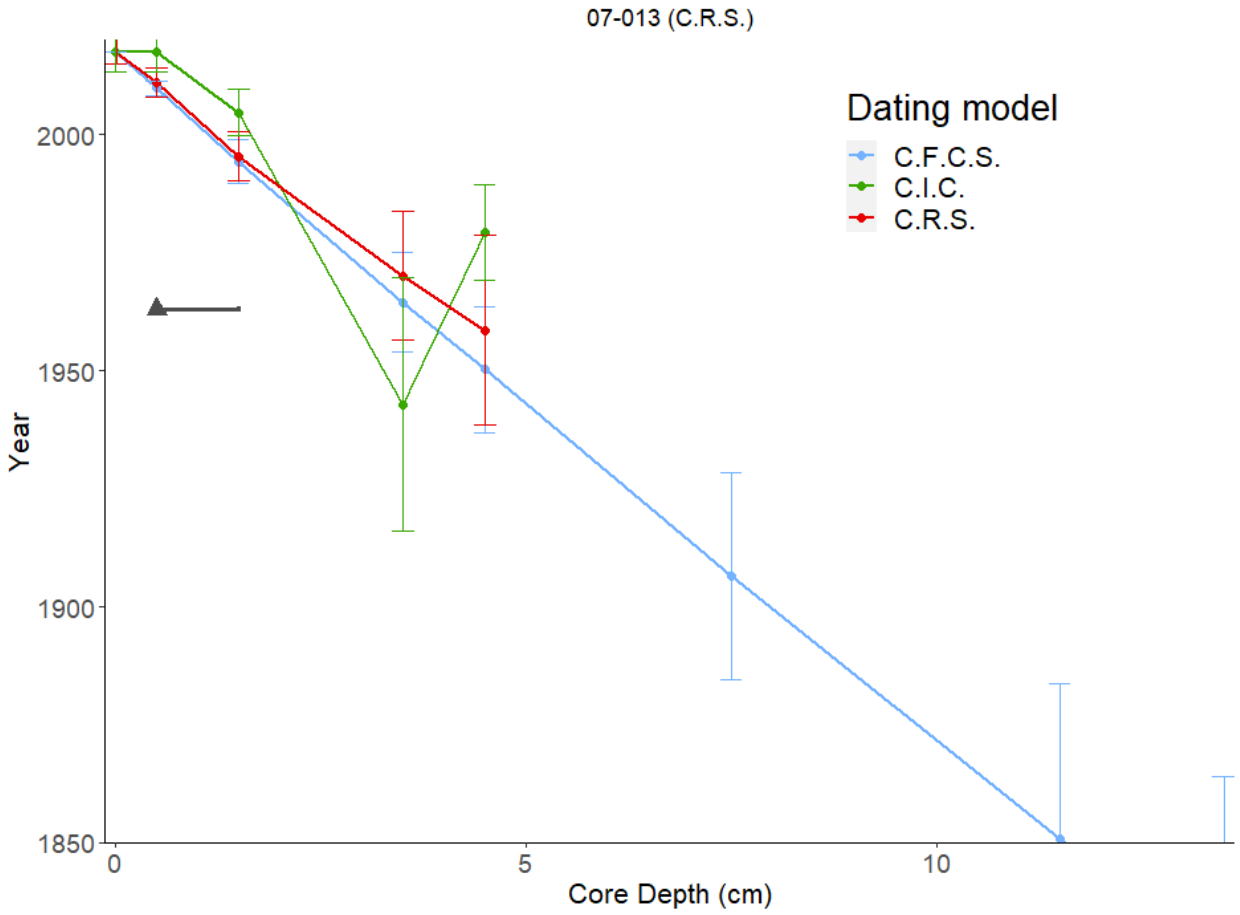
07-013 (C.R.S.)
Dating model
C.F.C.S.
C.I.C.
C.R.S.
Year
2000
1950
1900
1850
0
5
10
Core Depth (cm)

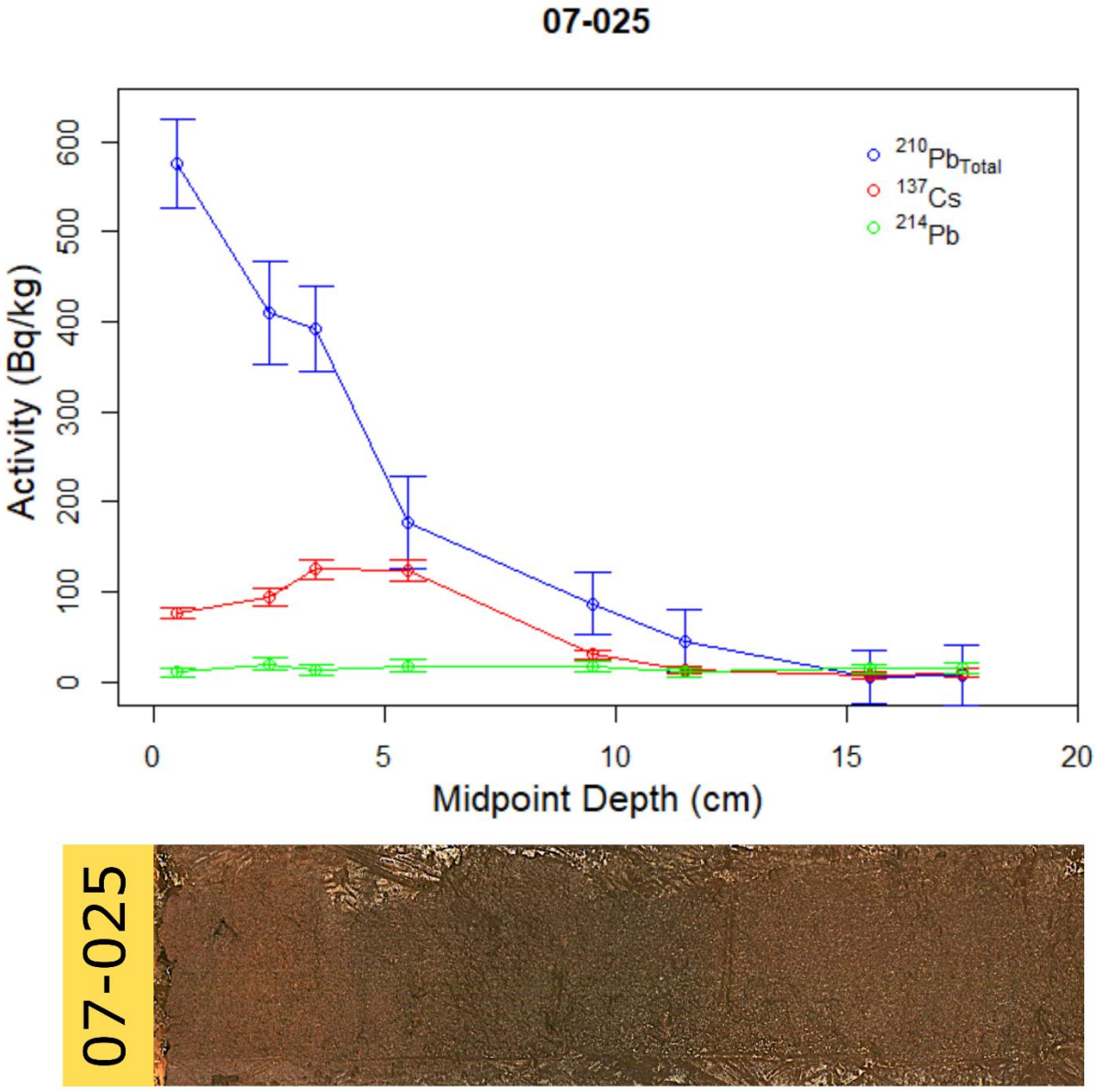
07-025
Activity (Bq/kg)
0
100
200
300
400
500
600
0
5
10
15
20
Midpoint Depth (cm)
$^{210}Pb_{Total}$
^{137}Cs
^{214}Pb

07-025

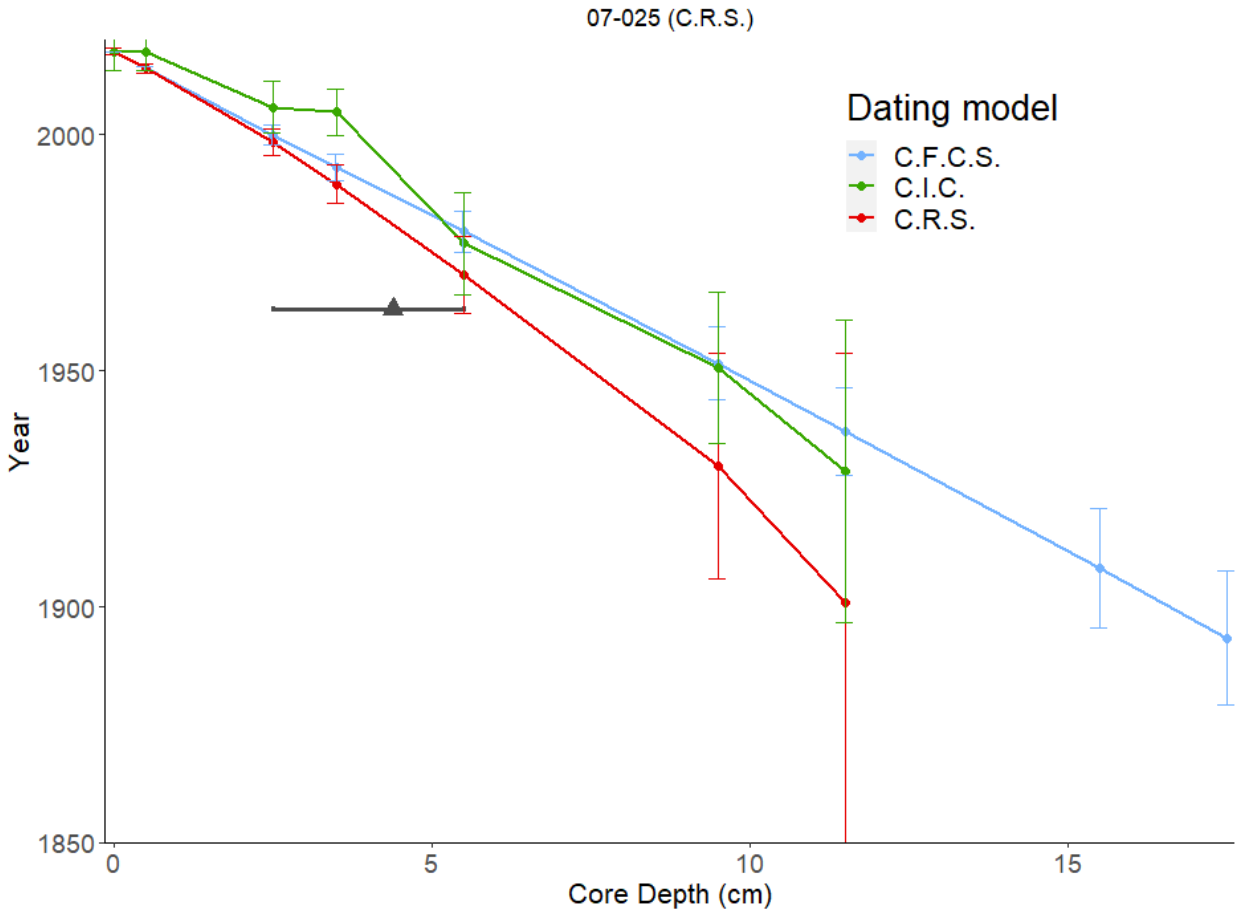
07-025 (C.R.S.)
Dating model
C.F.C.S.
C.I.C.
C.R.S.
Year
2000
1950
1900
1850
0
5
10
15
Core Depth (cm)

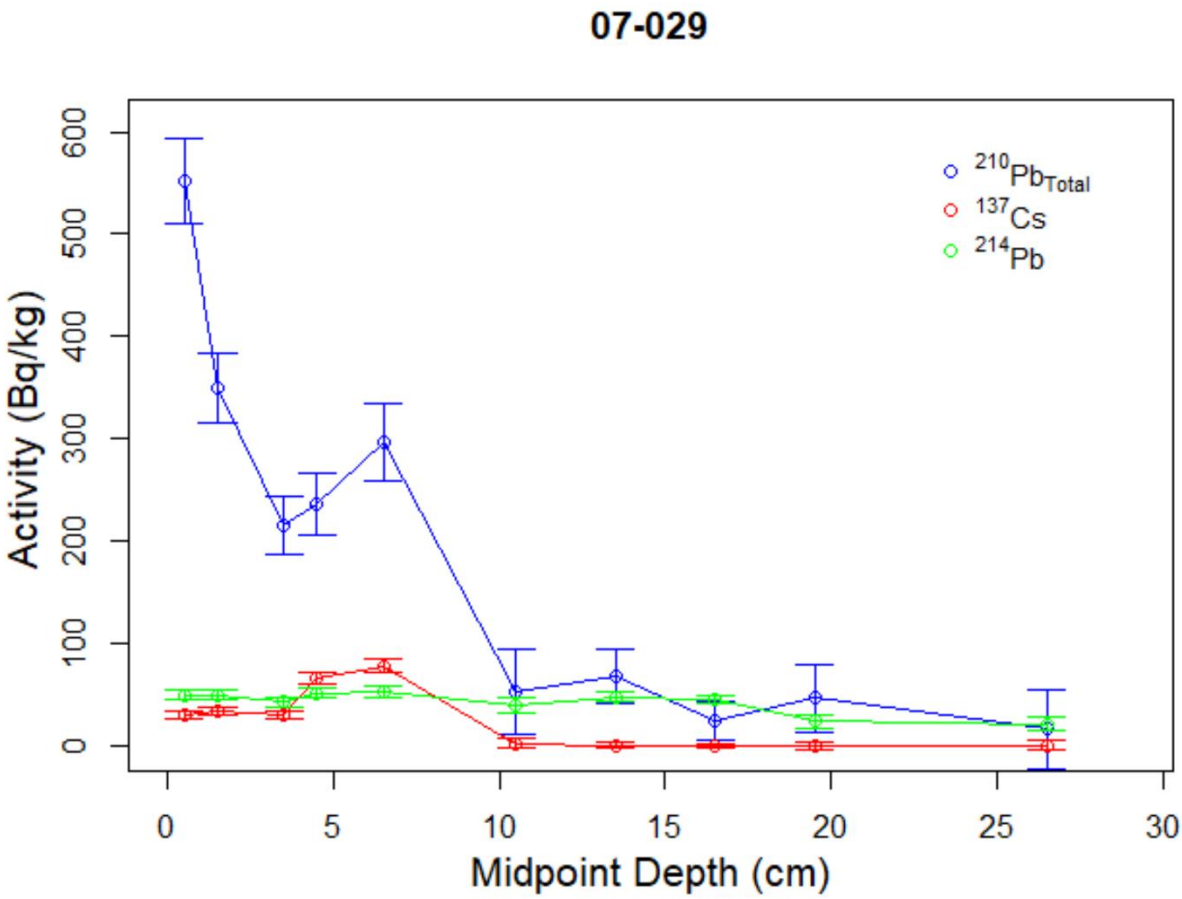
07-029
Activity (Bq/kg)
0
100
200
300
400
500
600
0
5
10
15
20
25
30
Midpoint Depth (cm)
$^{210}Pb_{Total}$
^{137}Cs
^{214}Pb


07-029

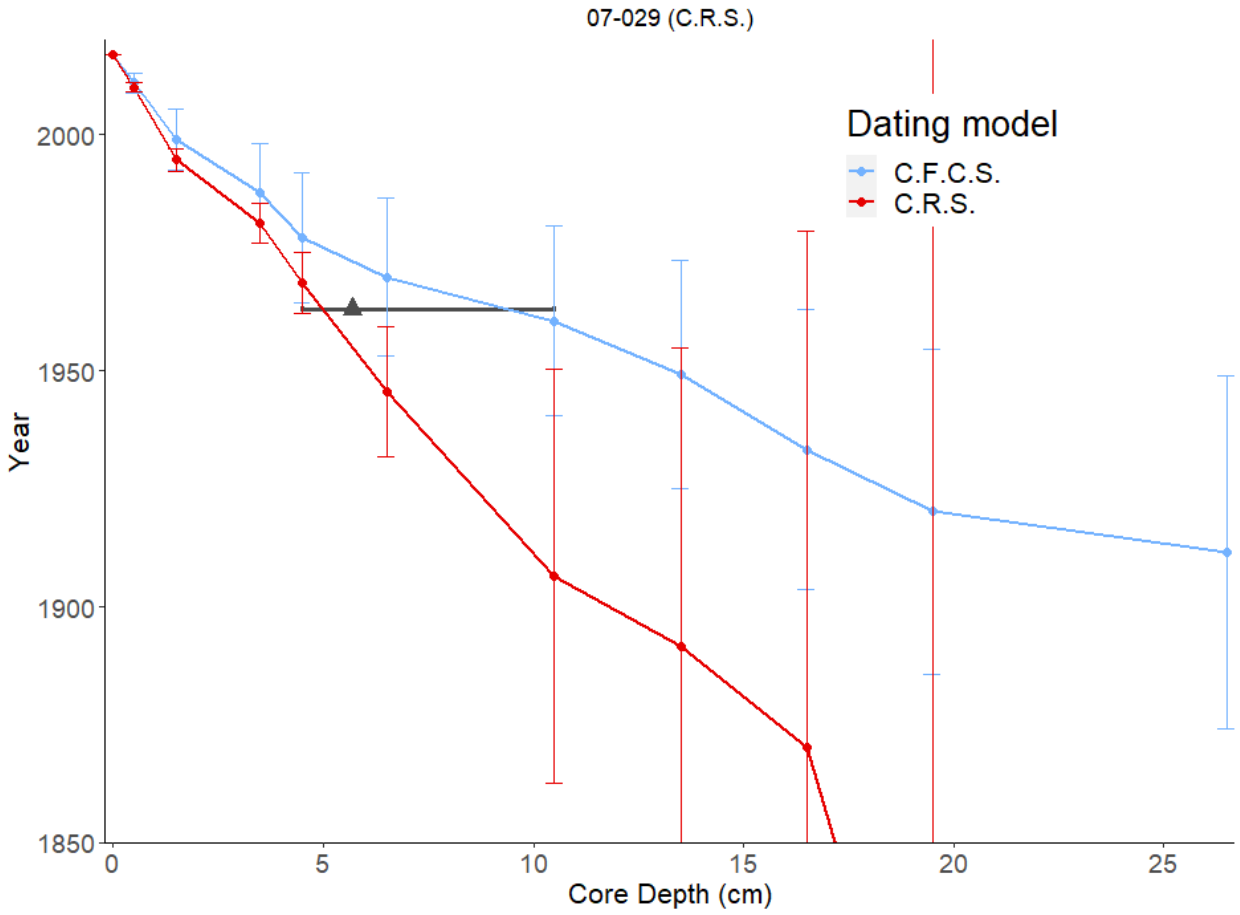
07-029 (C.R.S.)
Dating model
C.F.C.S.
C.R.S.
Year
2000
1950
1900
1850
0
5
10
15
20
25
Core Depth (cm)

d

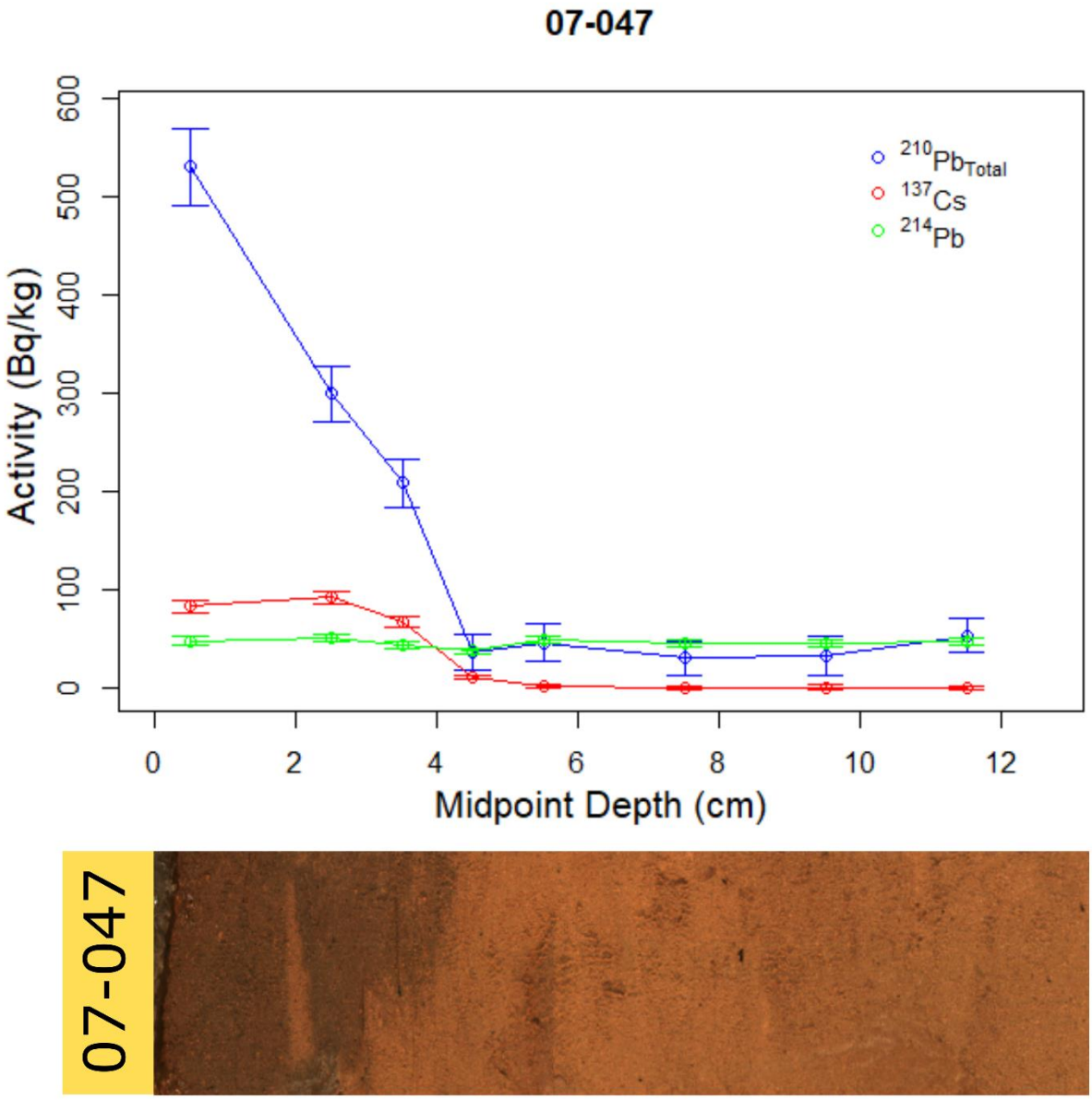
07-047
Activity (Bq/kg)
0
100
200
300
400
500
600
0
2
4
6
8
10
12
Midpoint Depth (cm)
$^{210}Pb_{Total}$
^{137}Cs
^{214}Pb

07-047

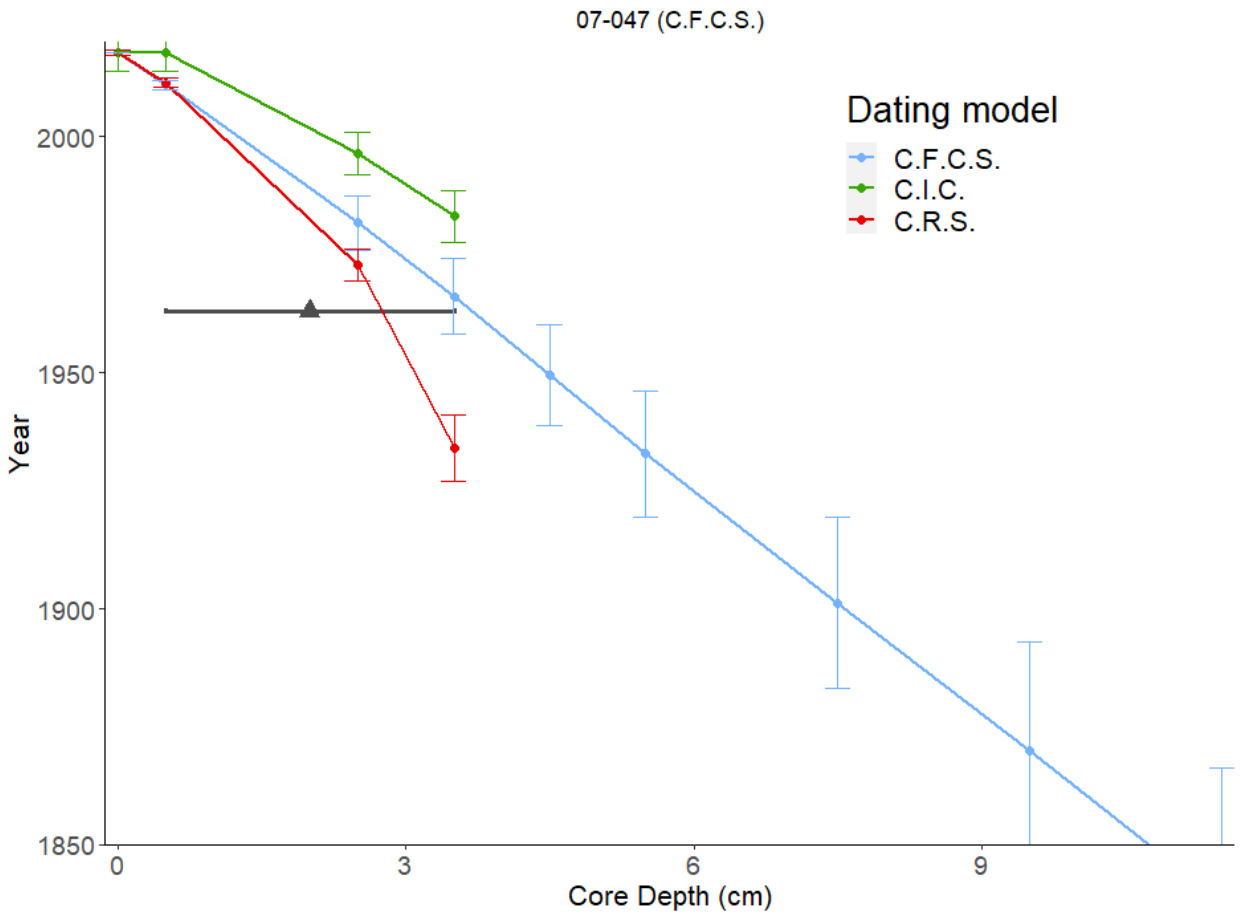
07-047 (C.F.C.S.)
Dating model
C.F.C.S.
C.I.C.
C.R.S.
Year
2000
1950
1900
1850
0
3
6
9
Core Depth (cm)

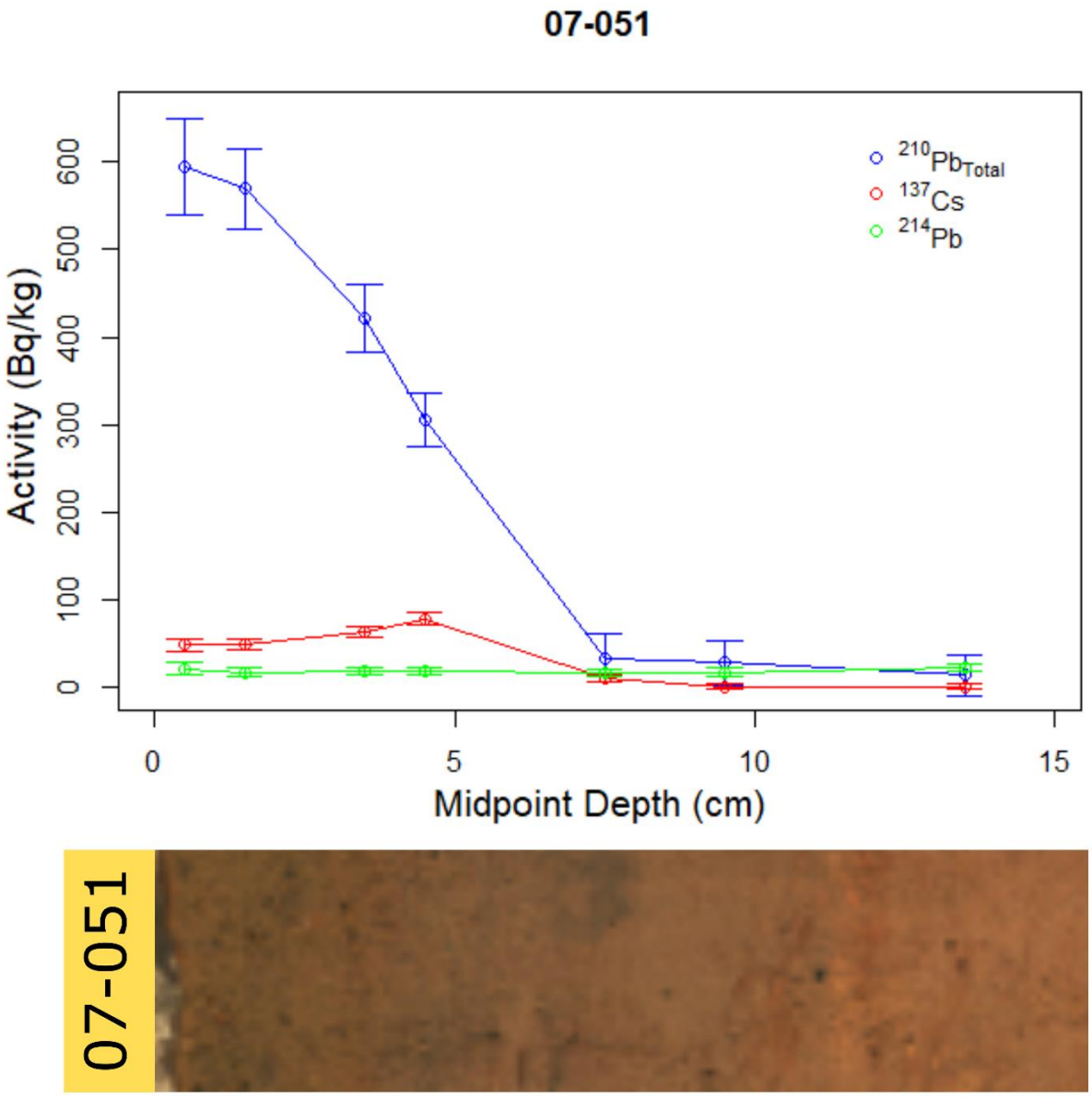
07-051
Activity (Bq/kg)
0
100
200
300
400
500
600
0
5
10
15
Midpoint Depth (cm)
$^{210}Pb_{Total}$
^{137}Cs
^{214}Pb

07-051

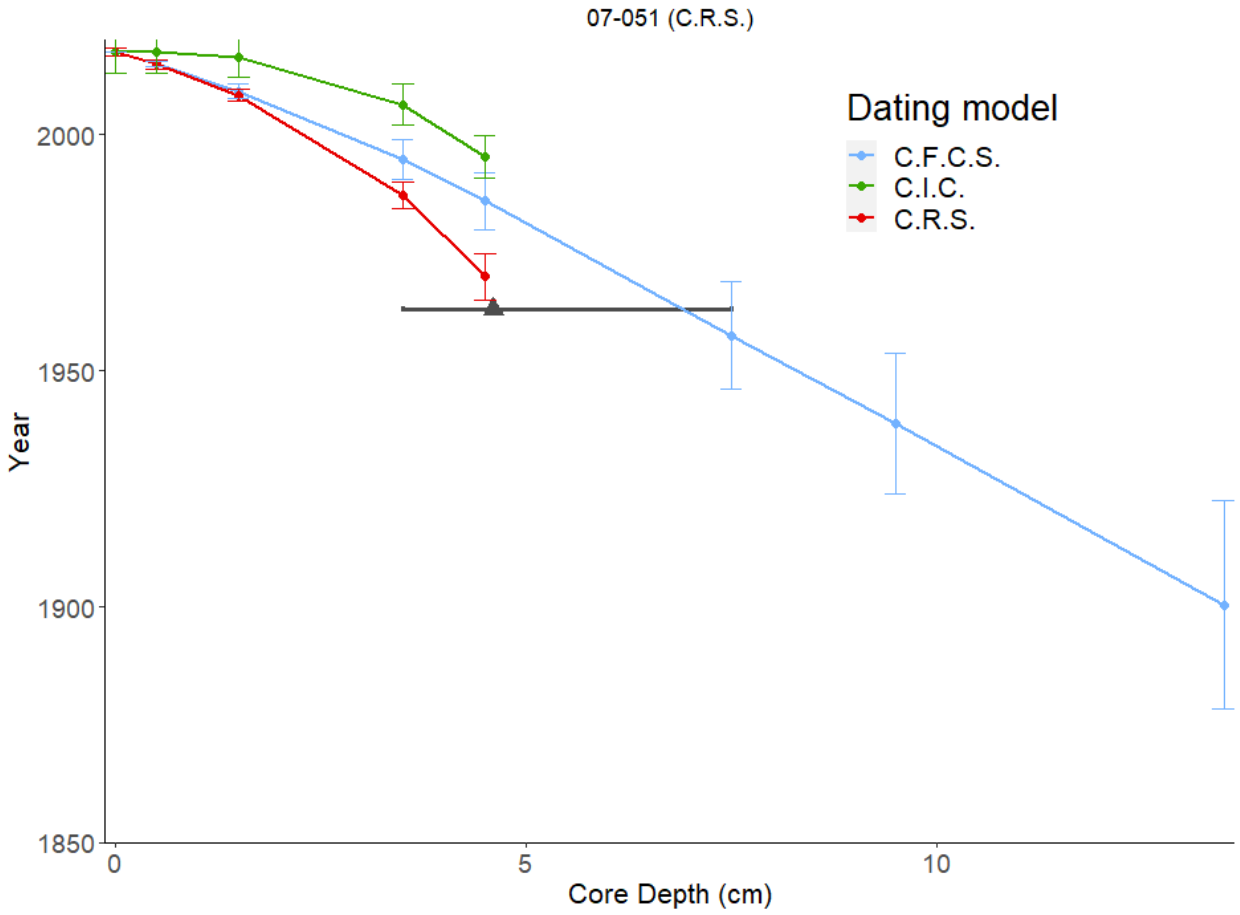
07-051 (C.R.S.)
Dating model
C.F.C.S.
C.I.C.
C.R.S.
Year
2000
1950
1900
1850
0
5
10
Core Depth (cm)

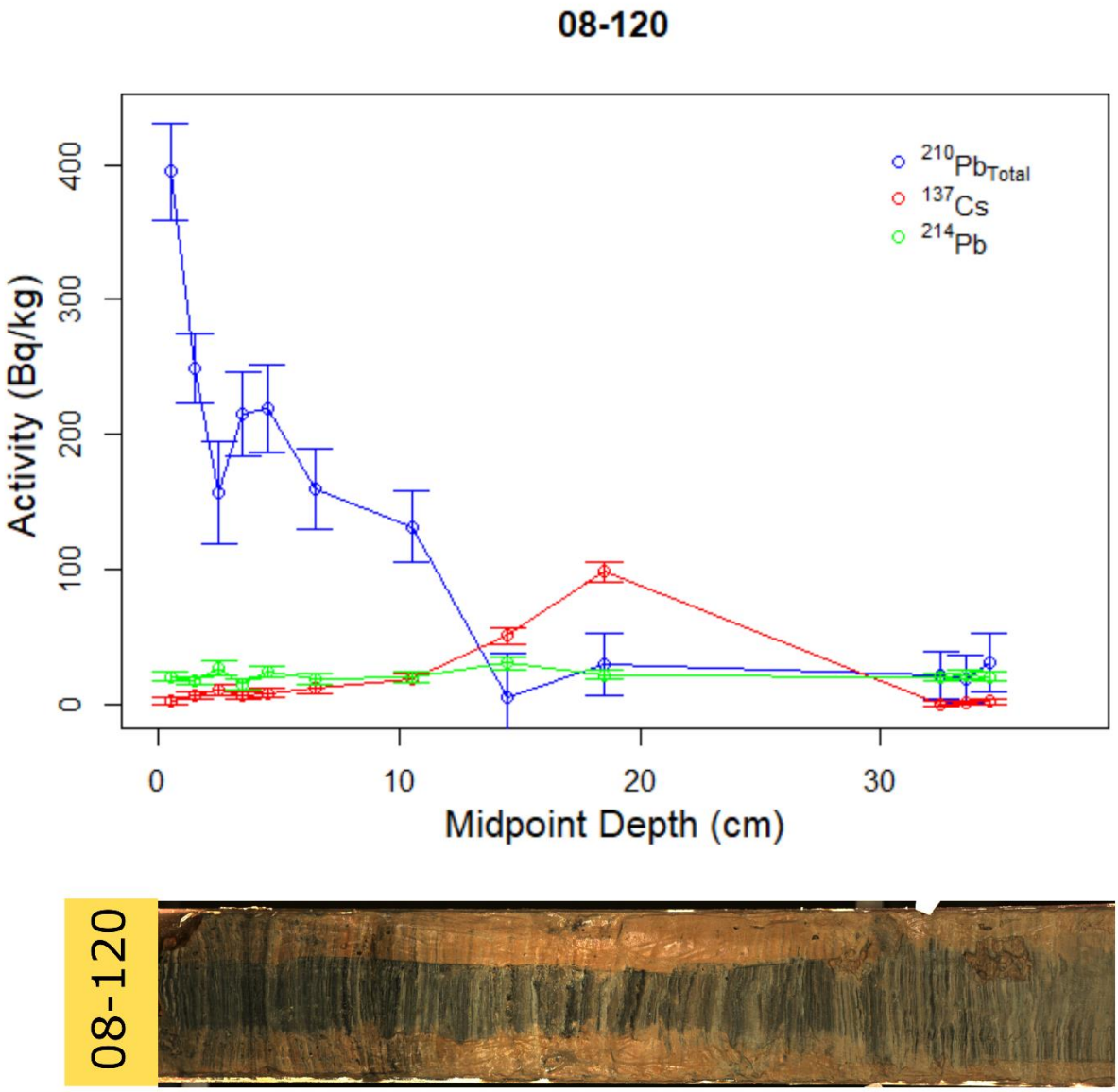
08-120
Activity (Bq/kg)
0
100
200
300
400
0
10
20
30
Midpoint Depth (cm)
$^{210}Pb_{Total}$
^{137}Cs
^{214}Pb
08-120

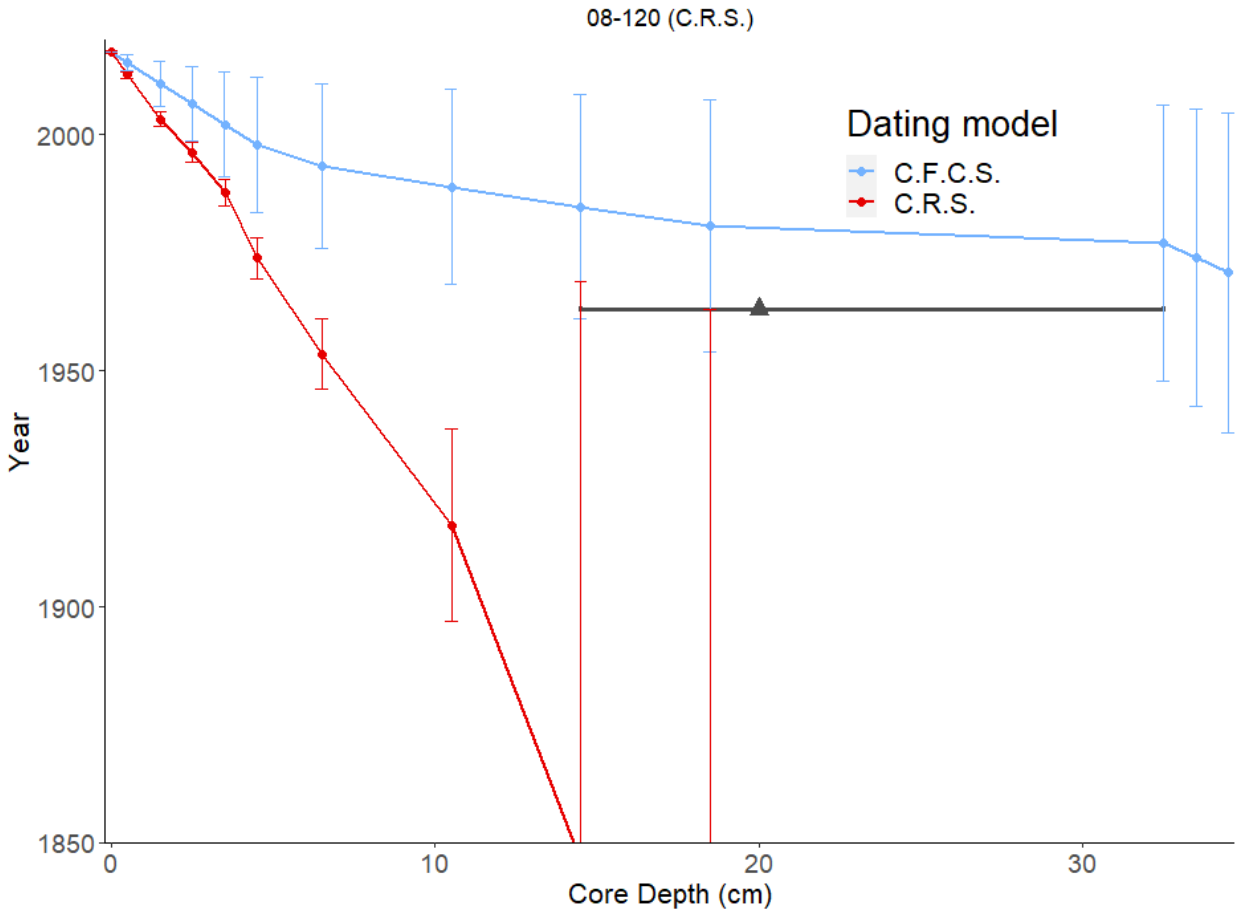
08-120 (C.R.S.)
Dating model
C.F.C.S.
C.R.S.
Year
2000
1950
1900
1850
0
10
20
30
Core Depth (cm)

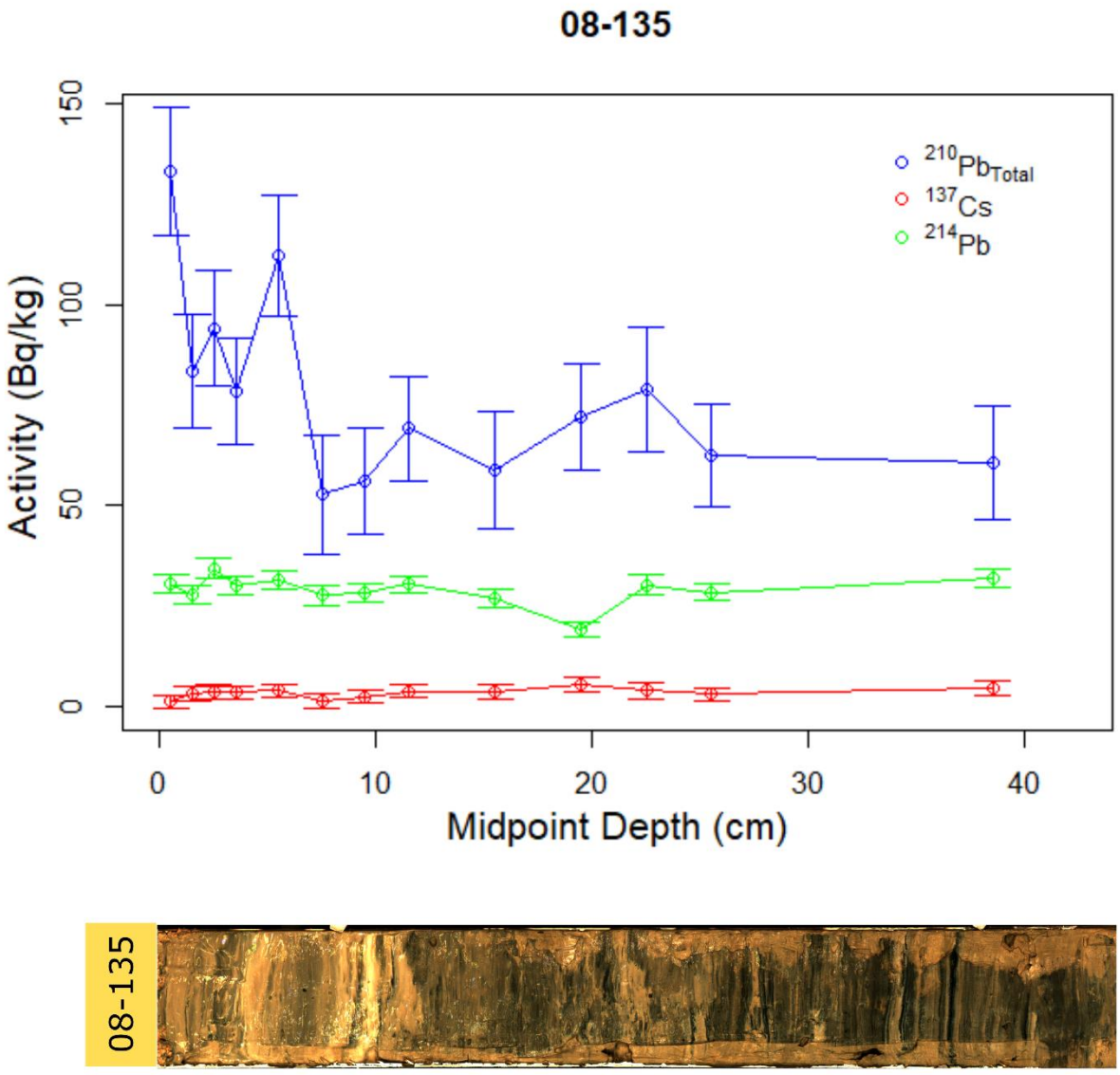
08-135
Activity (Bq/kg)
0
50
100
150
0
10
20
30
40
Midpoint Depth (cm)
$^{210}Pb_{Total}$
^{137}Cs
^{214}Pb

08-135

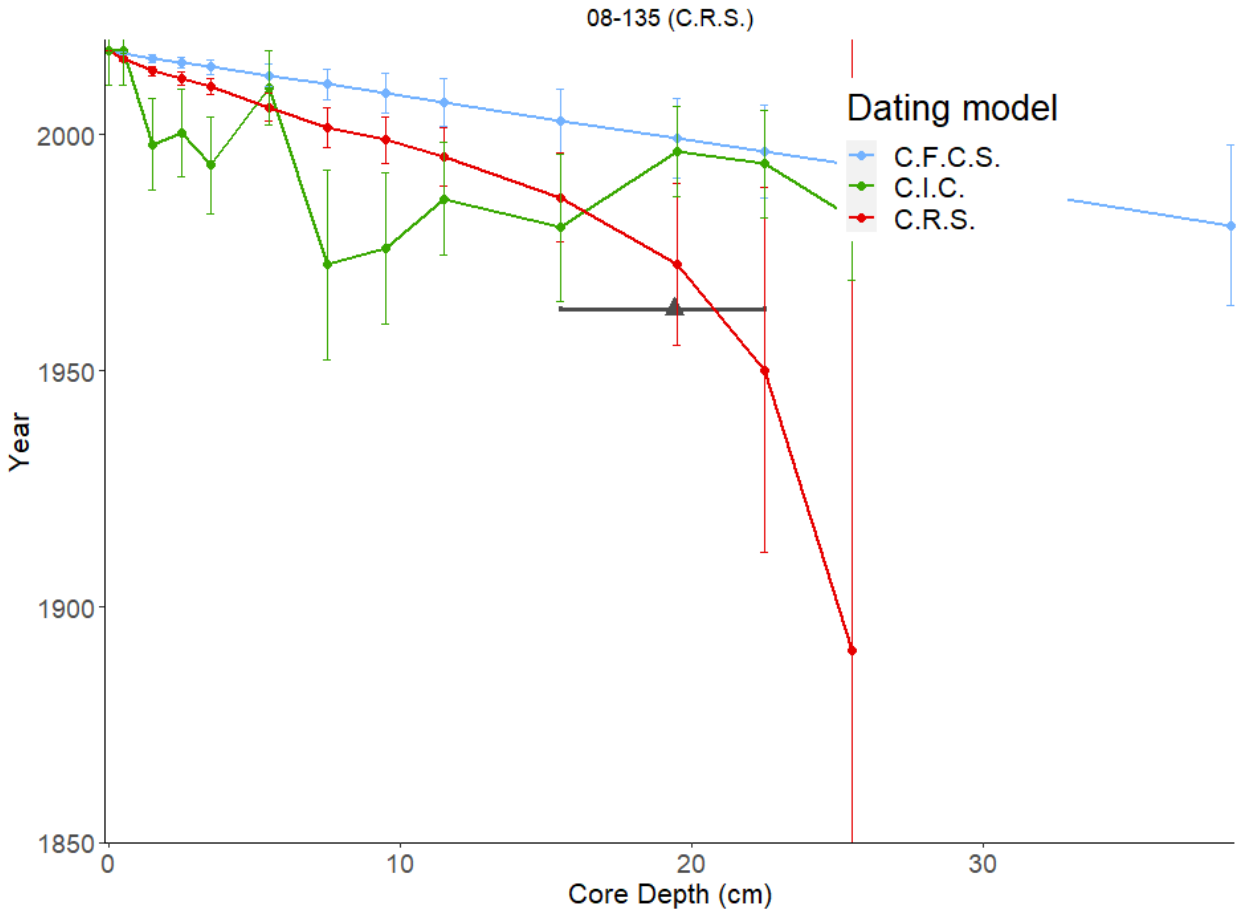
08-135 (C.R.S.)
Dating model
C.F.C.S.
C.I.C.
C.R.S.
Year
2000
1950
1900
1850
0
10
20
30
Core Depth (cm)

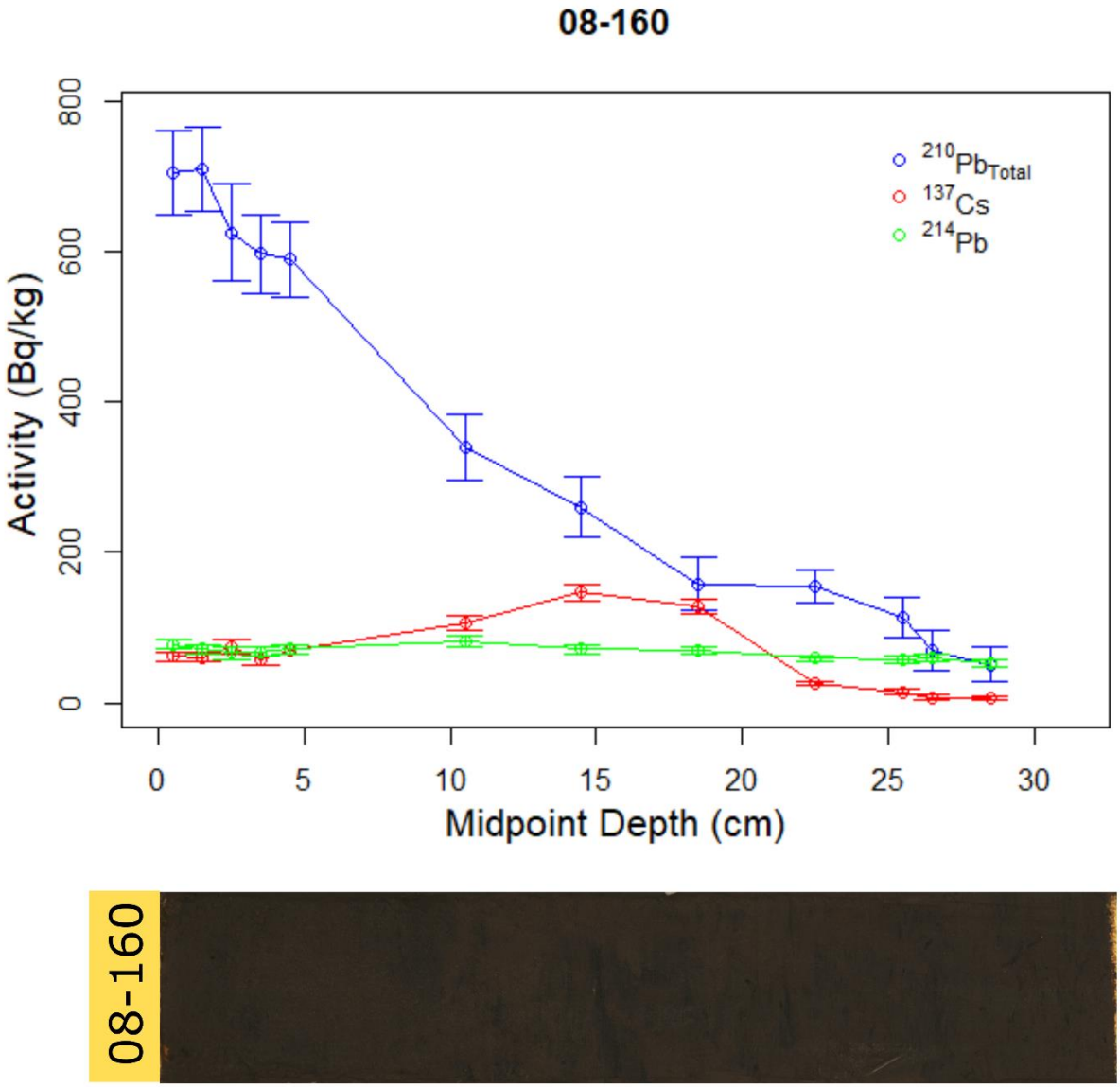
08-160
Activity (Bq/kg)
0
200
400
600
800
0
5
10
15
20
25
30
Midpoint Depth (cm)
$^{210}Pb_{Total}$
^{137}Cs
^{214}Pb
08-160

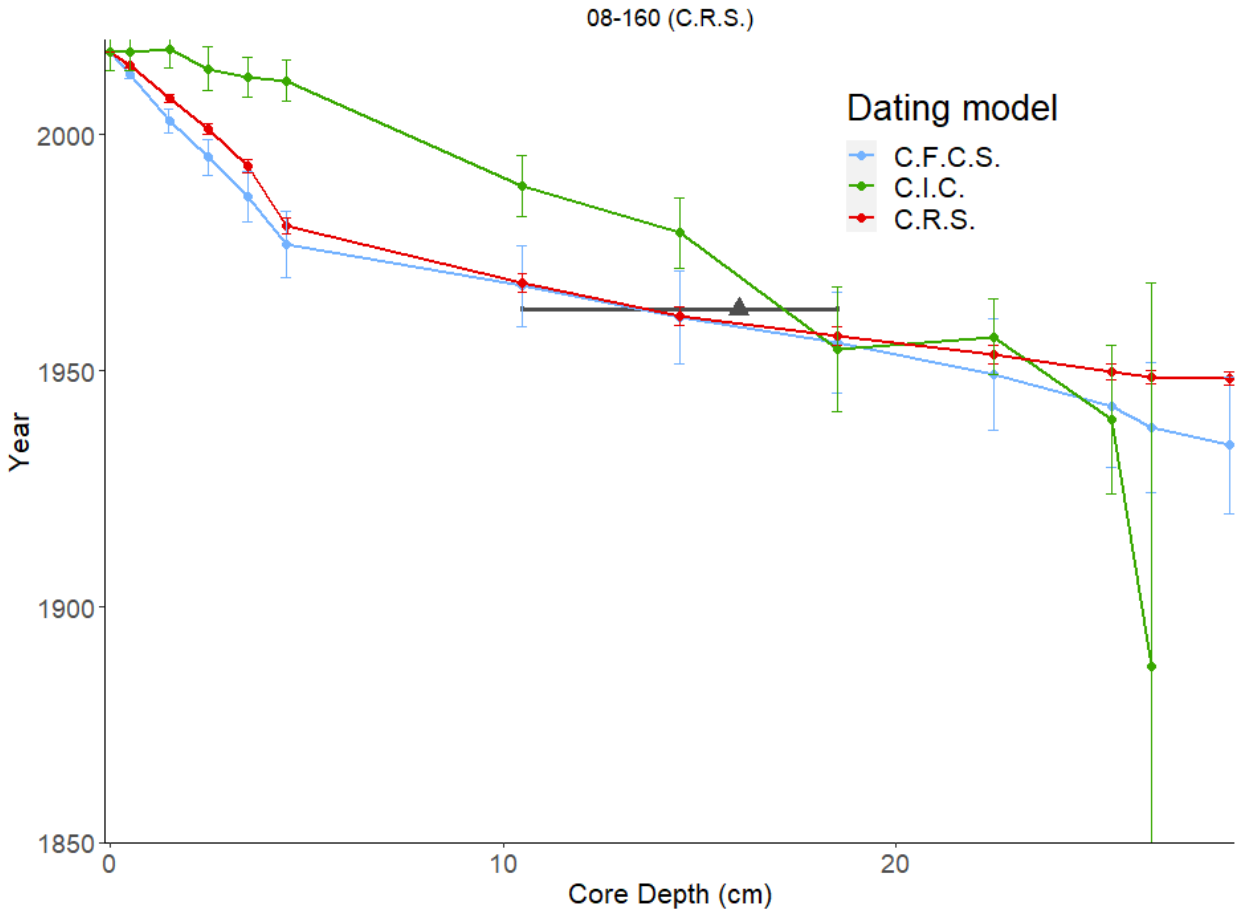
08-160 (C.R.S.)
Dating model
C.F.C.S.
C.I.C.
C.R.S.
Year
2000
1950
1900
1850
0
10
20
Core Depth (cm)

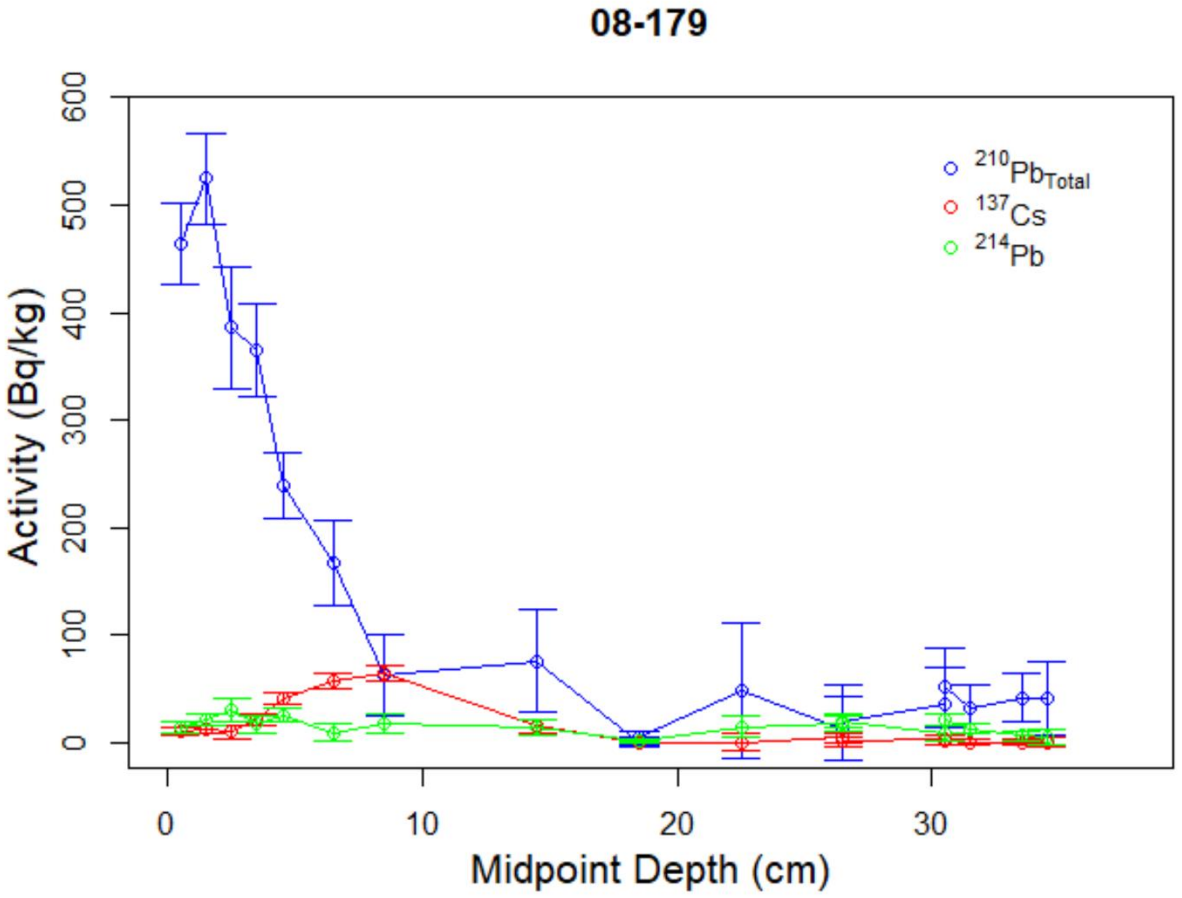
08-179
Activity (Bq/kg)
0
100
200
300
400
500
600
0
10
20
30
Midpoint Depth (cm)
$^{210}Pb_{Total}$
^{137}Cs
^{214}Pb


08-179

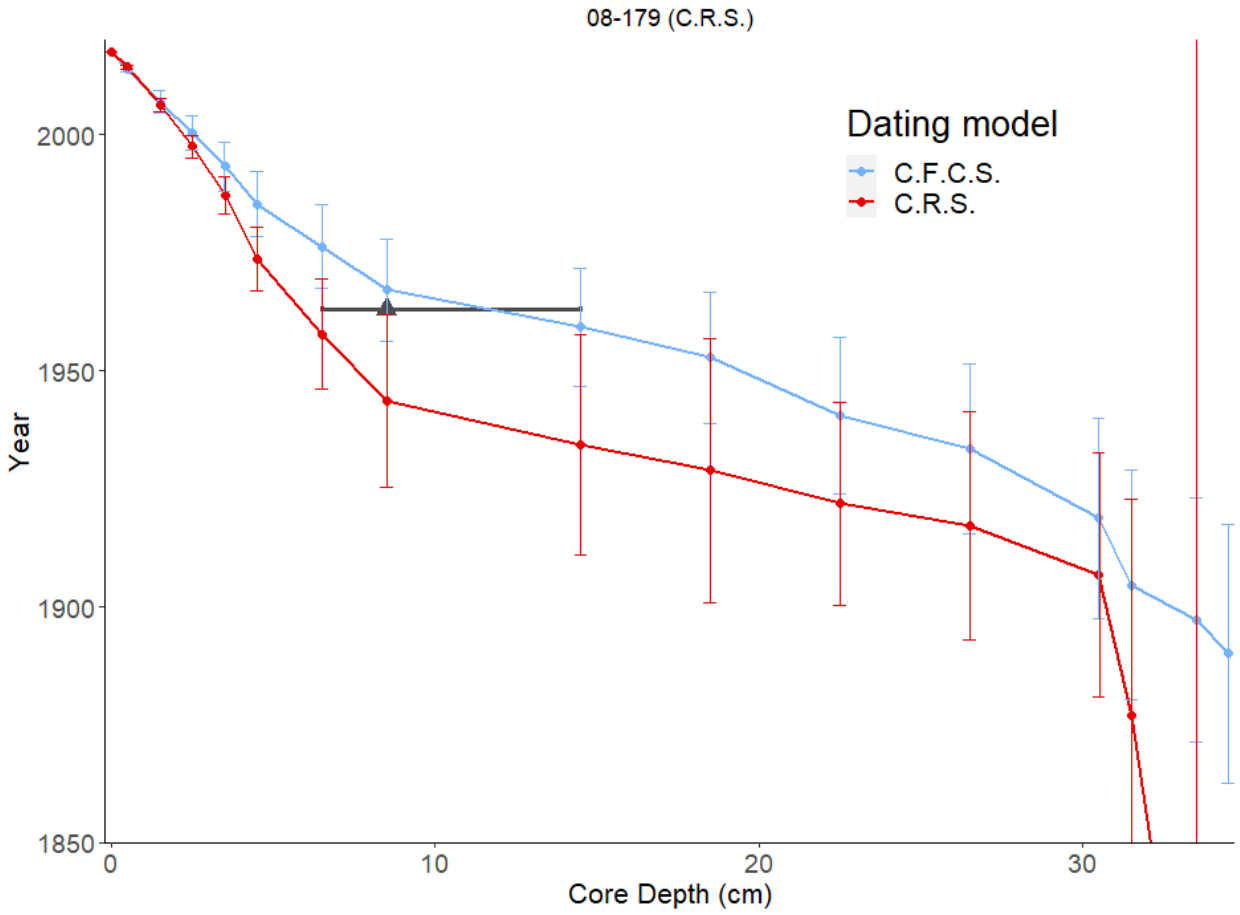
08-179 (C.R.S.)
Dating model
C.F.C.S.
C.R.S.
Year
2000
1950
1900
1850
0
10
20
30
Core Depth (cm)

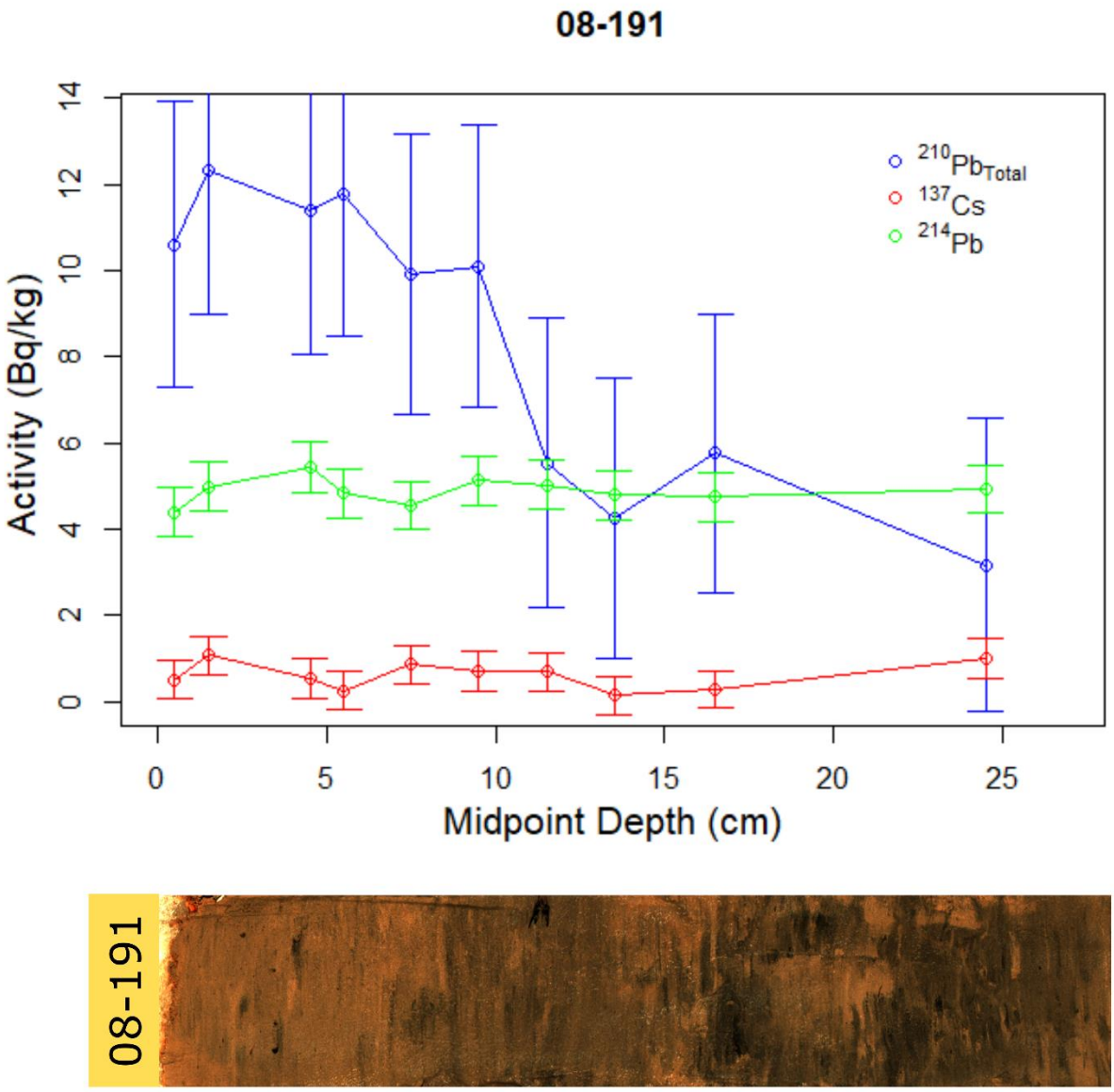
08-191
Activity (Bq/kg)
0
2
4
6
8
10
12
14
0
5
10
15
20
25
Midpoint Depth (cm)
$^{210}Pb_{Total}$
^{137}Cs
^{214}Pb

08-191

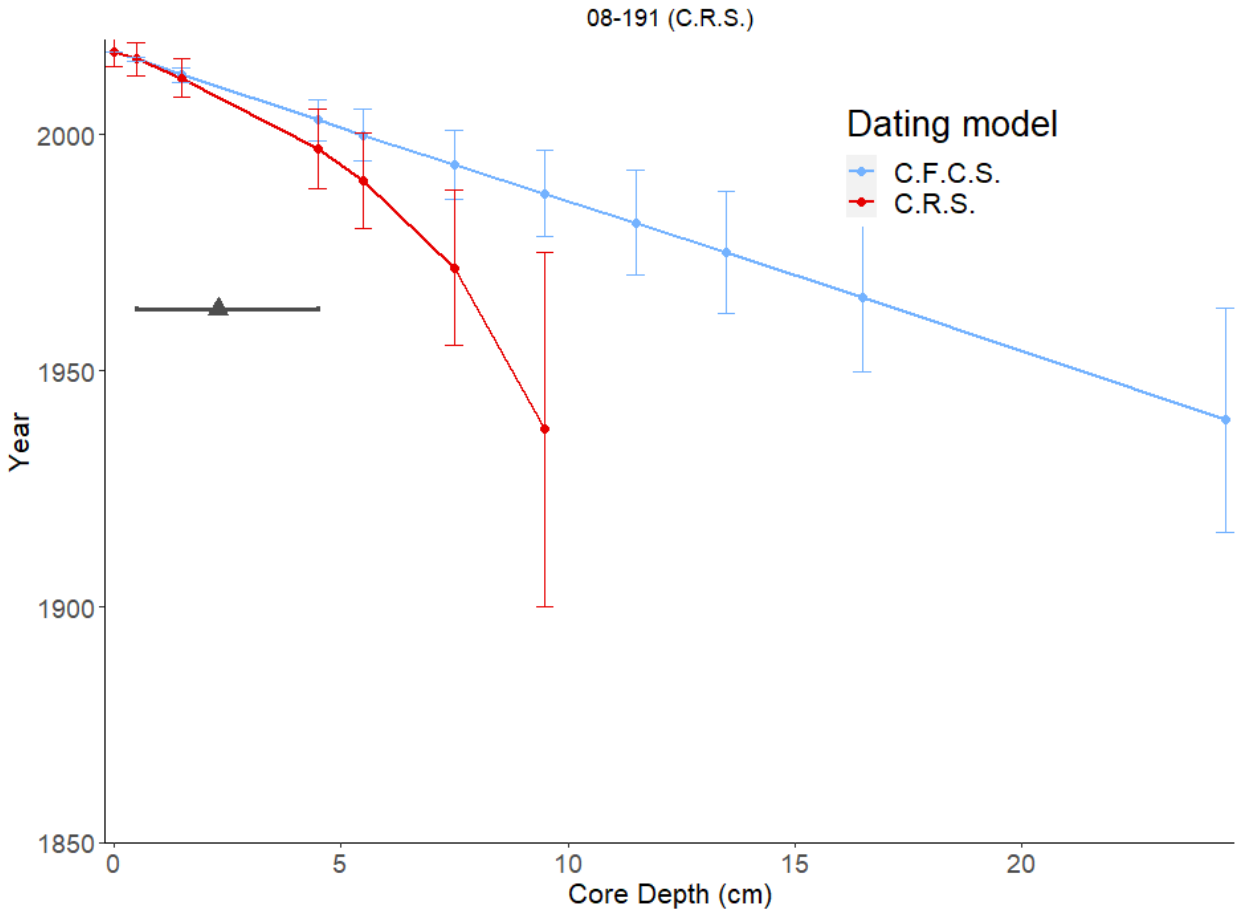
08-191 (C.R.S.)
Dating model
C.F.C.S.
C.R.S.
Year
2000
1950
1900
1850
0
5
10
15
20
Core Depth (cm)

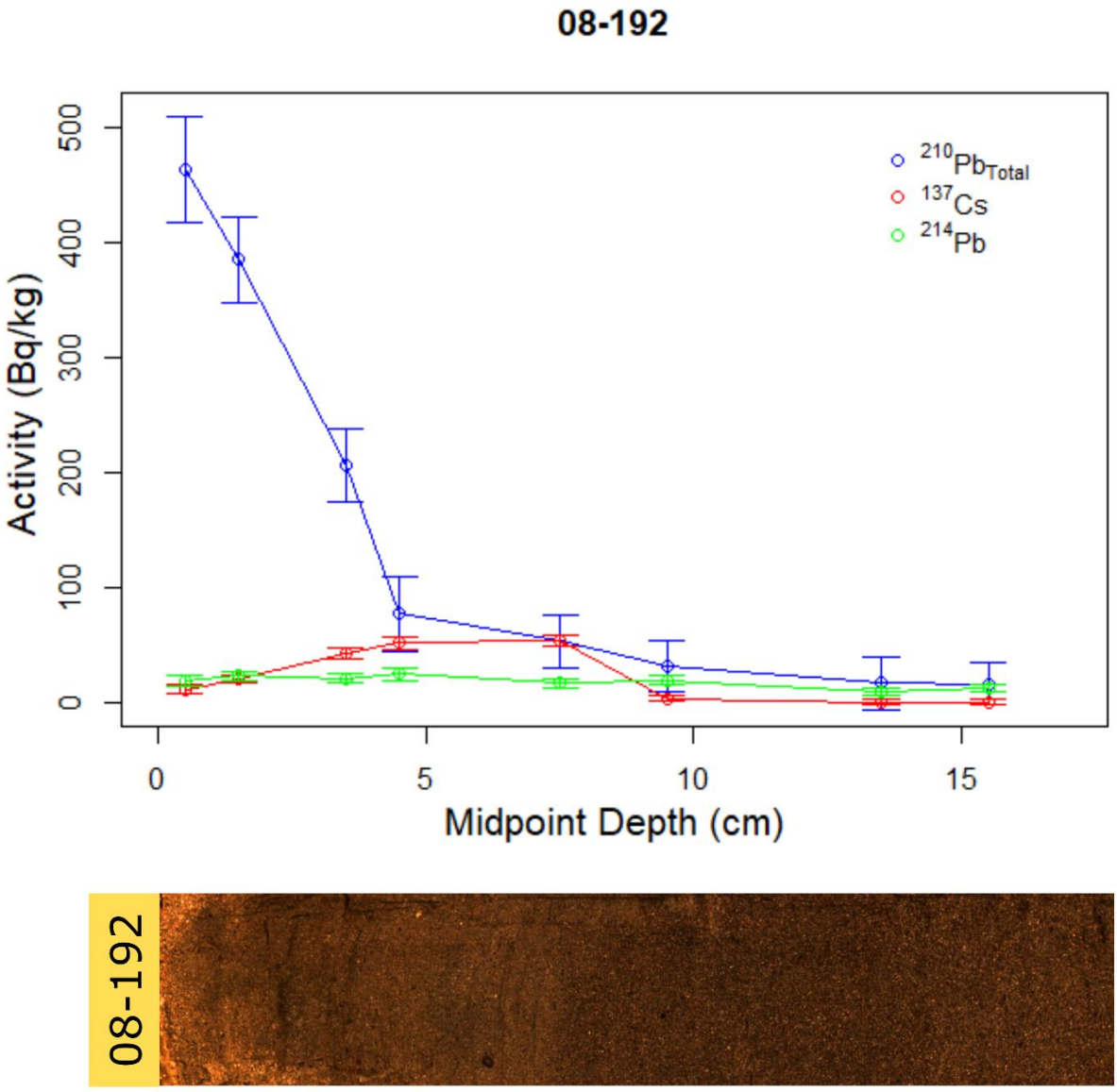
08-192
Activity (Bq/kg)
0
100
200
300
400
500
0
5
10
15
Midpoint Depth (cm)
$^{210}Pb_{Total}$
^{137}Cs
^{214}Pb

08-192

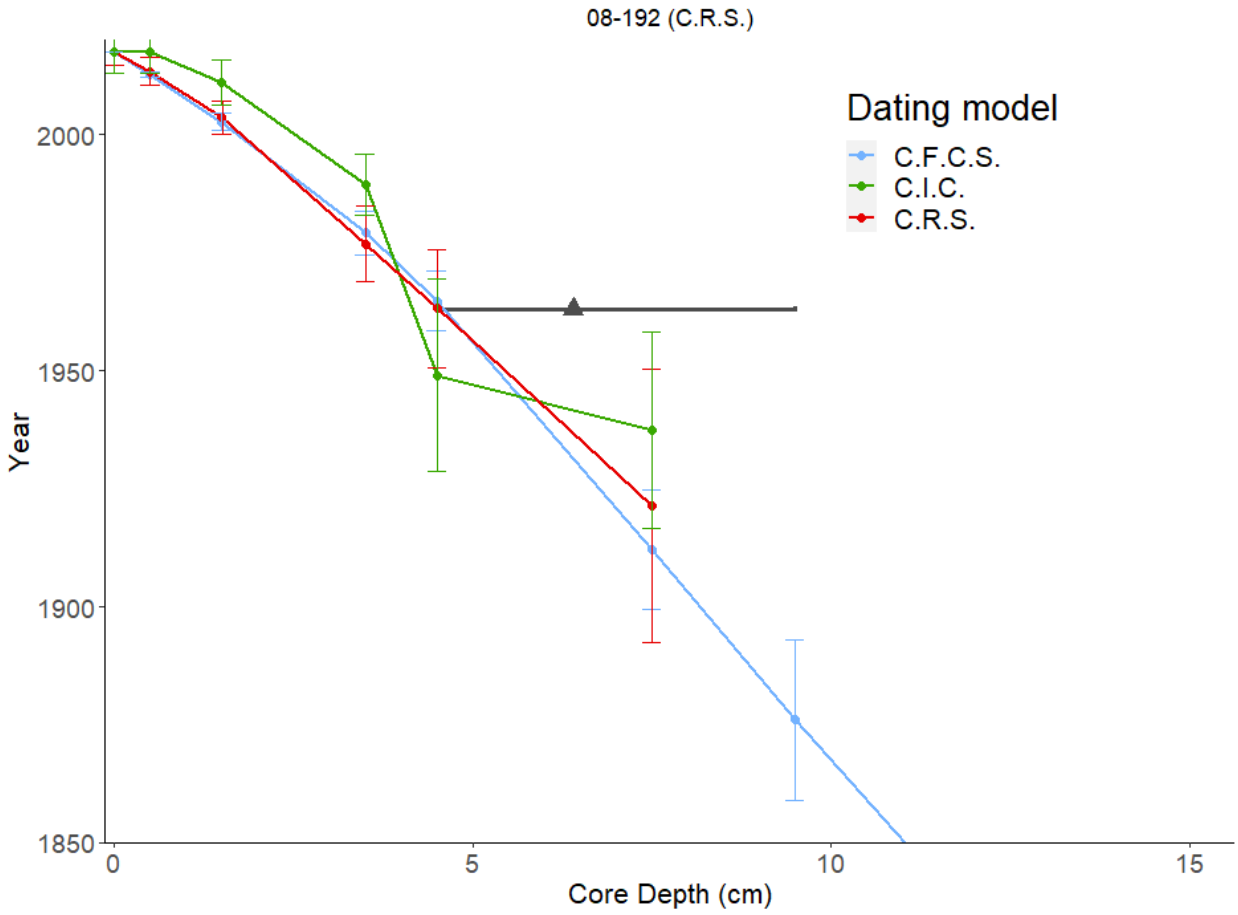
08-192 (C.R.S.)
Dating model
C.F.C.S.
C.I.C.
C.R.S.
Year
2000
1950
1900
1850
0
5
10
15
Core Depth (cm)

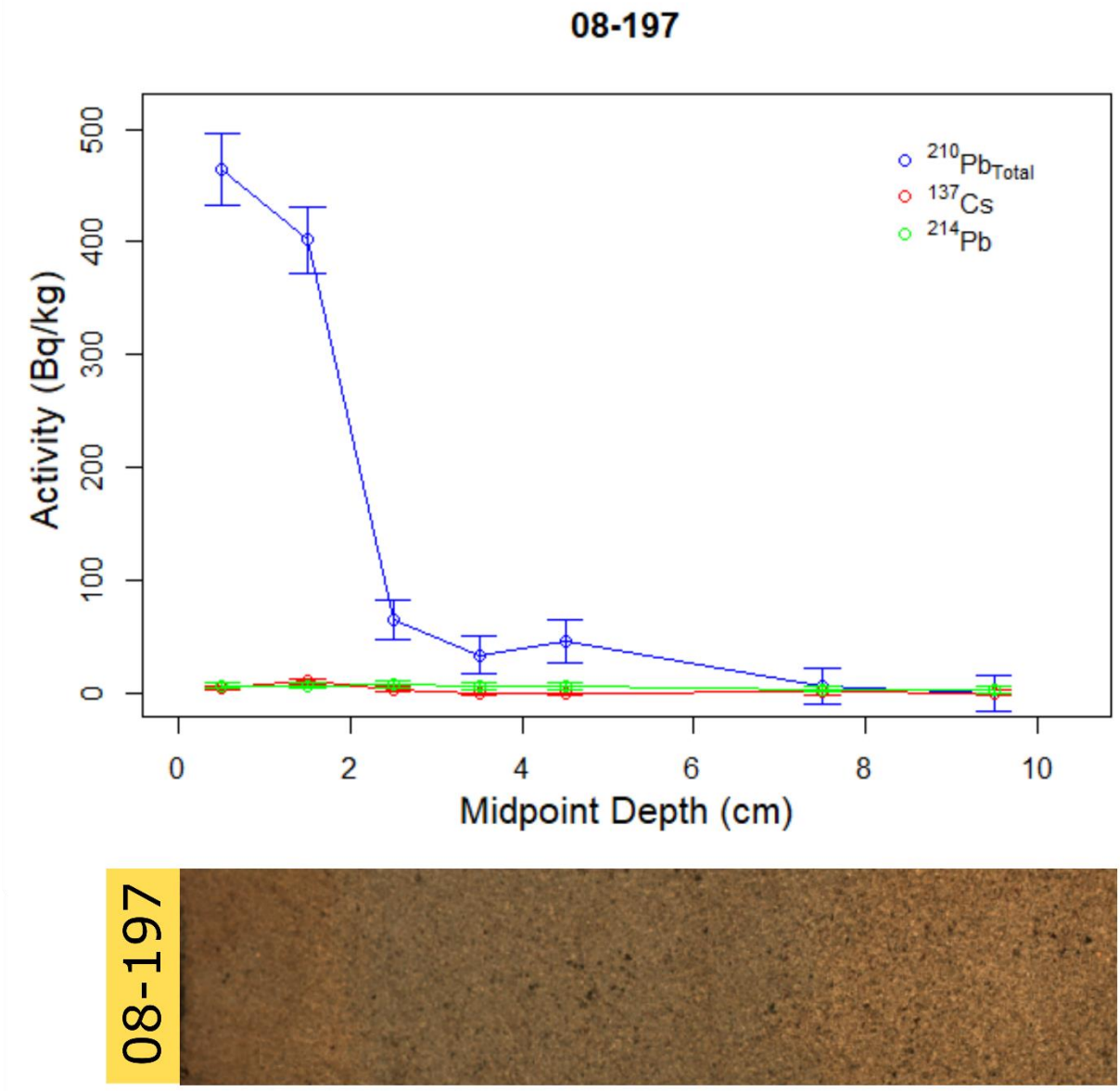
08-197
Activity (Bq/kg)
0
100
200
300
400
500
0
2
4
6
8
10
Midpoint Depth (cm)
210Pb Total
137Cs
214Pb

08-197

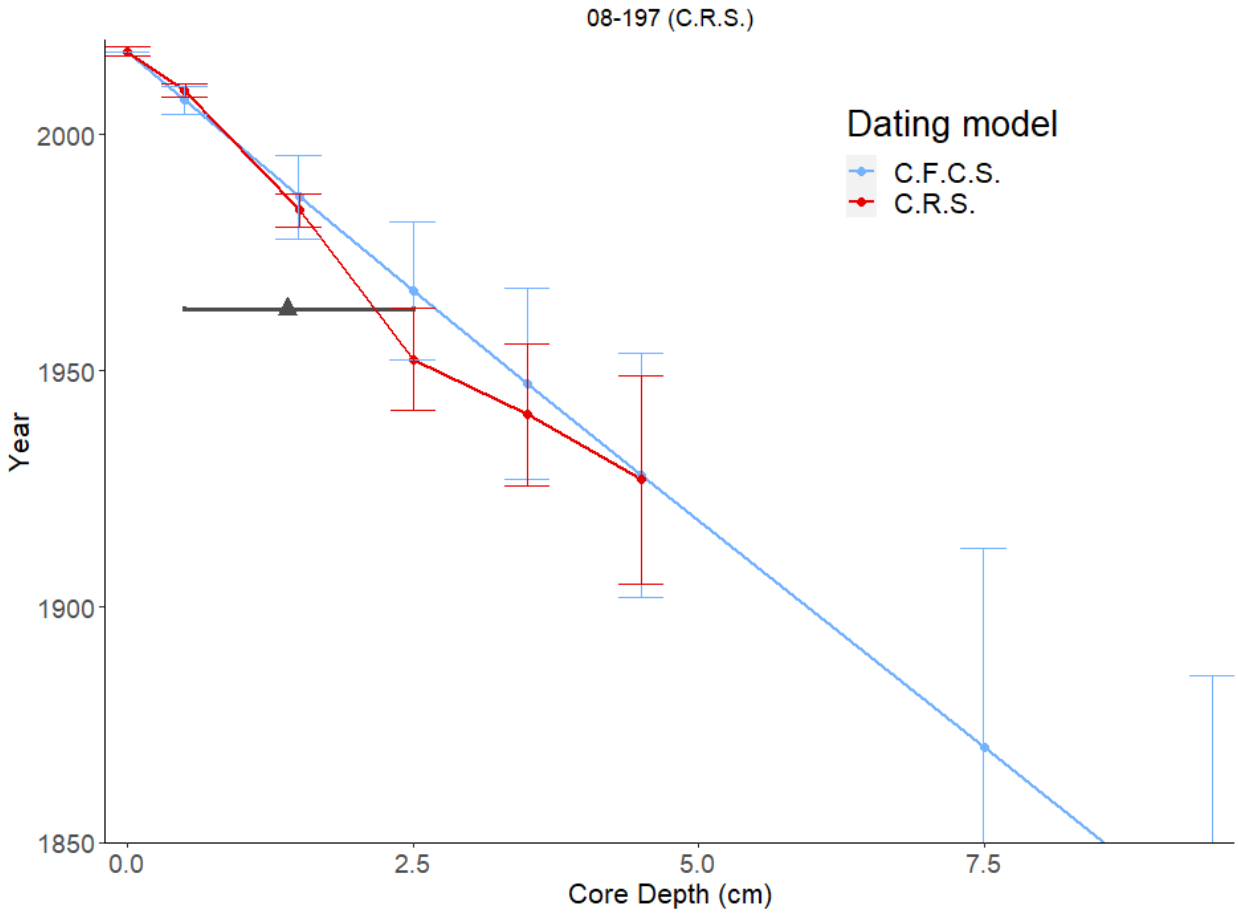
08-197 (C.R.S.)
Dating model
C.F.C.S.
C.R.S.
Year
2000
1950
1900
1850
0.0
2.5
5.0
7.5
Core Depth (cm)

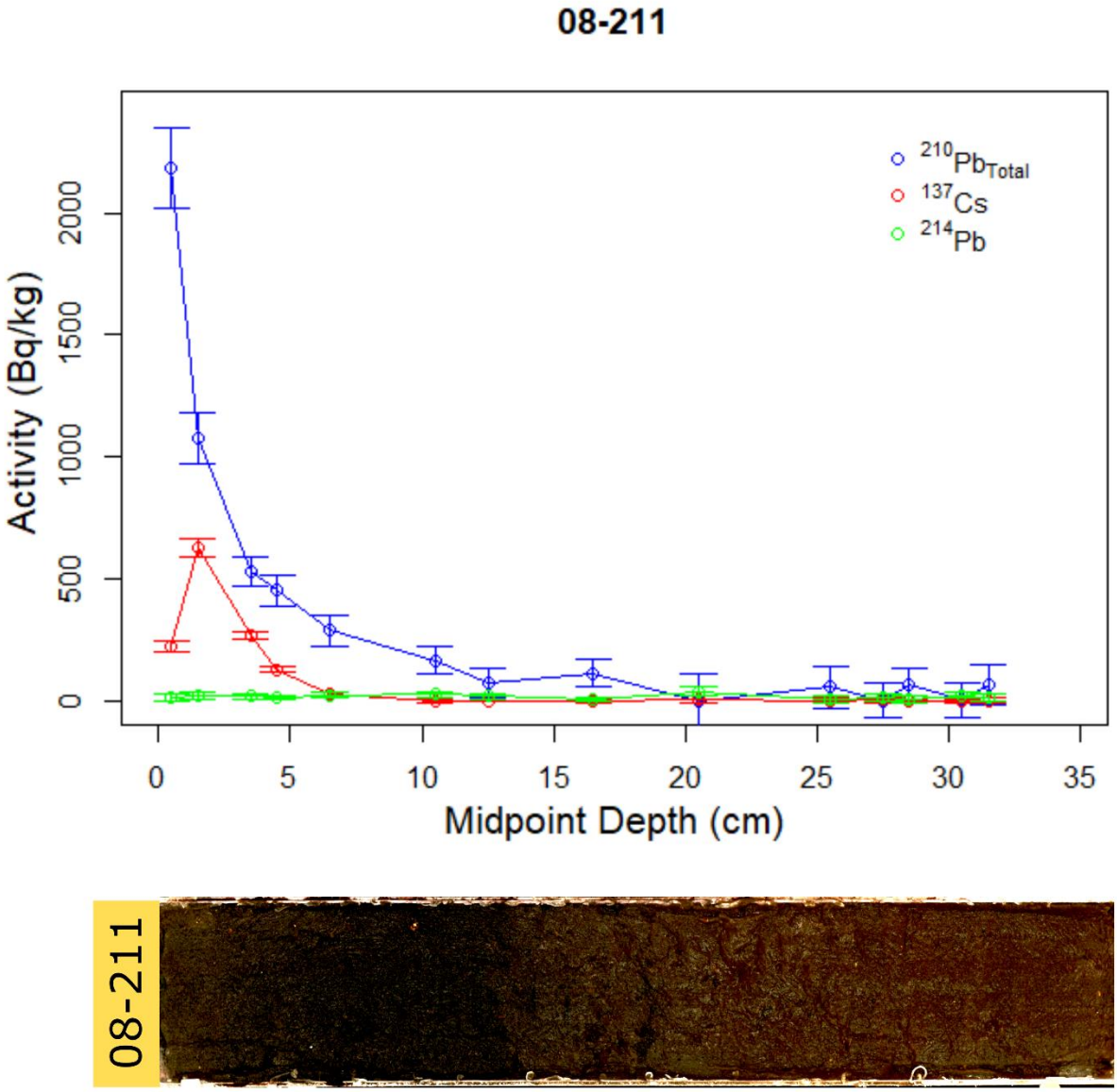
08-211
Activity (Bq/kg)
0
500
1000
1500
2000
0
5
10
15
20
25
30
35
Midpoint Depth (cm)
$^{210}Pb_{Total}$
^{137}Cs
^{214}Pb
08-211

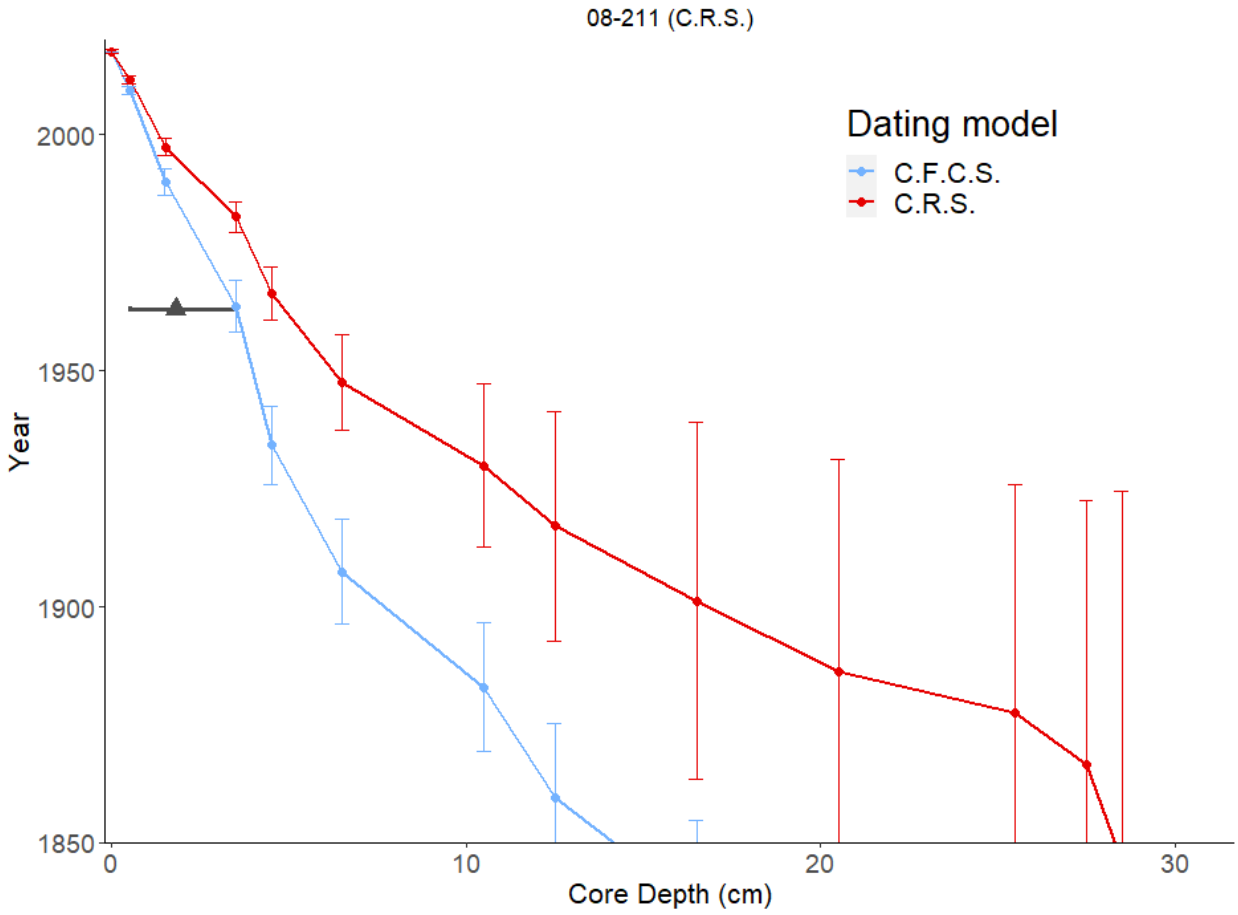
08-211 (C.R.S.)
Dating model
C.F.C.S.
C.R.S.
Year
2000
1950
1900
1850
0
10
20
30
Core Depth (cm)

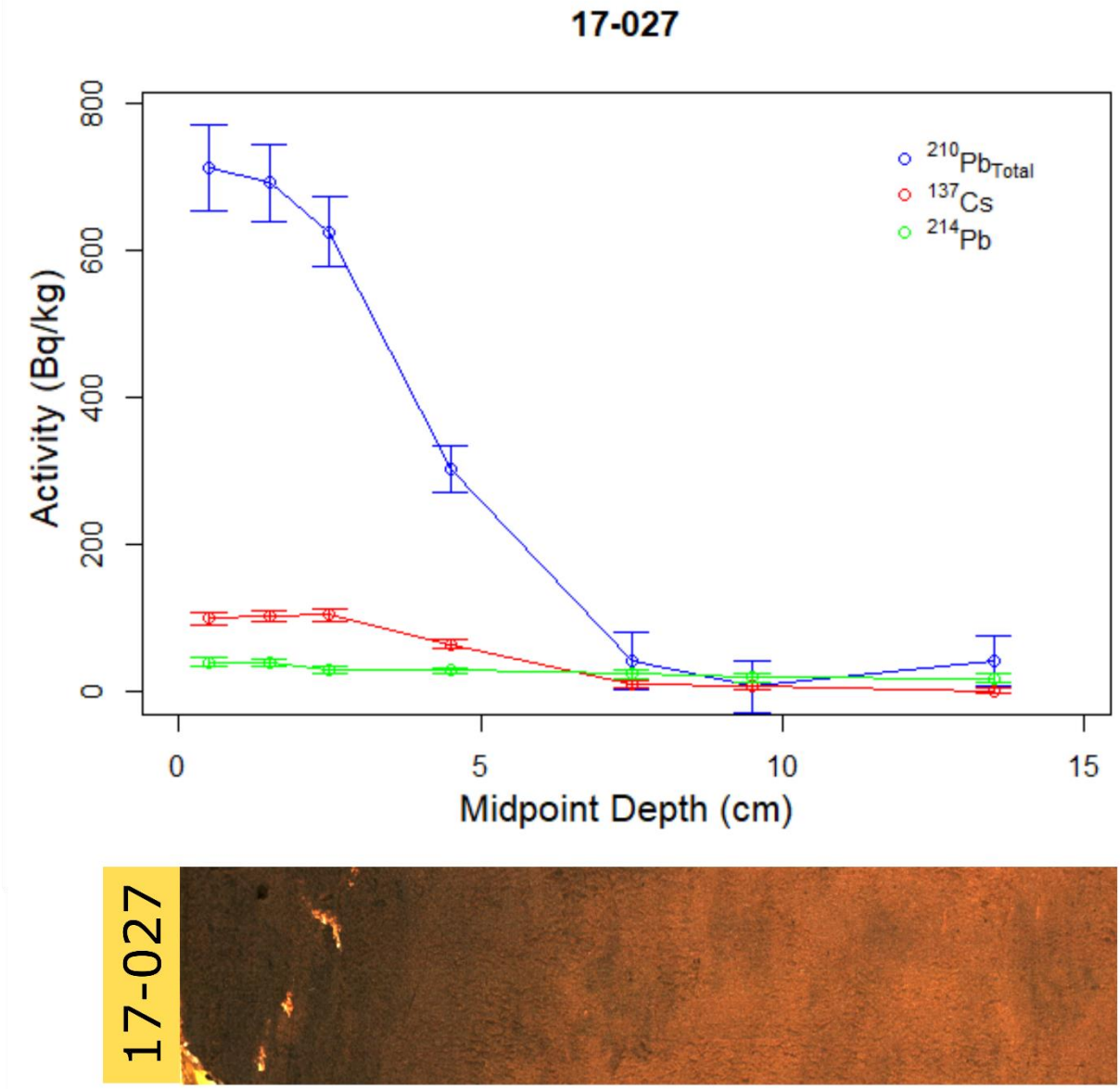
17-027
Activity (Bq/kg)
0
200
400
600
800
0
5
10
15
Midpoint Depth (cm)
210Pb Total
137Cs
214Pb

17-027

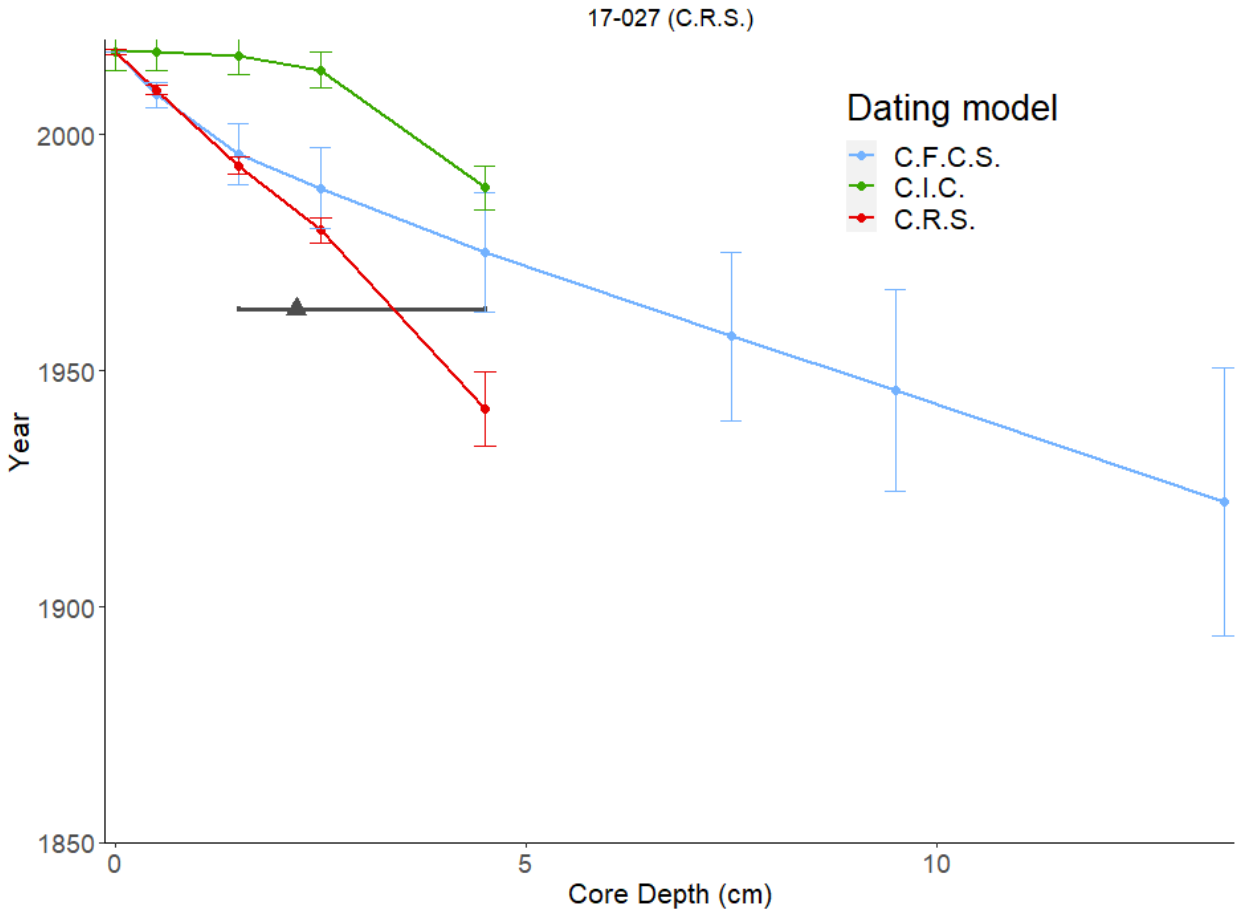
17-027 (C.R.S.)
Dating model
C.F.C.S.
C.I.C.
C.R.S.
Year
2000
1950
1900
1850
0
5
10
Core Depth (cm)

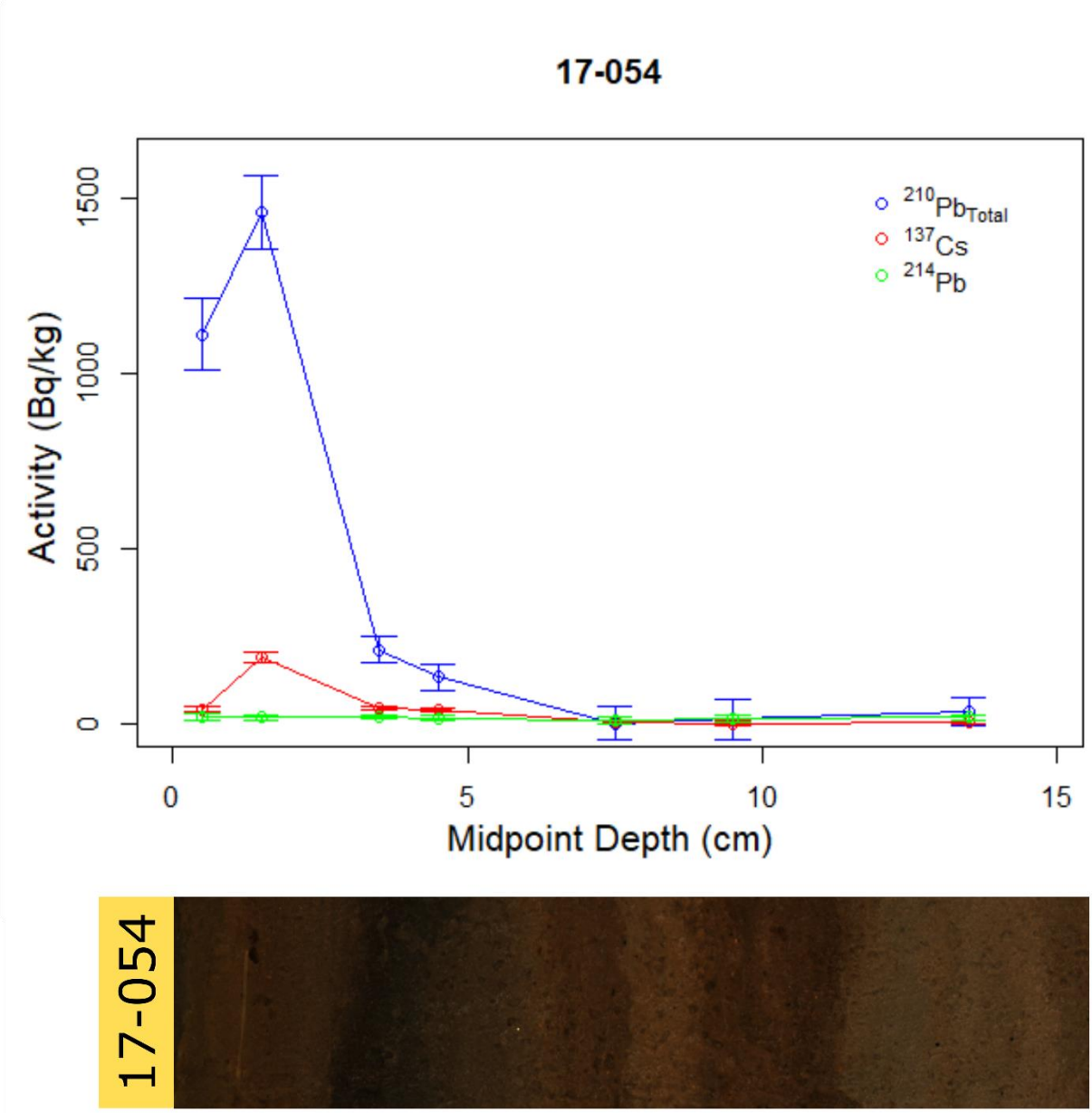
17-054
Activity (Bq/kg)
0
500
1000
1500
0
5
10
15
Midpoint Depth (cm)
210Pb Total
137Cs
214Pb

17-054

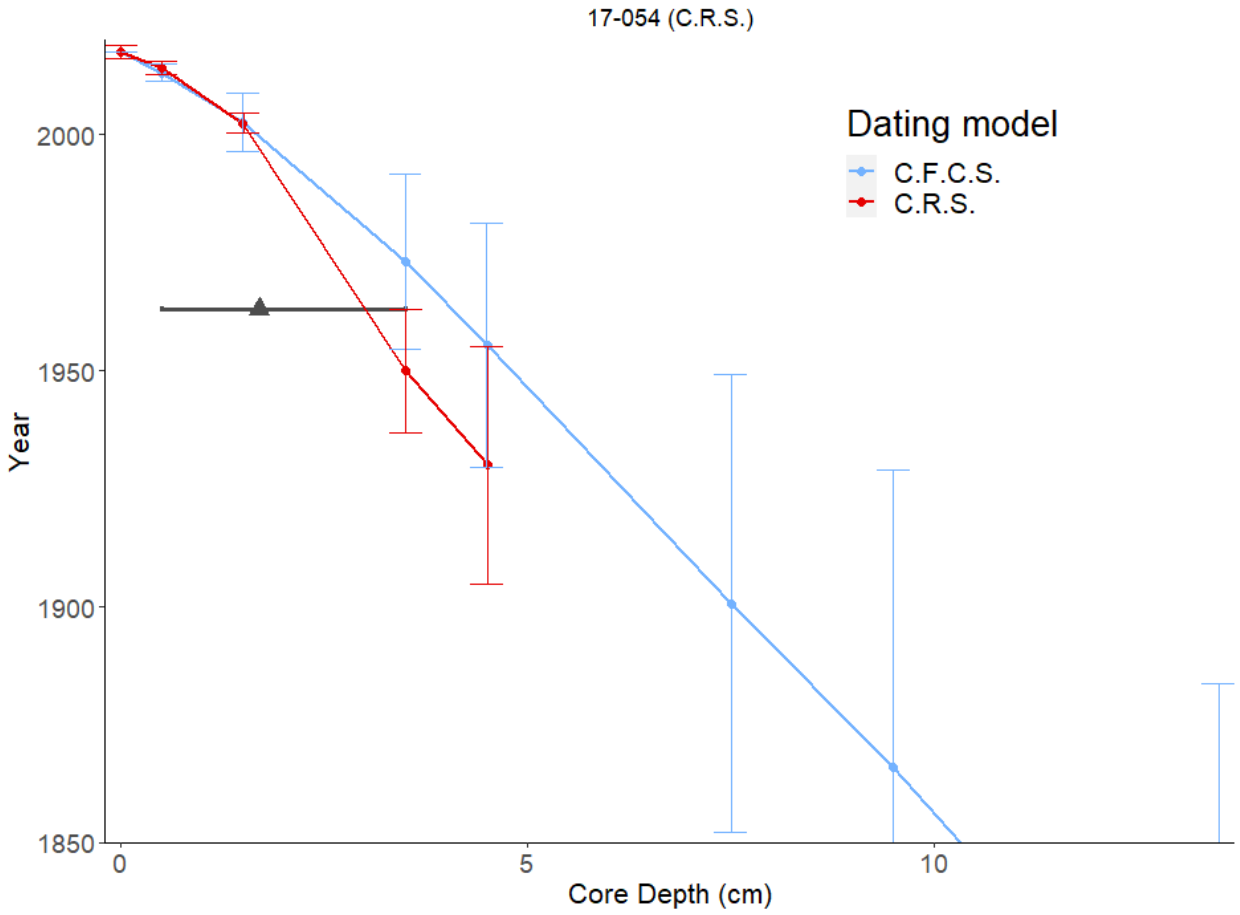
17-054 (C.R.S.)
Dating model
C.F.C.S.
C.R.S.
Year
2000
1950
1900
1850
0
5
10
Core Depth (cm)

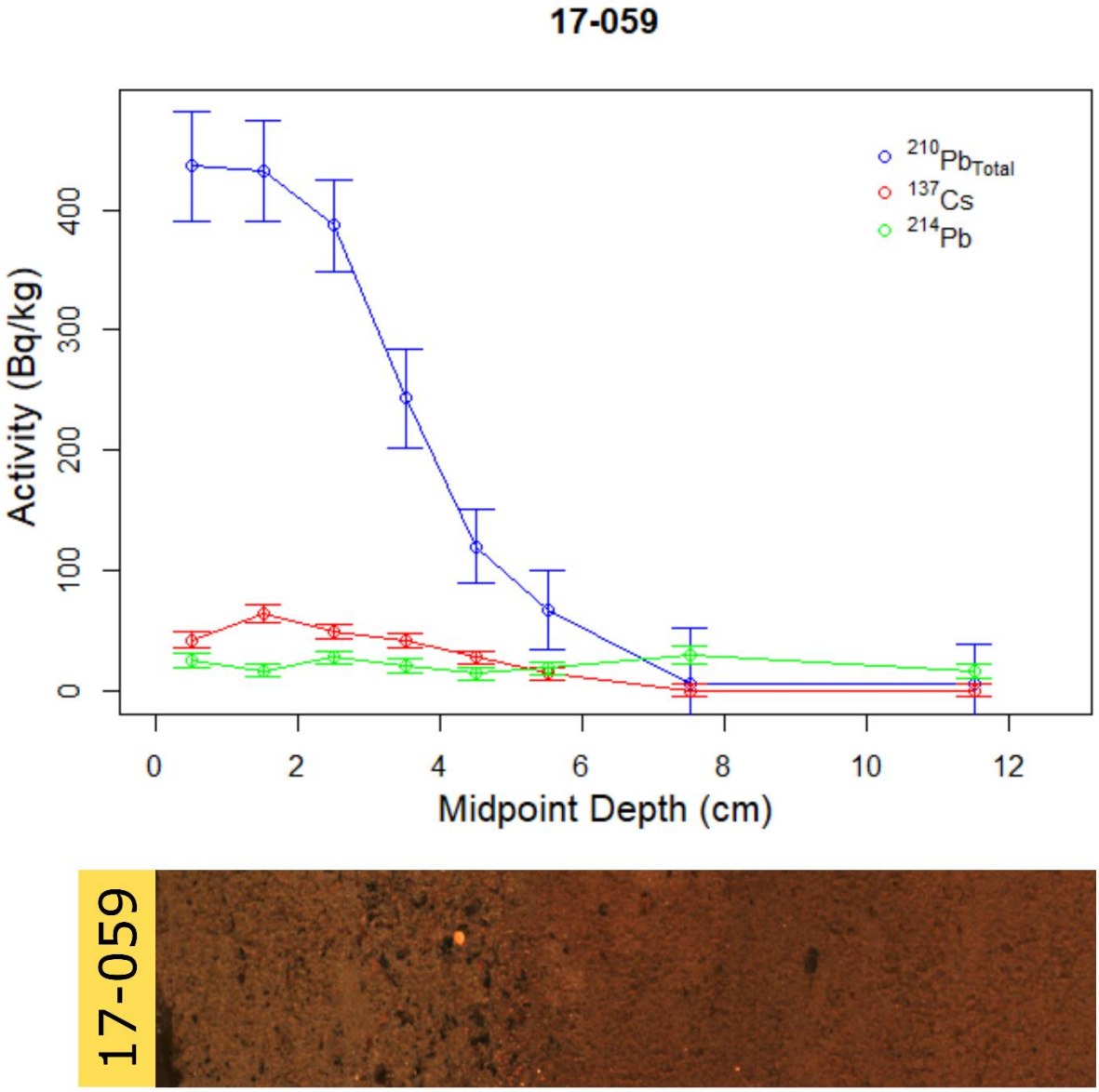
17-059
Activity (Bq/kg)
0
100
200
300
400
0
2
4
6
8
10
12
Midpoint Depth (cm)
210Pb Total
137Cs
214Pb

17-059

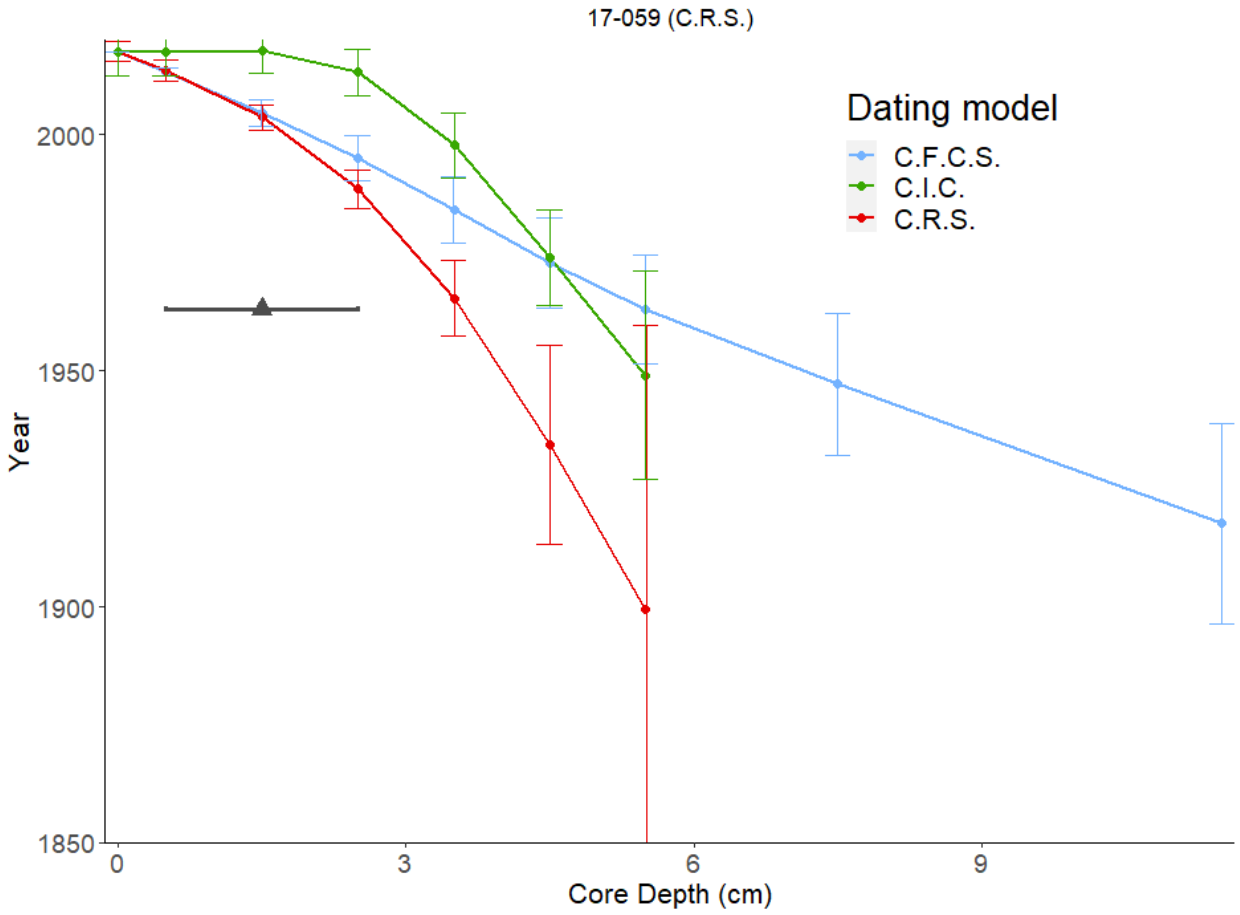
17-059 (C.R.S.)
Dating model
C.F.C.S.
C.I.C.
C.R.S.
Year
2000
1950
1900
1850
0
3
6
9
Core Depth (cm)

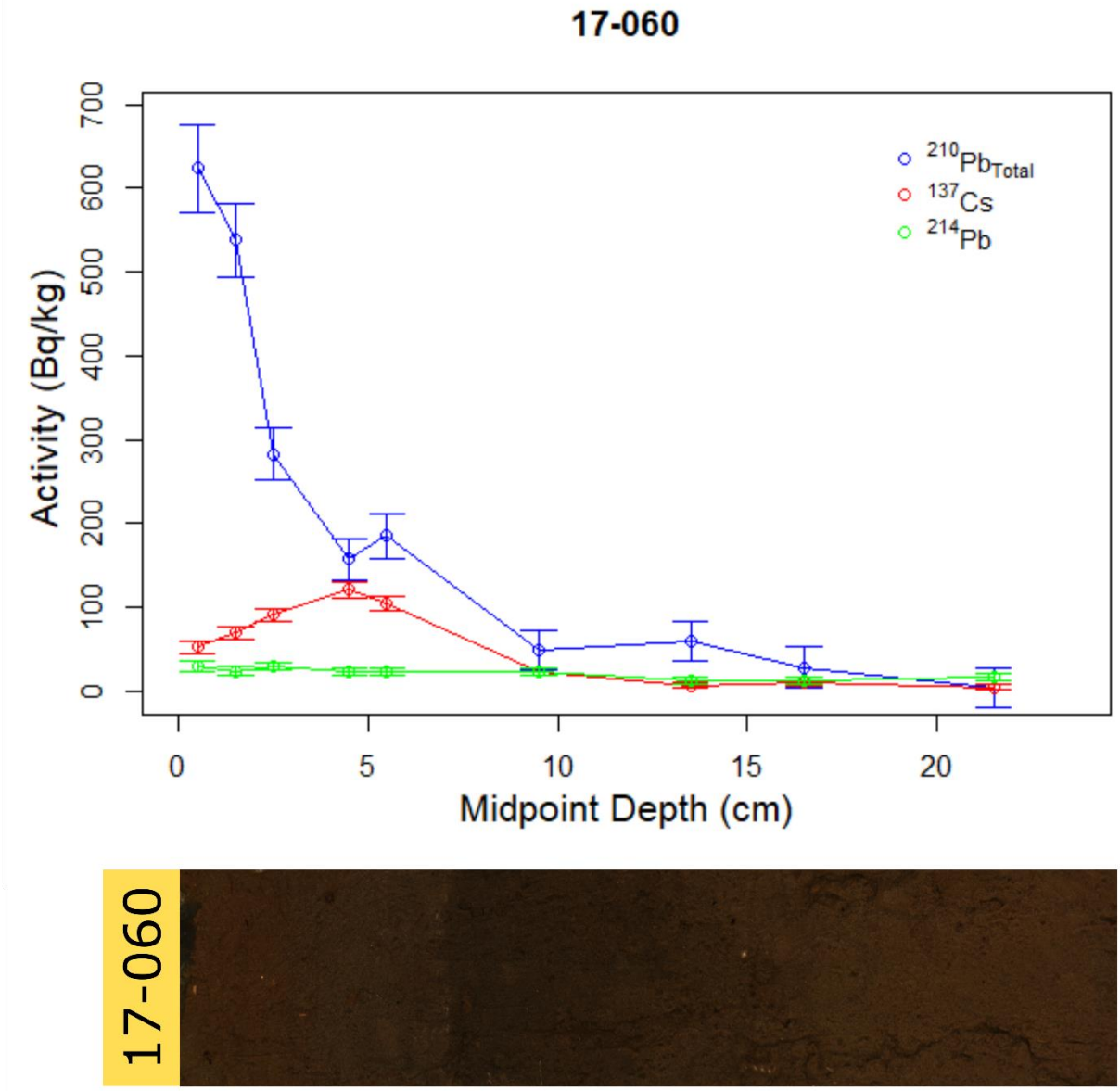
17-060
Activity (Bq/kg)
0
100
200
300
400
500
600
700
0
5
10
15
20
Midpoint Depth (cm)
210Pb Total
137Cs
214Pb

17-060

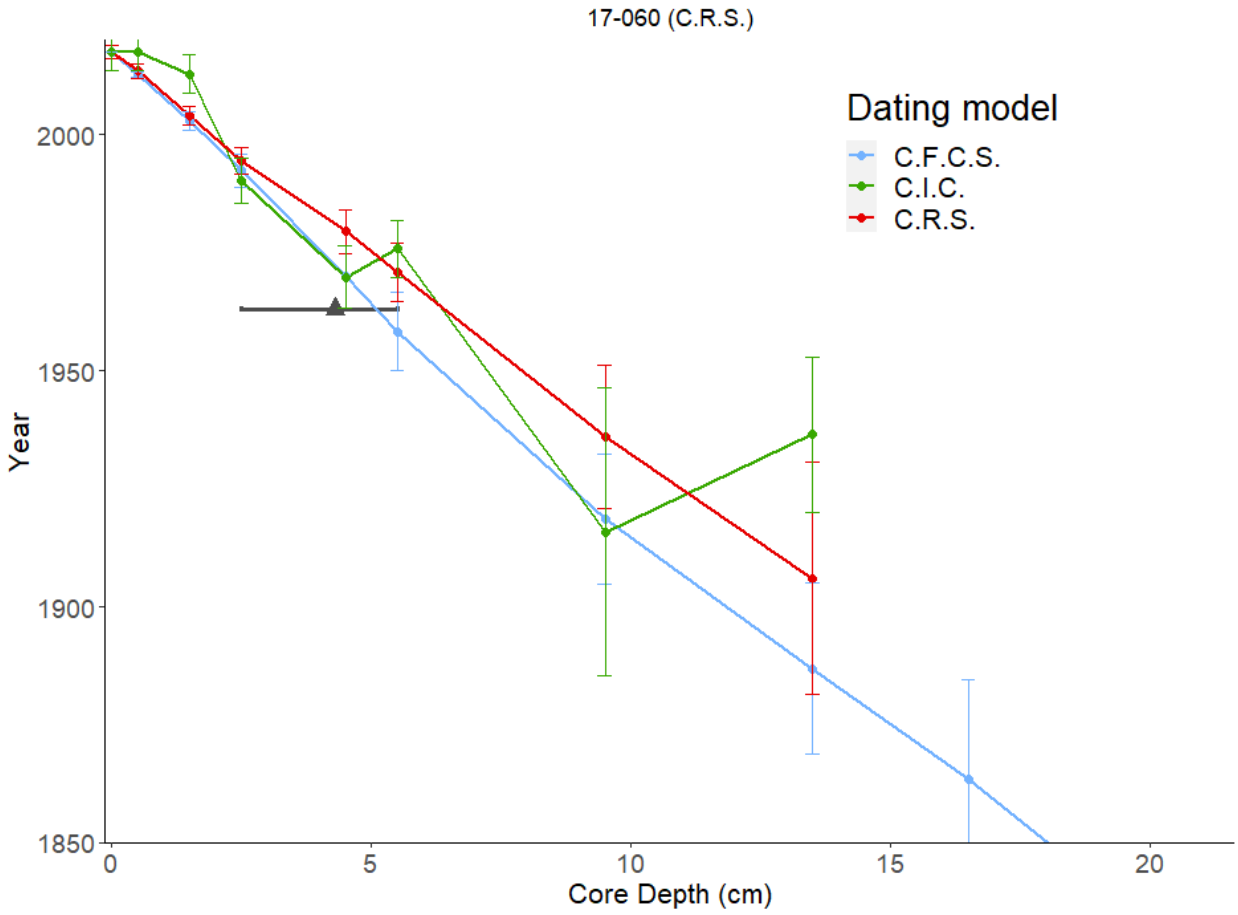
17-060 (C.R.S.)
Dating model
C.F.C.S.
C.I.C.
C.R.S.
Year
2000
1950
1900
1850
0
5
10
15
20
Core Depth (cm)

75

76

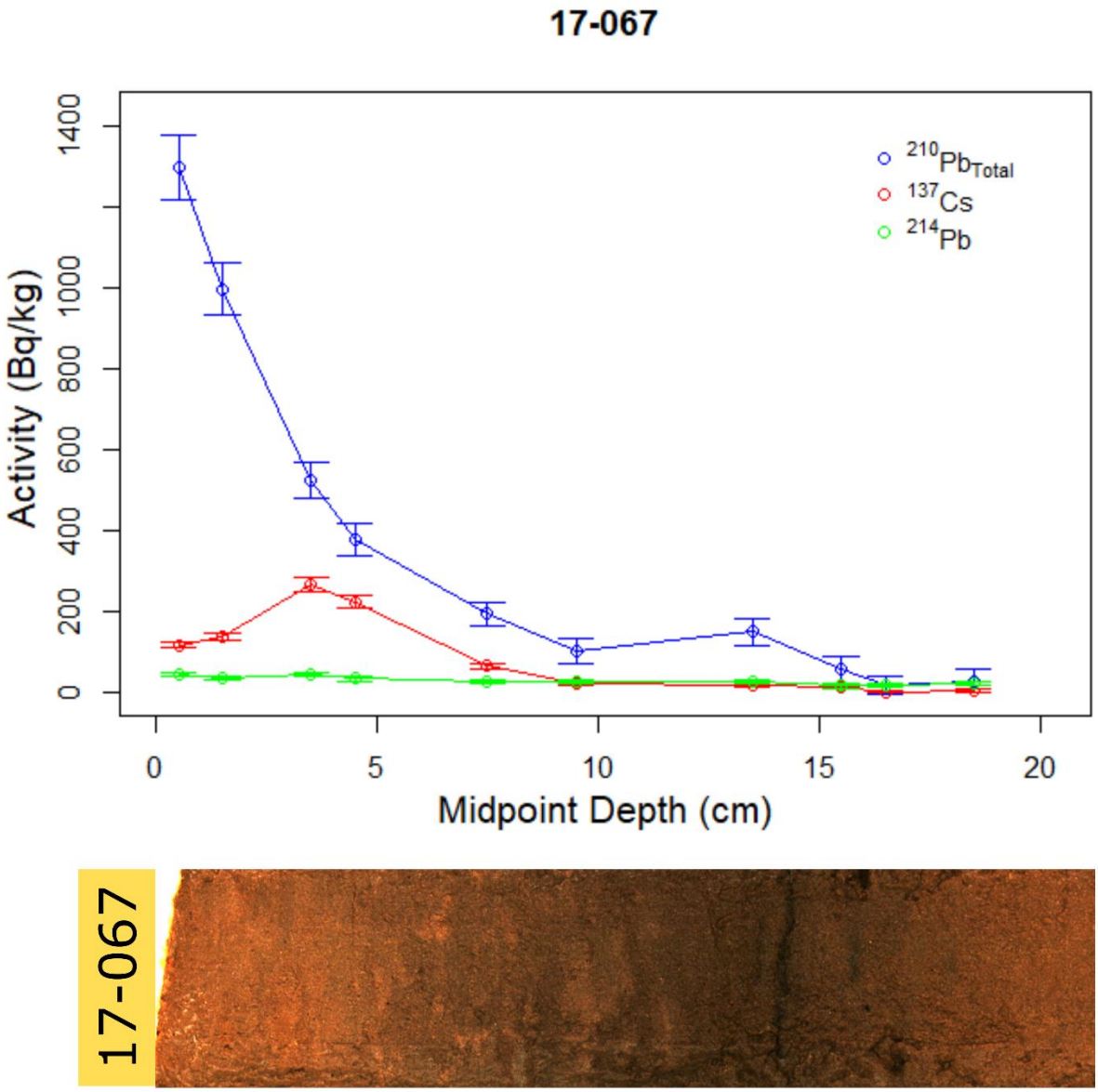
17-067
Activity (Bq/kg)
0
200
400
600
800
1000
1400
0
5
10
15
20
Midpoint Depth (cm)
$^{210}Pb_{Total}$
^{137}Cs
^{214}Pb

17-067

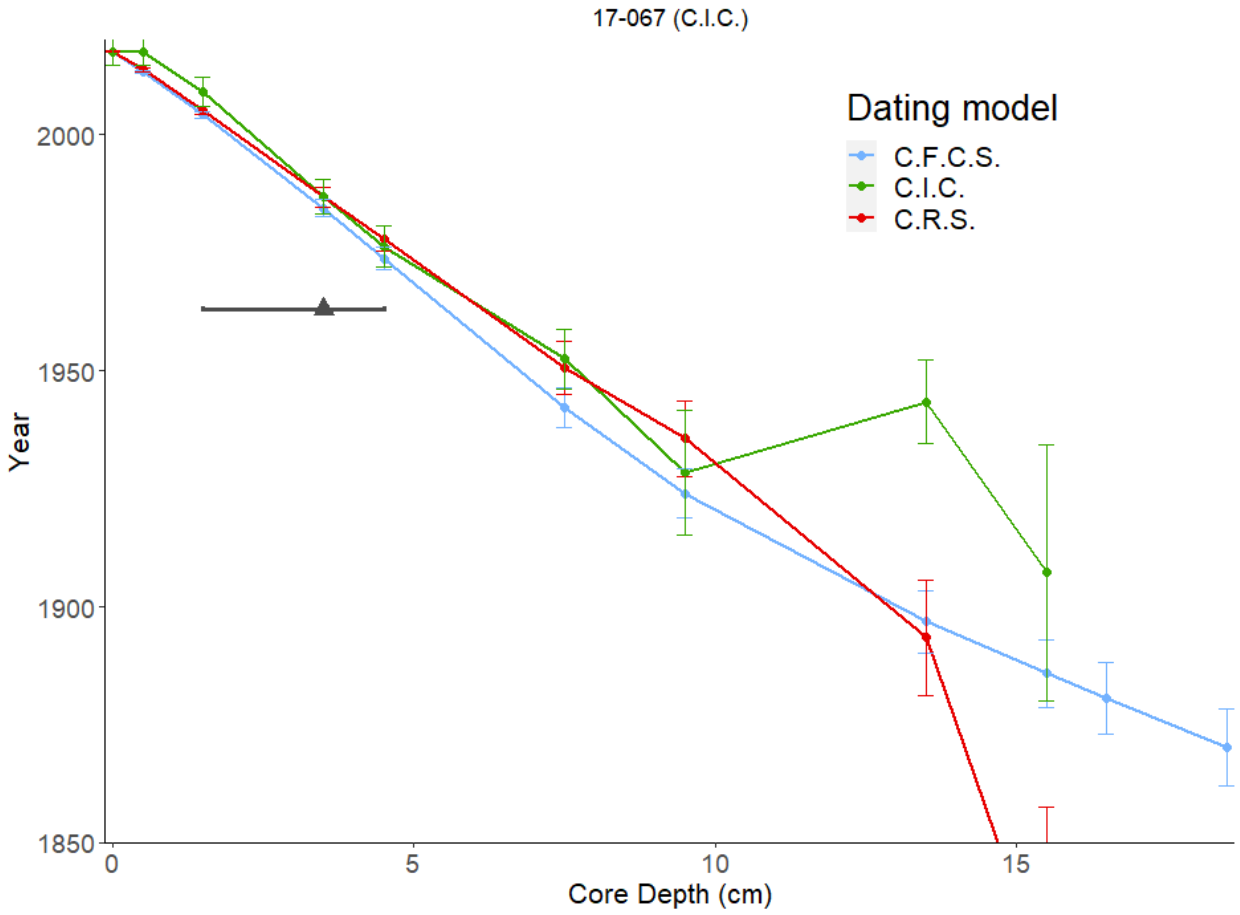
17-067 (C.I.C.)
Dating model
C.F.C.S.
C.I.C.
C.R.S.
Year
2000
1950
1900
1850
0
5
10
15
Core Depth (cm)

78

79

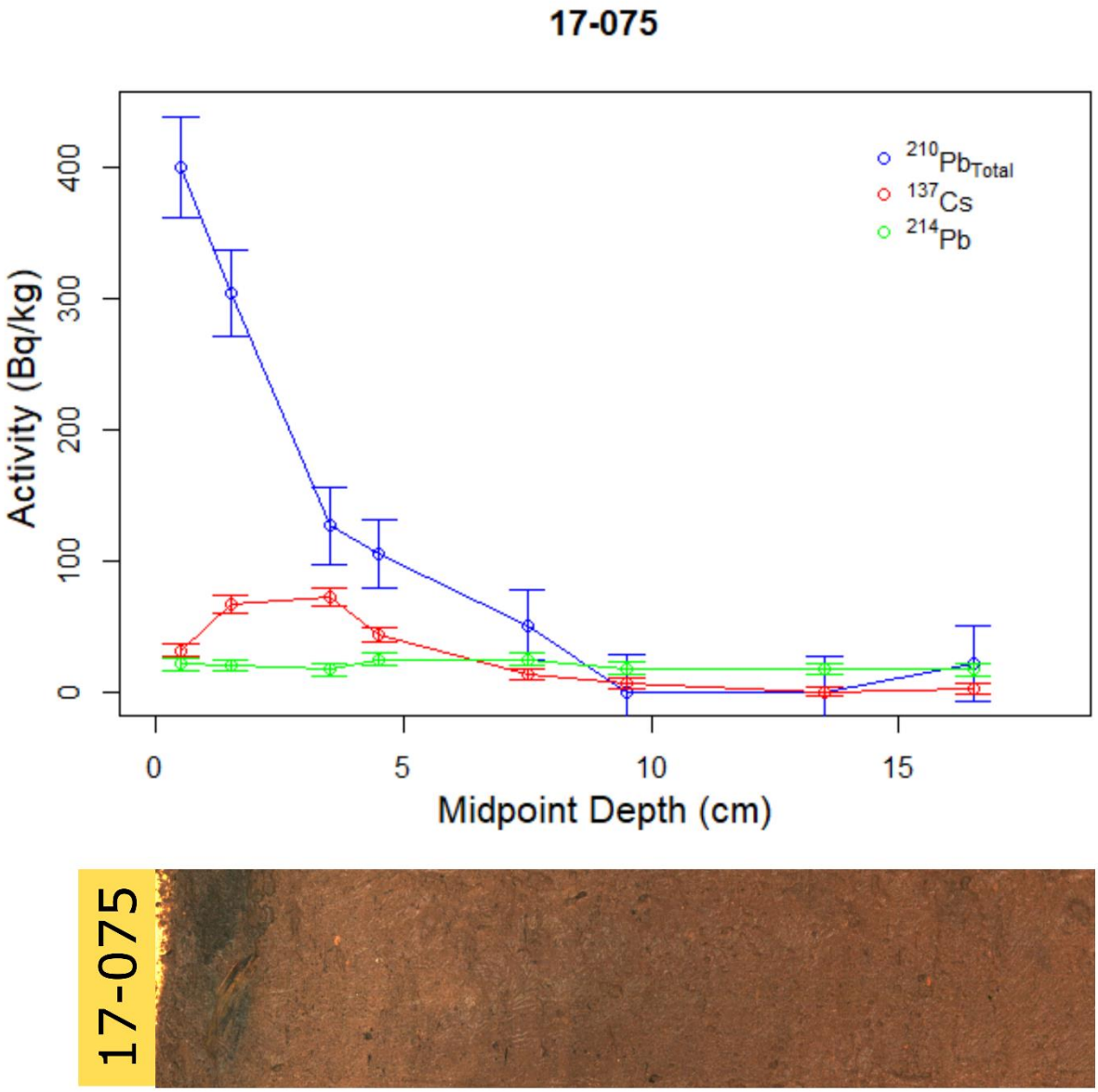
17-075
Activity (Bq/kg)
0
100
200
300
400
0
5
10
15
Midpoint Depth (cm)
$^{210}Pb_{Total}$
^{137}Cs
^{214}Pb

17-075

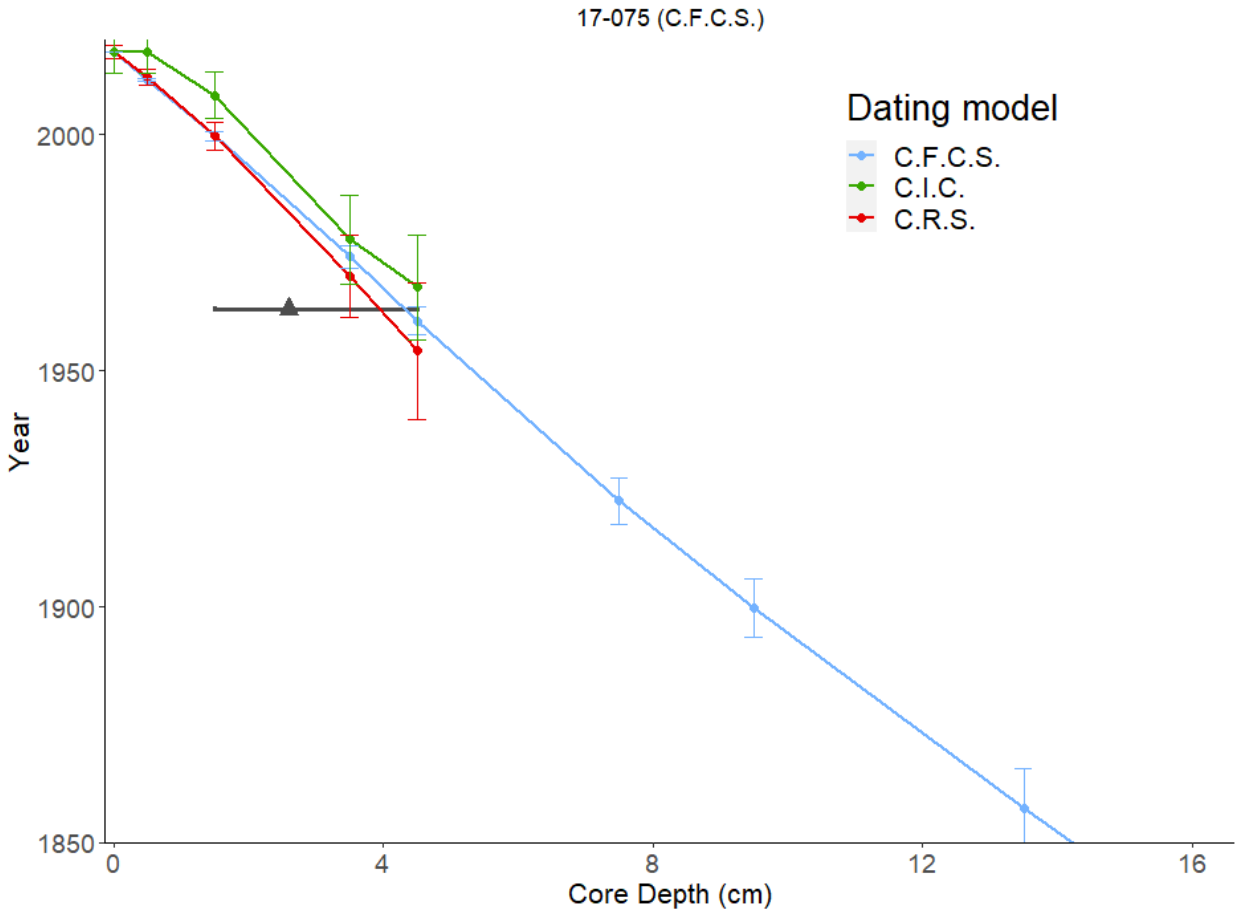
17-075 (C.F.C.S.)
Dating model
C.F.C.S.
C.I.C.
C.R.S.
Year
2000
1950
1900
1850
0
4
8
12
16
Core Depth (cm)

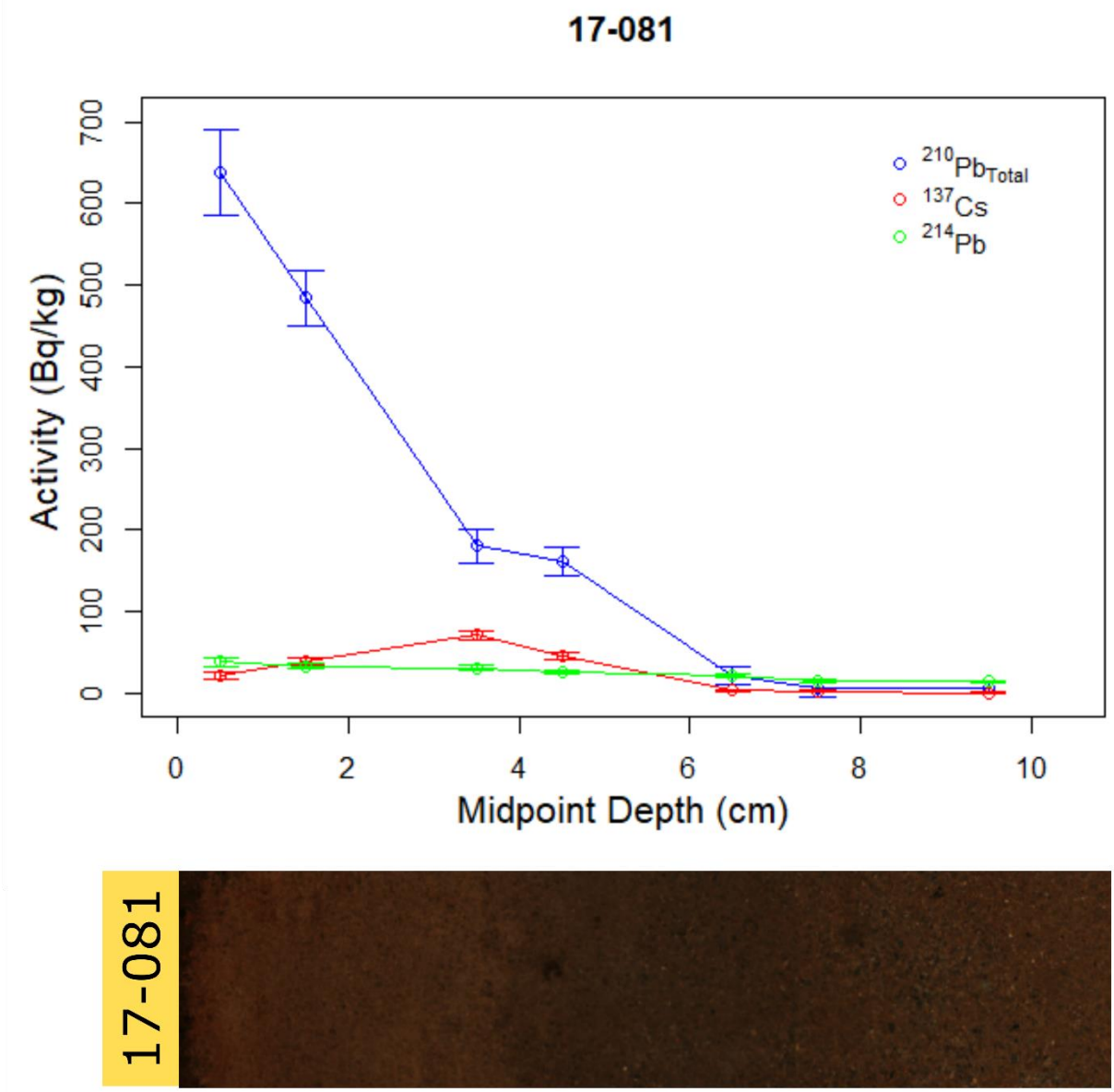
17-081
Activity (Bq/kg)
0
100
200
300
400
500
600
700
0
2
4
6
8
10
Midpoint Depth (cm)
$^{210}Pb_{Total}$
^{137}Cs
^{214}Pb

17-081

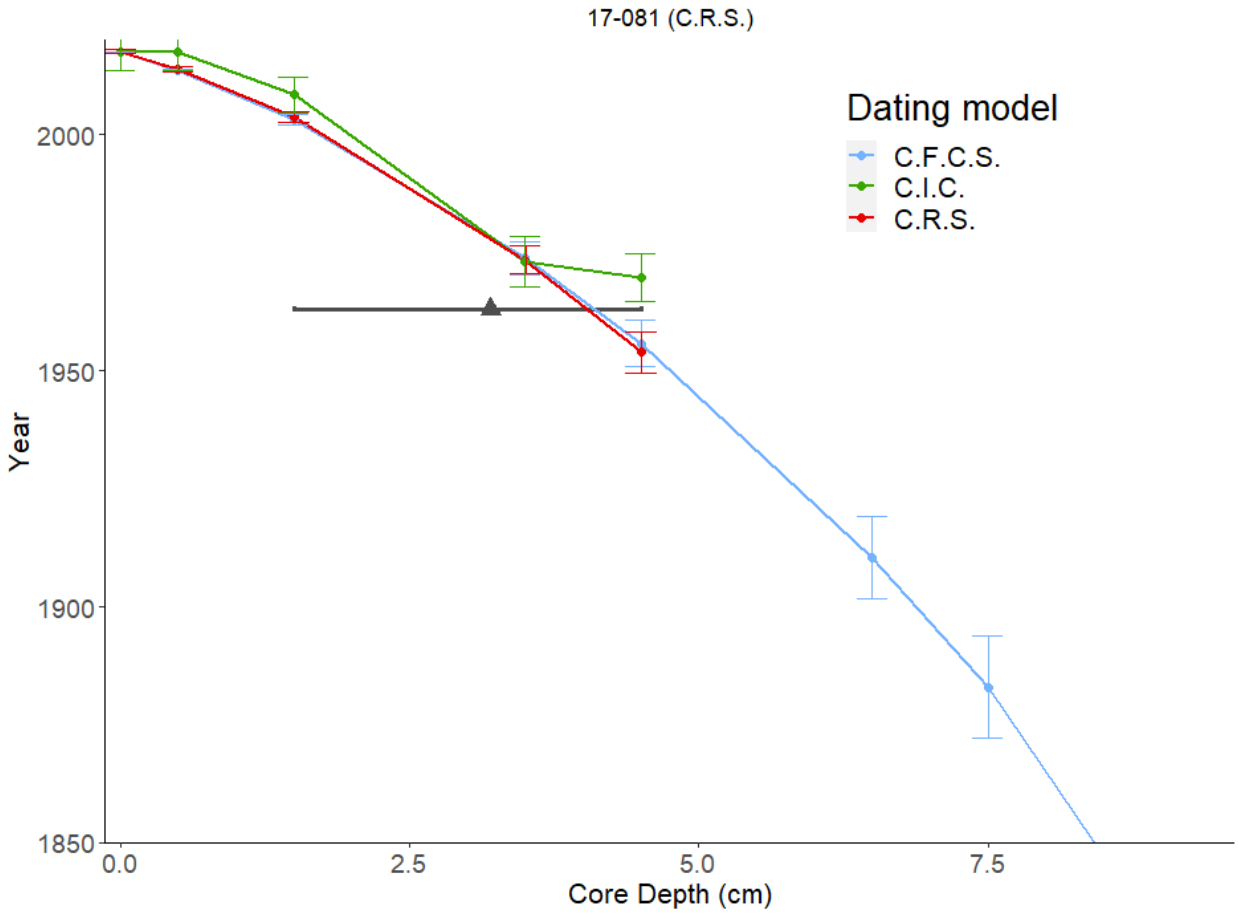
17-081 (C.R.S.)
Dating model
C.F.C.S.
C.I.C.
C.R.S.
Year
2000
1950
1900
1850
0.0
2.5
5.0
7.5
Core Depth (cm)

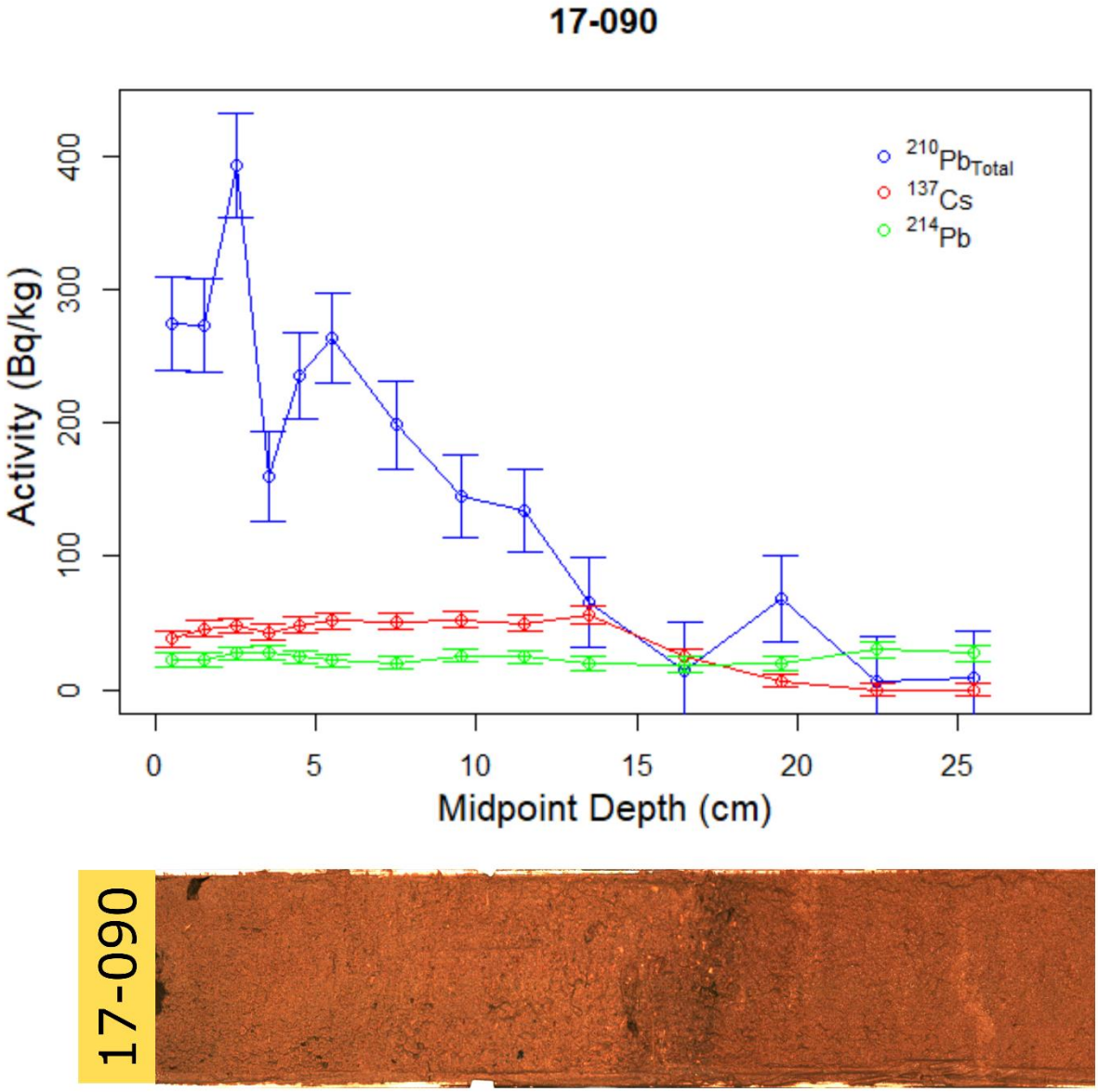
17-090
Activity (Bq/kg)
0
100
200
300
400
0
5
10
15
20
25
Midpoint Depth (cm)
210Pb Total
137Cs
214Pb

17-090

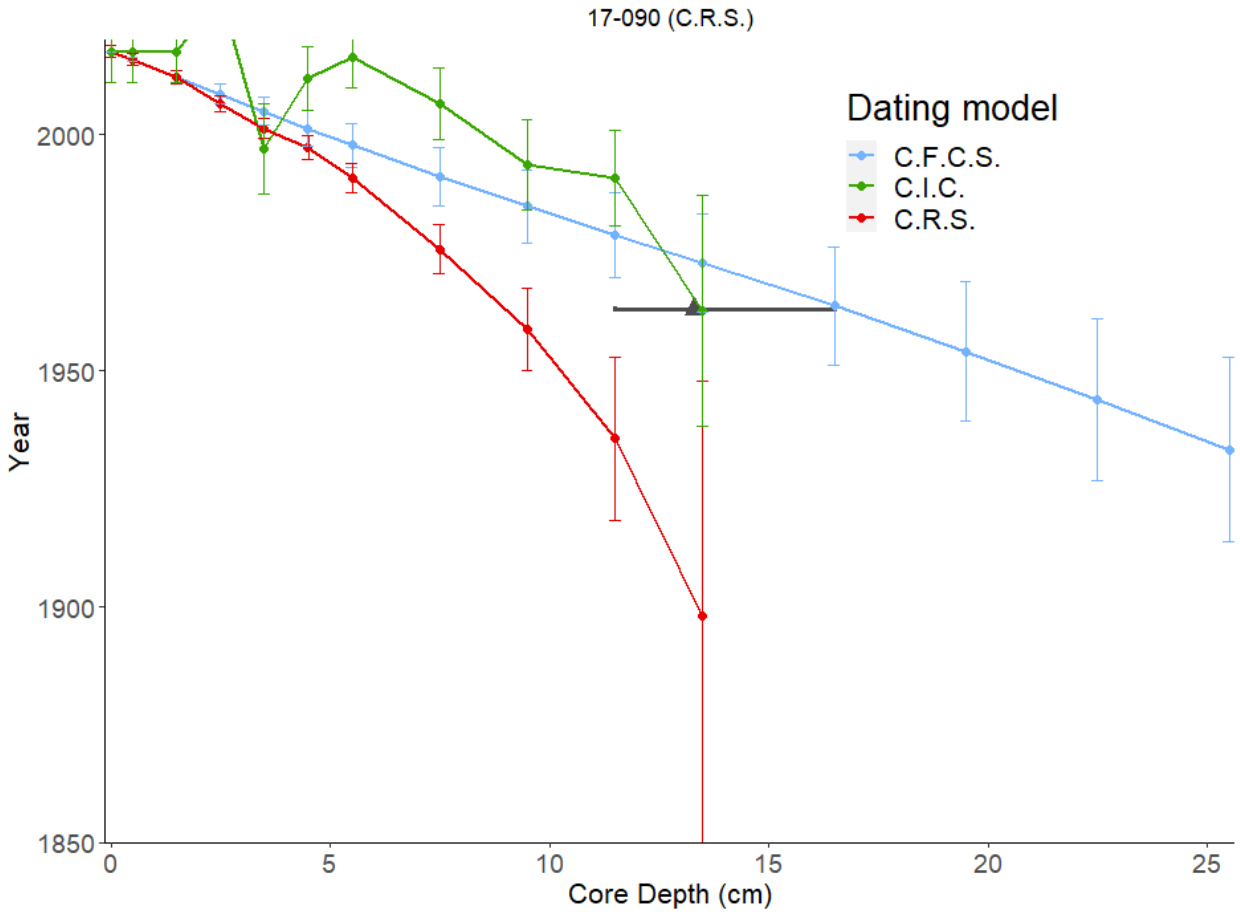
17-090 (C.R.S.)
Dating model
C.F.C.S.
C.I.C.
C.R.S.
Year
2000
1950
1900
1850
0
5
10
15
20
25
Core Depth (cm)

85

86

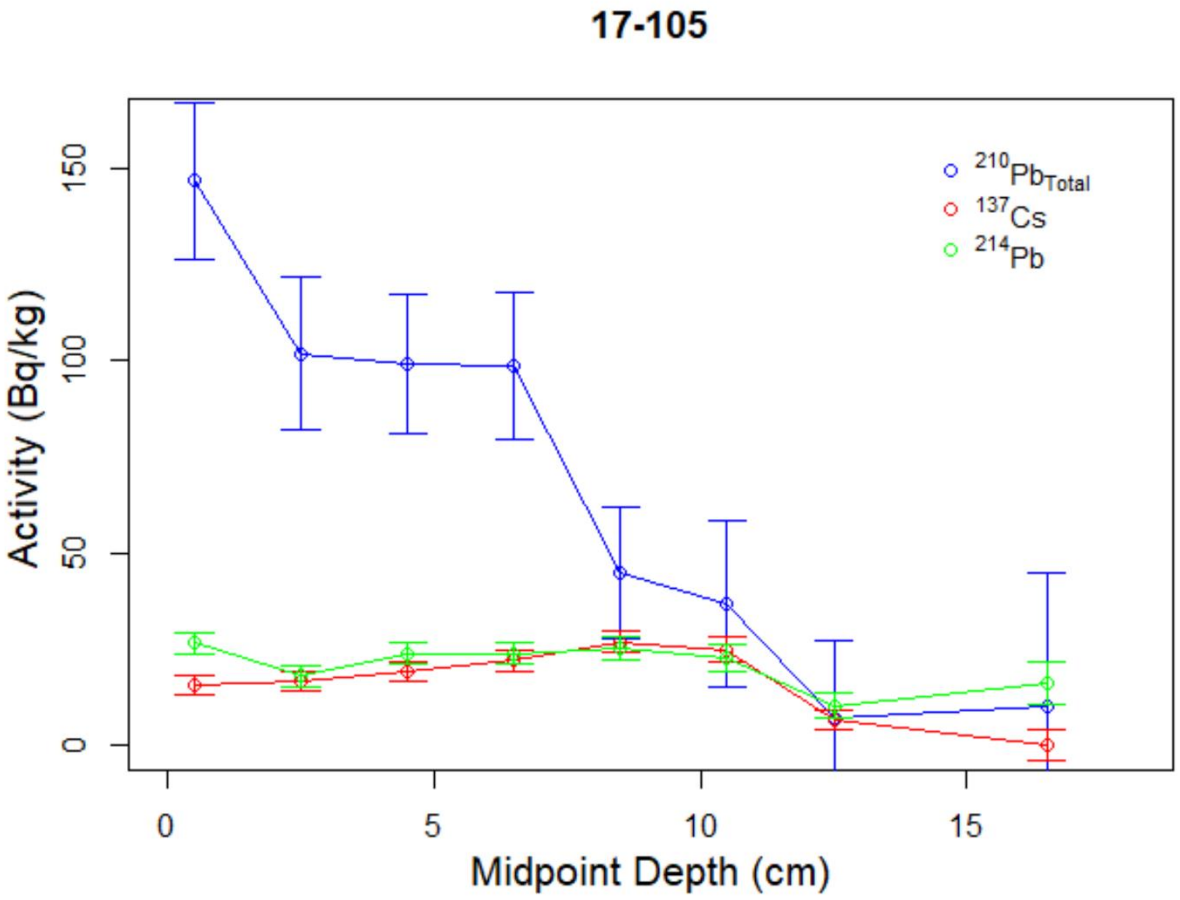
17-105
Activity (Bq/kg)
0
50
100
150
0
5
10
15
Midpoint Depth (cm)
$^{210}Pb_{Total}$
^{137}Cs
^{214}Pb

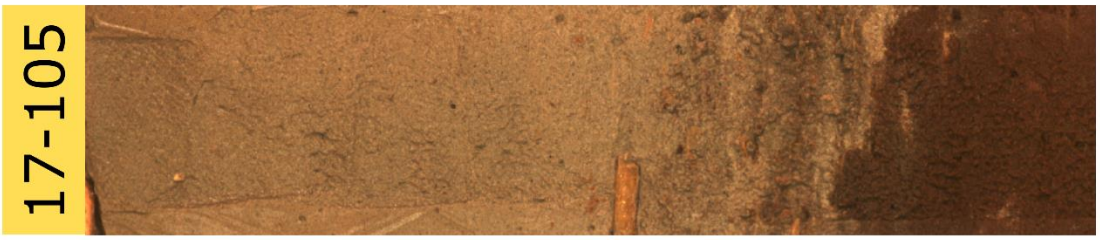
17-105

87

88

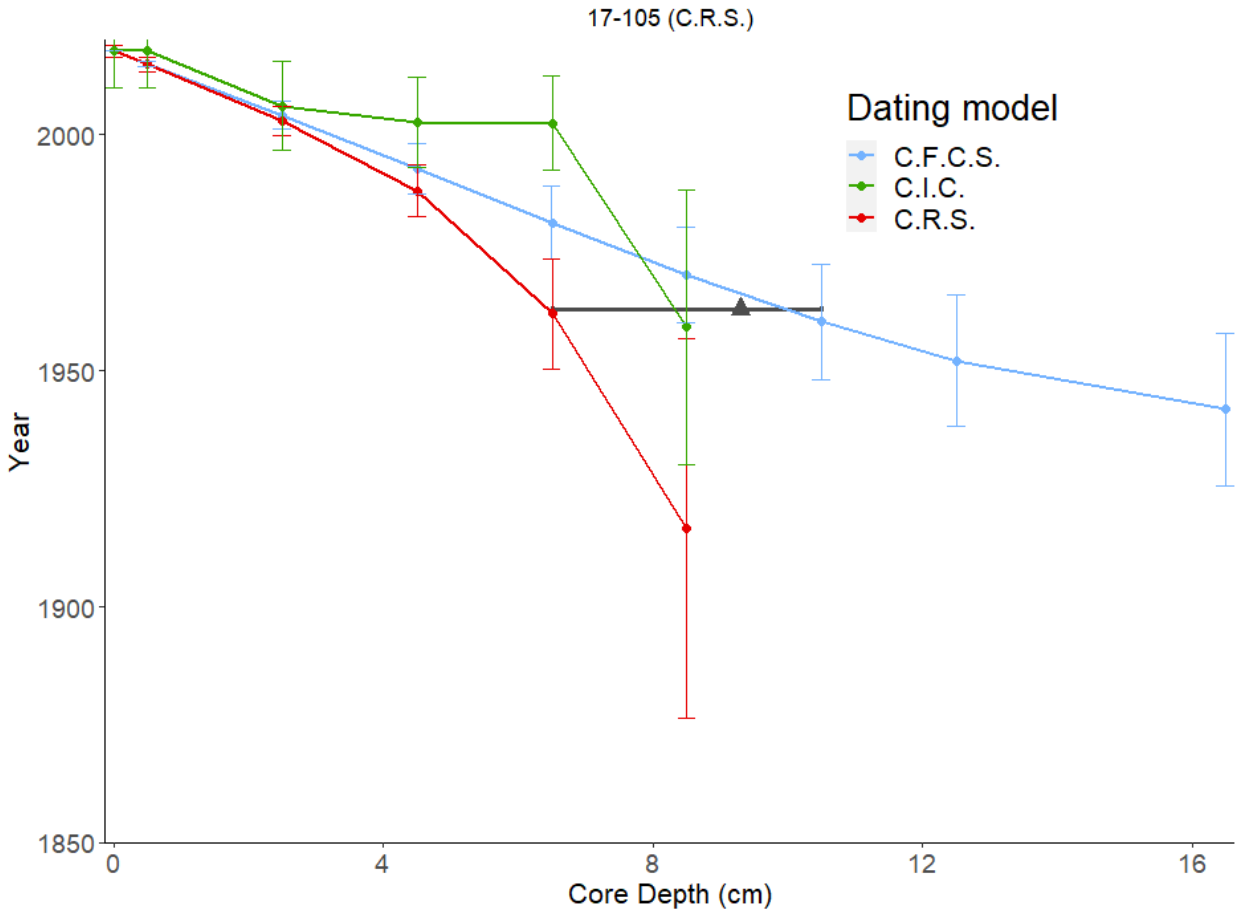
17-105 (C.R.S.)
Dating model
C.F.C.S.
C.I.C.
C.R.S.
Year
2000
1950
1900
1850
0
4
8
12
16
Core Depth (cm)

90 e

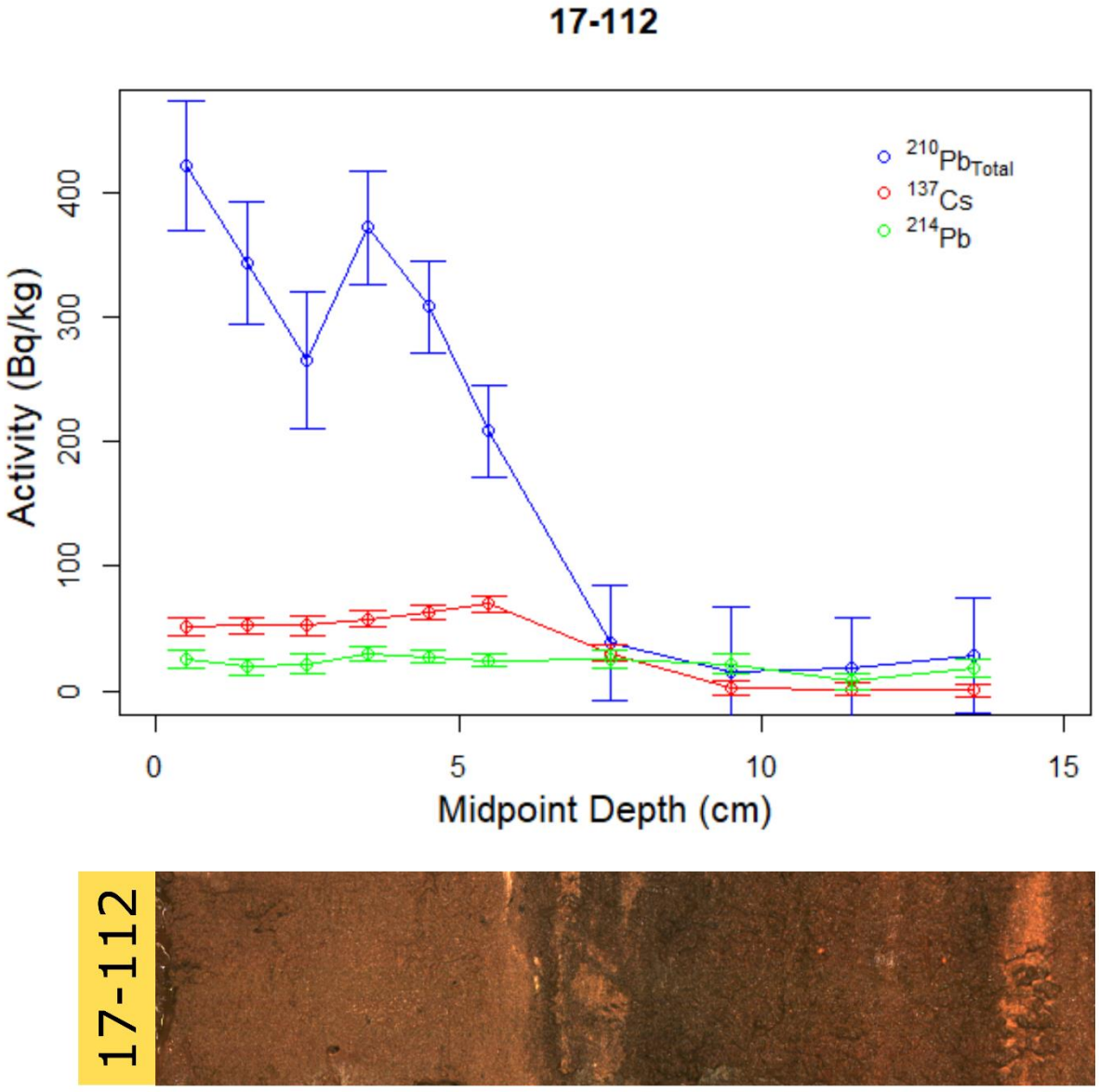
17-112
Activity (Bq/kg)
0
100
200
300
400
0
5
10
15
Midpoint Depth (cm)
$^{210}Pb_{Total}$
^{137}Cs
^{214}Pb
17-112

91

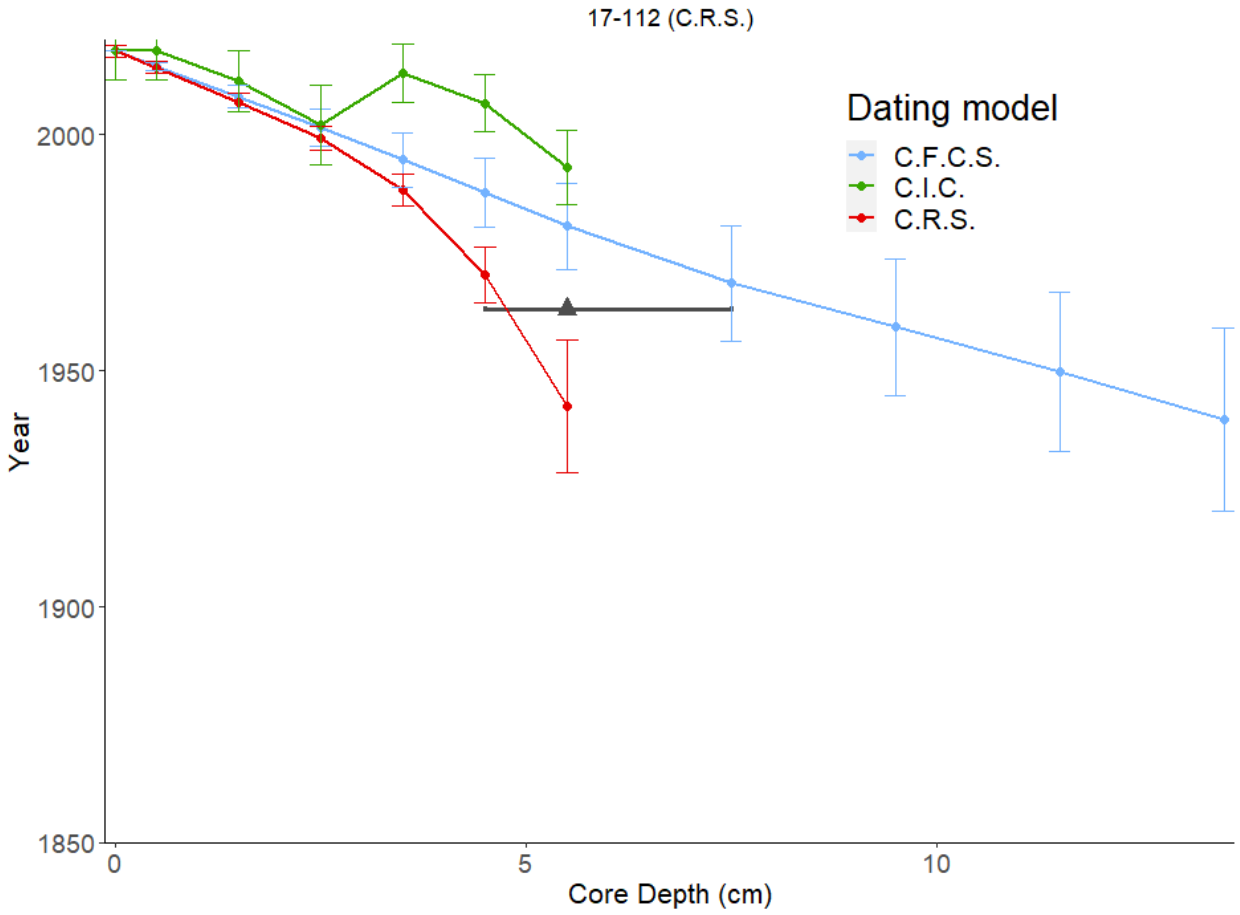
17-112 (C.R.S.)
Dating model
C.F.C.S.
C.I.C.
C.R.S.
Year
2000
1950
1900
1850
0
5
10
Core Depth (cm)

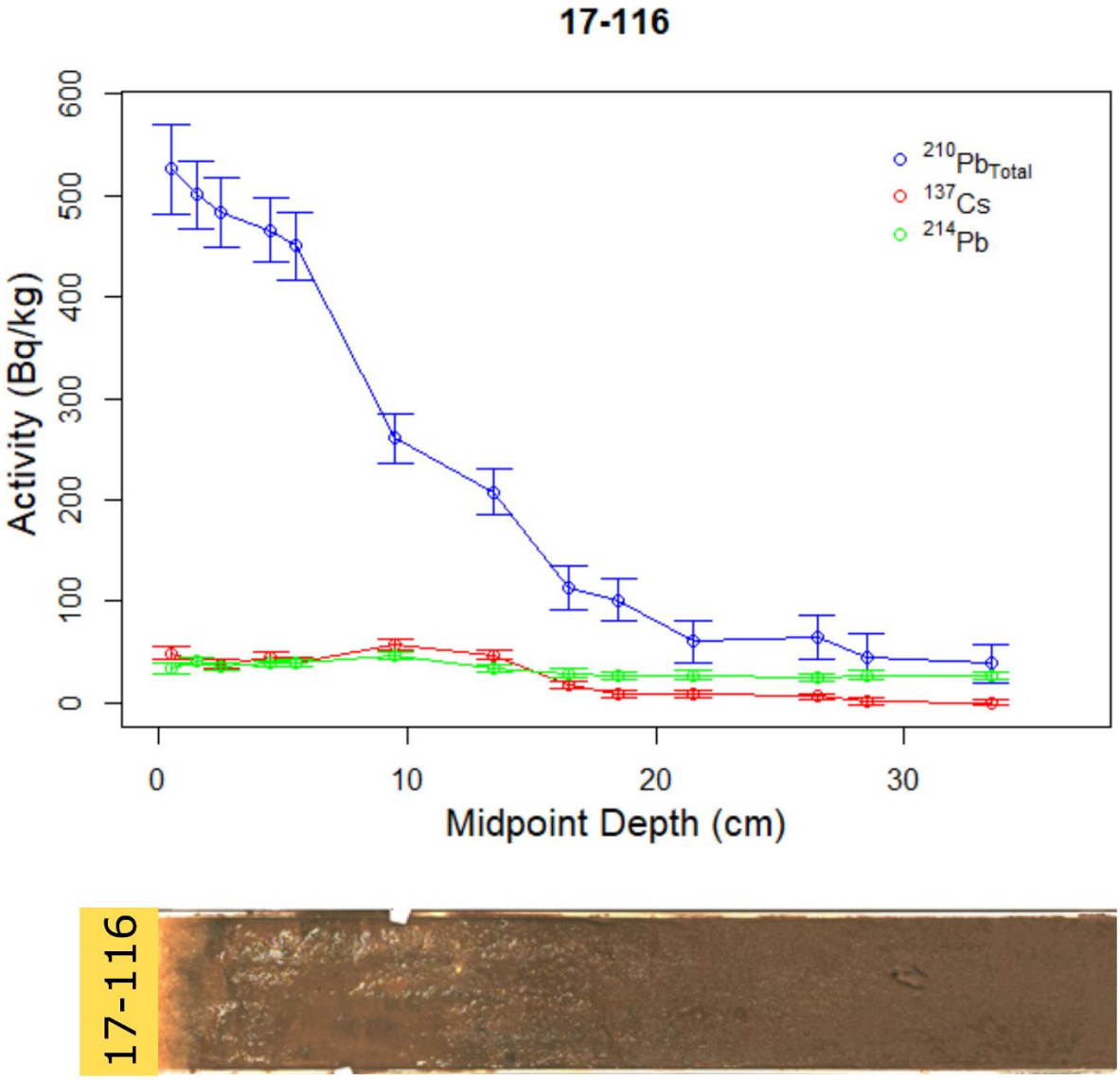
17-116
Activity (Bq/kg)
0
100
200
300
400
500
600
0
10
20
30
Midpoint Depth (cm)
$^{210}Pb_{Total}$
^{137}Cs
^{214}Pb
17-116

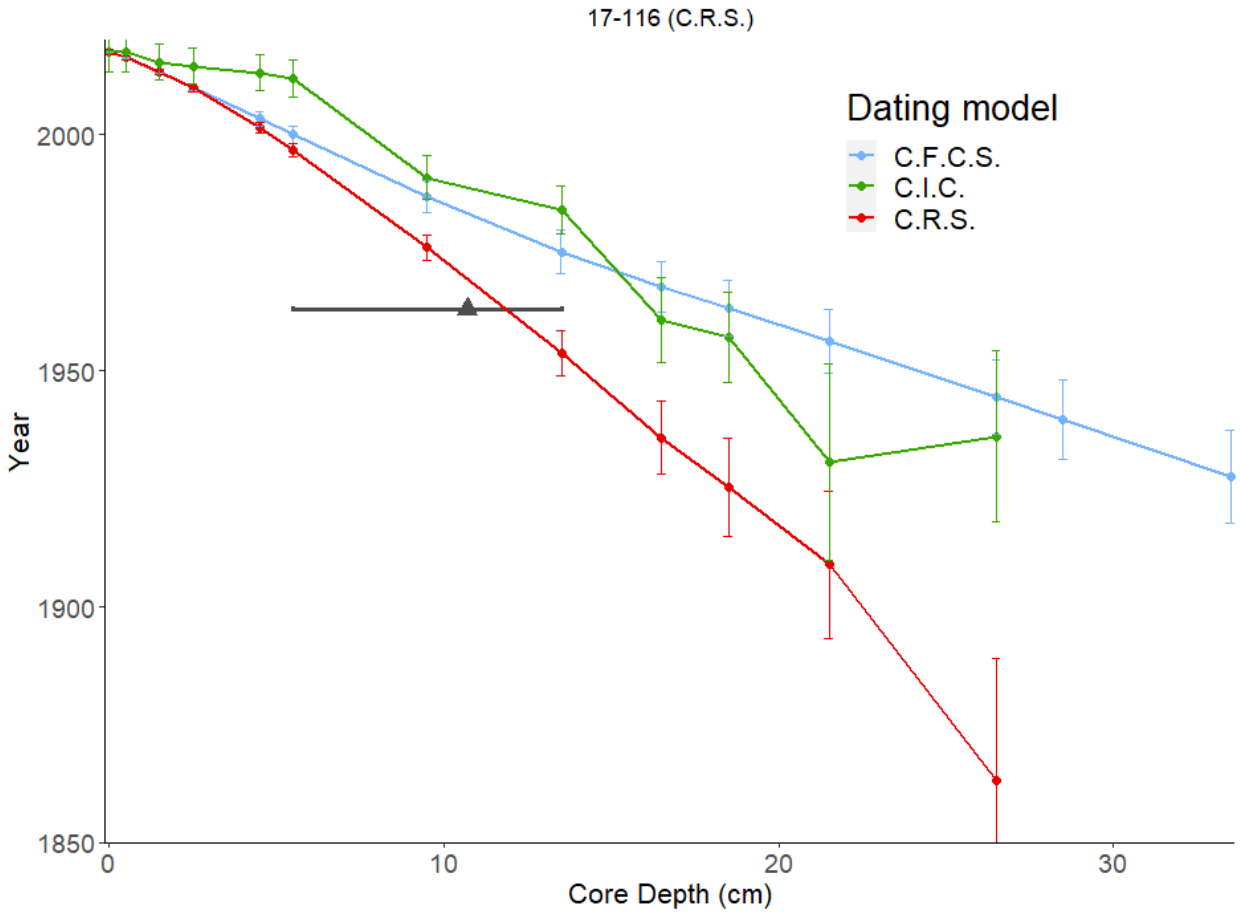
17-116 (C.R.S.)
Dating model
C.F.C.S.
C.I.C.
C.R.S.
Year
2000
1950
1900
1850
0
10
20
30
Core Depth (cm)